Dissertation

Functional characterization of CALR mutations in human HSPCs using CRISPR/Cas9 genome engineering.

submitted by

Johannes Foßelteder, MSc

for the Academic Degree of

Doctor of Philosophy (PhD)

at the

Medical University of Graz

Department of Internal Medicine, Division of Hematology

under the supervision of

Ass.-Prof. Dr.med.univ. Andreas Reinisch, PhD

2023

Statutory Declaration

I hereby declare that this thesis is my own original work and that I have fully acknowledged by name all of those individuals and organizations that have contributed to the research for this thesis. Due acknowledgement has been made in the text to all other material used. Throughout this thesis and in all related publications I followed the “Guidelines of the Medical University of Graz on Good Scientific Practice”.

Date	Signature
15.02.2023	e.h. Johannes Foßelteder

Disclosures

Part of this thesis has been published in Foßelteder J, Pabst G, Sconocchia T, Schlacher A, Auinger L, Kashofer K, Beham-Schmid C, Trajanoski S, Waskow C, Schöll W, Sill H, Zebisch A, Wölfler A, Thomas D, Reinisch A. Human gene-engineered calreticulin mutant stem cells recapitulate MPN hallmarks and identify targetable vulnerabilities. Leukemia 2023.

Co-authors:

Gabriel Pabst[1,2,3], Tommaso Sconocchia[1], Angelika Schlacher[1], Lisa Auinger[1], Karl Kashofer[4], Christine Beham-Schmid[4], Slave Trajanoski[5], Claudia Waskow[6,7], Wolfgang Schöll[8], Heinz Sill[1], Armin Zebisch[1,9], Albert Wölfler[1], Daniel Thomas[10,11], and Andreas Reinisch[1,12]

[1]Department of Internal Medicine, Division of Hematology, Medical University of Graz, Graz, Austria; [2]Research Institute of Molecular Pathology (IMP), Vienna BioCenter (VBC), Vienna, Austria; [3]Vienna BioCenter PhD Program, Doctoral School of the University of Vienna and Medical University of Vienna, Vienna BioCenter (VBC), Vienna, Austria; [4]Diagnostic & Research Institute of Pathology, Medical University of Graz, Graz, Austria; [5]Core Facility Computational Bioanalytics, Medical University of Graz, Graz, Austria; [6]Leibniz Institute on Aging, Fritz Lipmann Institute, Jena, Germany; [7]Institute of Biochemistry and Biophysics, Faculty of Biological Sciences, Friedrich-Schiller-University, Jena, Germany; [8]Department of Obstetrics and Gynecology, Medical University of Graz, Graz, Austria; [9]Otto Loewi Research Center for Vascular Biology, Immunology and Inflammation, Division of Pharmacology, Medical University of Graz, Graz, Austria; [10]Cancer Program, Precision Medicine Theme, South Australian Health and Medical Research Institute (SAHMRI), Adelaide, Australia; [11]Adelaide Medical School, The University of Adelaide, Adelaide, Australia; [12]Department of Blood Group Serology and Transfusion Medicine, Medical University of Graz, Graz, Austria;

All co-authors agreed to the use of their data in this thesis.

Acknowledgements

First and foremost, I want to thank my supervisor and mentor Ass.-Prof. Dr. Andreas Reinisch for his guidance in the last 4 years. I'm very thankful for our good relationship that always felt like friendship, for all the time he spent away from his family discussing research questions with me and helping me improve my presentation and writing skills. His dedication to science always impressed and inspired me.

Furthermore, I want to thank my co-supervisors and members of my "Thesis Committee" Univ.-Prof. Dr. Albert Wölfler and Ass.-Prof. Dr. Julia Kargl for regularly and critically reviewing my work and for their support that helped me to drive forward my projects.

Special thanks to Prof. Dr. Daniel Thomas for his critical comments and priceless scientific input of MPN and CALR knowledge, that greatly shaped the underlying project of this thesis.

I would like to thank all the lab members and colleagues that accompanied me along my PhD journey. I'm grateful for their scientific support by discussing experiments and sharing experience but equally for all the fun we had in between. I enjoyed every lunch break, game or movie night and other lab activities we spent together. Thank you, Angelika Schlacher, Gabriel Pabst, Lisa Auinger, Erdem Özkaya, Tommaso Sconocchia, Sara Nieß-Mahmoud, Afrim Avdili, Karin Lind, Bianca Perfler, Daniela Thaler, and Margaretha Frühwirth.

Huge thanks to my parents for their unconditional love and support throughout my entire life. They enabled me to build my career in the best possible way.

Moreover, I want to thank my girlfriend for her endless love and support. Thank you for always staying with me, accepting my long working hours in the lab and for building me up after a rough day.

Lastly, I would like to acknowledge the funding from the Medical University of Graz through the PhD Program Molecular Medicine "MolMed".

Table of Contents

1. Abbreviations and Definitions

7-AAD	7-Aminoactinomycin D
AAV	Adeno-associated virus
AML	Acute myeloid leukemia
BFP	Blue fluorescent protein
BM	Bone marrow
BFU-E	Burst forming unit – erythrocyte
BSA	Bovine serum albumin
CALR	Calreticulin
CAR	Chimeric antigen receptor
Cas	CRISPR-associated protein
CEL-NOS	Chronic eosinophilic leukemia, not otherwise specified
CFU-GM	Colony forming unit – granulocyte/macrophage
CFU-M	Colony forming unit – macrophage
CML	Chronic myeloid leukemia
CNL	Chronic neutrophilic leukemia
CRISPR	Clustered regularly interspaced short palindromic repeats
crRNA	CRISPR RNA
DAB	3,3'-Diaminobenzidine
DAPI	4′,6-diamidino-2-phenylindole
DSB	Double strand break
ddPCR	Droplet digital PCR
DMSO	Dimethyl sulfoxide
ET	Essential thrombocythemia
EPO	Erythropoietin
ER	Endoplasmic reticulum
ERAD	ER associated degradation
ESC	Embryonic stem cell
FACS	Fluorescence activated cell sorting
FLT3L	FMS-like tyrosine kinase 3 ligand

GFP	Green fluorescent protein
GM-CSF	Granulocyte-macrophage colony-stimulating factor
GOF	Gain-of-function
gRNA	Guide RNA
GSEA	Gene set enrichment analysis
HDR	Homology directed repair
HRP	Horseradish peroxidase
HSC	Hematopoietic stem cell
HSCT	Hematopoietic stem cell transplantation
HSPC	Hematopoietic stem and progenitor cell
hTERT	Human telomerase reverse transcriptase
IL2RG	Interleukin 2 receptor gamma subunit
IL-3	Interleukin 3
IL-6	Interleukin 6
IL-9	Interleukin 9
INDEL	Insertion and deletion
iPSC	Induced pluripotent stem cell
ITR	Inverted terminal repeat
JAK2	Janus kinase 2
KI	Knock-in
KO	Knock-out
LDL	Low-density lipoprotein
LHA	Left homology arm
Lin	Lineage markers
LOF	loss-of-function
MHC	Major histocompatibility complex
MISTRG	M-CSF, IL-3/GM-CSF, SIRPa, TPO, Rag2, IL2Rg
MNC	Mononuclear cells
MOI	Multiplicity of infection
MPD	Myeloproliferative disorder
MPL	Myeloproliferative leukemia virus proto-oncogene

MPN	Myeloproliferative neoplasm
MPN-U	Myeloproliferative neoplasm unclassifiable
NHEJ	Non-homologous end joining
NMD	Nonsense-mediated decay
NOD	Non-obese diabetic
NSG	NOD SCID IL2Rg
NSGS	NSG-SGM3
ORF	Open reading frame
OS	Overall survival
PAM	Protospacer adjacent motif
PB	Peripheral blood
PBS	Phosphate buffered saline
PCR	Polymerase chain reaction
PDI	Protein disulfide isomerase
PDX	Patient-derived xenograft
PEI	Polyethylenimine
PMF	Primary myelofibrosis
polyA	Polyadenylation signal
PV	Polycythemia vera
RBC	Red blood cell
rDNA	Recombinant DNA
RHA	Right homology arm
RNP	Ribonucleoprotein
RT-qPCR	Reverse transcription quantitative polymerase chain reaction
sAML	secondary AML
SCD	Sickle cell disease
SCID	Severe combined immunodeficiency
SCF	Stem cell factor
SEM	Standard error of mean
SFFV	Spleen focus forming virus
sgRNA	Single guide RNA

SIRPα	Signal regulatory protein alpha
SOCE	Store operated calcium entry
SR1	StemRegenin 1
ssODN	Single-stranded oligodeoxynucleotide
TALEN	Transcription activator-like effector nuclease
TCR	T-cell receptor
TPO	Thrombopoietin
TpoR	Thrombopoietin receptor
tracrRNA	Trans-activating crRNA
UCB	Umbilical cord blood
UPR	Unfolded protein response
ZFN	Zinc finger nuclease

2. Zusammenfassung

Myeloproliferative Neoplasien sind maligne Erkrankungen der blutbildenden Stammzellen des Knochenmarks, die sich durch eine erhöhte Bildung von myeloischen Zellen wie rote Blutkörperchen, weiße Blutkörperchen und Blutplättchen kennzeichnen. Mutationen im Calreticulin Gen führen dabei zur vermehrten Bildung von Blutplättchen und ihren Vorläuferzellen und sind häufige Auslöser für Philadelphia-Chromosom negative Neoplasien wie Essentielle Thrombozythämie und Primäre Myelofibrose. MPN Patienten haben oftmals ein erhöhtes Risiko für Thrombosen und für die Progression in eine sekundäre akute myeloische Leukämie.

Der heutige Wissensstand zur Wirkweise von mutiertem Calreticulin beruht auf Studien mit genetisch veränderten Mausmodellen und Krebszelllinien. Diese präklinischen Modelle ermöglichten die teilweise Entschlüsselung des pathogenen Wirkmechanismus. Ihre Validität wird jedoch durch unphysiologische Charakteristika wie die ektopische Überexpression von Calreticulin, sowie durch weitreichende Unterschiede in den zellulären und molekularen Mechanismen von Maus und Mensch eingeschränkt. Dies erschwert die Translation von neuen Erkenntnissen in die Klinik.

Aus diesen Gründen entwickelten wir ein humanisiertes präklinisches Modell für Calreticulin-mutierte Myeloproliferative Neoplasien. Genetische Manipulation mittels der „Genschere“ CRISPR/Cas9 in Kombination mit Adeno-assoziierten Viren erlaubte uns die zwei häufigsten Calreticulin Mutationen am endogenen DNA Locus von primären hämatopoetischen Stammzellen präzise nachzubilden. In *in vitro* und *in vivo E*xperimenten konnten diese genetisch manipulierten Zellen den krankmachenden, myeloproliferativen Thrombopoetin-unabhängigen Phänotyp reproduzieren. Vor allem im präklinischen Mausmodell konnten wir die Ausbildung wichtiger klinischer Merkmale myeloproliferativer Neoplasien wie eine gesteigerte Megakaryopoese, sowie eine Knochenmarksfibrose mit einhergehender Splenomegalie nachweisen.

In gesunden Stammzellen führen Calreticulin Mutationen zu frühen transkriptionellen Veränderungen, sowie zu einer Aktivierung von Stressregulationsmechanismen im Endoplasmatischen Retikulum. Diese neuen Erkenntnisse wurden herangezogen, um neue Calreticulin Mutations-spezifische Therapieansätze zu entwickeln. Das hier beschriebene präklinische Modell kann translationale Forschung und die Entwicklung weiterer Mutations-spezifischer Therapeutika ermöglichen.

3. Abstract

Myeloproliferative neoplasms are a group of clonal hematopoietic stem cell disorders, characterized by overproduction of various mature myeloid lineage-derived cell types. Calreticulin mutations are important oncogenic drivers of Philadelphia chromosome negative myeloproliferative neoplasms including essential thrombocythemia and primary myelofibrosis, where patients face a high thrombotic risk caused by excessive platelet counts and the risk for transformation into secondary acute myeloid leukemia. Mutant calreticulin, while causing and fueling these diseases, presents a promising target with high therapeutic potential.

Current knowledge of mutant calreticulin's mechanism-of-action is derived from genetically engineered mouse models or immortalized cancer cell lines. While these models proofed very valuable for gaining new insights in the past, ectopic over-expression of calreticulin and cross-species differences in molecular mechanisms in these models impede clinical translation of the findings.

To overcome these limitations, we developed the first human gene-engineered model of calreticulin mutant myeloproliferative neoplasms. We utilized a sophisticated approach combining the CRISPR/Cas9 technology and adeno-associated viral vector transfer to site specifically introduce the two most common calreticulin mutations in primary human hematopoietic stem and progenitor cells. This approach allowed the establishment of a reproducible and trackable myeloproliferative phenotype *in vitro* and in xenografted mice. The novel model described here, represents important clinical disease hallmarks like thrombopoietin-independent megakaryopoiesis, bone marrow fibrosis with linked splenomegaly and excessive growth of megakaryocyte progenitors.

The introduction of calreticulin mutations in healthy hematopoietic stem and progenitor cells allowed to reveal early transcriptional rewiring upon mutation acquisition and the induction of an endoplasmic reticulum stress response. Novel insights gained through our model enabled the identification of mutation-specific vulnerabilities that can be exploited by proteasome and chaperone inhibition to selectively eradicate mutant cells.

The humanized primary cell-based model described here, improves current calreticulin mutant models and provides a platform for molecular investigations as well as for testing of novel therapeutic compounds.

4. Introduction

4.1 *CALR* mutations in myeloproliferative neoplasms (MPN)

MPNs are a group of malignant hematological disorders that were identified in the late nineteenth and early twentieth century (2-6). In 1951, William Dameshek recognized the commonality between these bone marrow (BM) -derived disorders and united them under the term myeloproliferative disorders (MPD) (7, 8). They share the common characteristic of aberrantly increased proliferation of myeloid progenitors, which in turn leads to the accumulation of pathologic high levels of mature blood cells. These features separate MPNs from the dominating myeloid malignancy in adults: acute myeloid leukemia (AML), where immature blasts expand and circulate in the blood due to a block in differentiation. Over the years, the diagnosis of individual MPD entities improved and new classifications were created.

Today, the term MPN is predominantly used and the most recent classification of MPNs was performed in 2022 by the WHO (9-11), where MPNs were subdivided into eight distinct pathologic entities, namely chronic myeloid leukemia (CML), polycythemia vera (PV), essential thrombocythemia (ET), primary myelofibrosis (PMF), chronic eosinophilic leukemia – not otherwise specified (CEL-NOS), chronic neutrophilic leukemia (CNL), juvenile myelomonocytic leukemia (JMML), and MPN unclassifiable (MPN-U) **(Figure 1A)**. The discovery of the Philadelphia (Ph) chromosome, a translocation between chromosomes 9 and 22, that leads to the expression of the novel fusion protein BCR-ABL in CML patients, led to an early separation of Ph-positive (+) CML from the other Ph-negative (-) MPNs (12, 13). The yearly incidence rate of MPNs is about 2 cases per 100,000 persons ranging from 0.1 to 4.0. The highest incidence is reported for PV, followed by CML, ET and PMF which are very similar, whereas CEL, CNS, JMML and MPN-U are very rare (14-17) **(Figure 1B)**. The median age at diagnosis is between 60 and 70 years, making MPNs diseases of the elderly population as it is the case for most cancers.

In this study, we focus on the Ph (-) “classical” MPNs PV, ET and PMF (18). PV refers to an increase in red blood cells that concomitantly increases the risk for patients to form arterial and venous blood clots that may cause heart attacks, strokes, and deep vein thrombosis (19). Treatment strategies therefore focus on mitigating the thromboembolic risk with acetylsalicylic acid and decreasing blood counts either via phlebotomy or cytoreductive drugs such as hydroxyurea. Additional therapeutic options include interferon alpha or the JAK1/2 inhibitor ruxolitinib (20-22).

The median overall survival (OS) of PV patients is 15 years with a 5-year survival rate of 85%, showing that clinical symptoms can be handled for the majority of patients (23).

ET patients are diagnosed with increased platelet counts in the periphery accompanied by accumulation of clusters of abnormal megakaryocytes in the BM (24). Similar to PV, ET patients suffer from bleeding related symptoms which are mainly related to thrombotic events that need to be monitored closely as they present the major cause of mortality. Treatment of ET relies on managing the thrombotic risk either with acetylsalicylic acid or by reducing platelet counts via hydroxyurea, anagrelide or interferon-α (25-29). ET patients show superior survival compared to PV with a median OS of 18 years and a 5-year survival rate of > 85% (23).

Lastly, PMF is characterized by occurring BM fibrosis without prior history of other MPNs. BM fibrosis is thought to be caused by an increase in abnormal megakaryocytes that stimulate surrounding non-malignant fibroblasts to deposit collagen fibers (30). Excessive BM scarring causes extramedullary hematopoiesis, where the main site of blood production shifts into the spleen which in turn enlarges (splenomegaly). Progressing fibrosis usually leads to pancytopenia which increases the risk for bleeding complications due to a reduction in red blood cells and platelets as well as the risk for infections due to reduced leukocytes (31). Cases of PMF with pre-fibrotic stages exist but are very difficult to diagnose and might be mistakenly classified as ET resulting in inappropriate treatment (32). Treatment options for PMF patients include cytoreductive therapy with JAK2 inhibitors (ruxolitinib or fedratinib) (33, 34). In younger, fit patients hematopoietic stem cell transplantation (HSCT) represents the only curative approach (31, 35). PMF patients have the highest mortality rate among MPNs with a median survival of 4.5 years (23). Additionally, PV and ET patients might progress to more severe secondary myelofibrosis termed post-PV MF and post-ET MF that are similarly treated to PMF and all MPNs have an increased risk for transformation to secondary AML (sAML) (36).

The pathogenic driver mutations in MPNs were identified within the last 20 years and are predominantly found in three genes: Janus kinase 2 (*JAK2*), calreticulin (*CALR*) and myeloproliferative leukemia virus proto-oncogene (*MPL*). Mutations in these genes are generally found to be mutually exclusive although isolated cases with two co-occurring mutations were reported (37, 38). Furthermore, all three mutations were detected in hematopoietic stem cells (HSC) strengthening the theory that these diseases are clonal stem cell disorders (39).

The *JAK2*^{V617F} mutation was described first in 2005 and is found in > 60% of all MPN cases. It accounts for 95% of cases in PV and 50-60% in ET and PMF (40, 41). This was followed by the discovery of activating point mutations in *MPL* (W515K/L) encoding the thrombopoietin receptor (TpoR) that occur in 2-10% of ET and PMF patients and are absent in PV (42, 43). More recently, in 2013, frameshift mutations in *CALR* were reported and are found in approximately 30-40% of ET and PMF patients (44, 45) **(Figure 1C)**. This dissertation specifically focuses on *CALR* mutant MPNs and hence *CALR* will be elaborated in more detail.

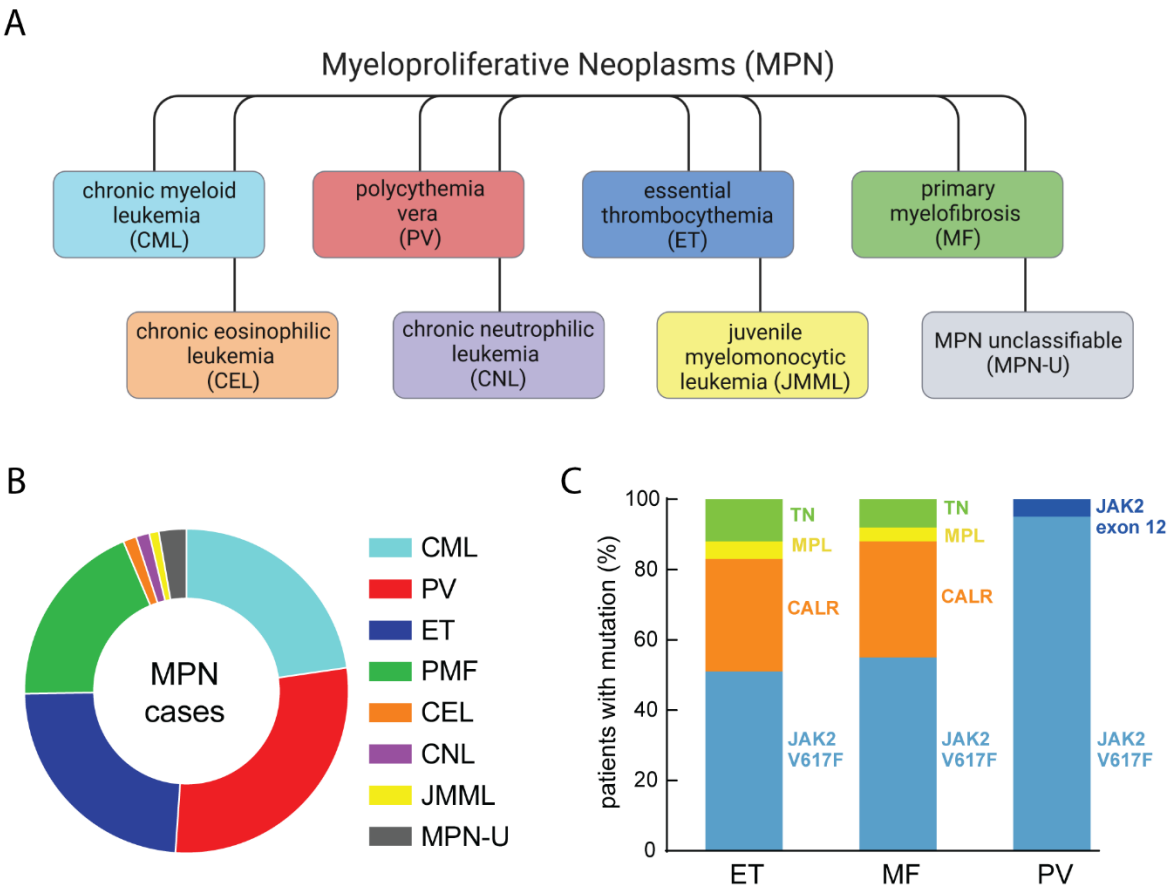

Figure 1. MPN classification and mutational landscape.

(A) MPNs were sub-classified into eight distinct entities by the WHO in 2022. **(B)** Pie chart showing the distribution of MPN cases into the respective sub-classes. Data is derived from the Surveillance, Epidemiology, and End Results (SEER) Program, National Institute of Health (NIH), USA as well as from two peer reviewed publications (46, 47). **(C)** Bar graph showing the frequency of driver mutations in the "classical" MPNs PV, ET and MF. TN stands for "triple negative" and represents patients where no mutation in either *JAK2*, *MPL* or *CALR* was found. Reproduced with modifications from (48) with permission via the CC BY-NC license (https://creativecommons.org/licenses/by-nc/4.0/).

CALR is a soluble endoplasmic reticulum (ER)-resident protein, that has been extensively studied in the past due to its manifold roles in regulating cellular homeostasis. It comprises three domains: i) a globular N-domain containing lectin domains for the binding of N-glycosylated proteins, ii) a P-domain forming an extended flexible loop for binding of additional co-chaperones to mediate protein folding and iii) a helical C-domain containing mainly acidic negatively charged amino acids that allow binding of several Ca^{2+} ions contributing to calcium buffering and storage in the ER. The C-terminus ends with a KDEL signal sequence that directs *CALR* to the ER and ensures its retention within (49-51) **(Figure 2A)**.

CALR interacts with many other chaperones like calnexin (*CANX*), BiP (*HSPA5*), GRP94 (*HSP90B1*) and protein disulfide isomerases (PDI) and was reported to directly bind ERp57 (*PDIA3*) via its P-domain to facilitate protein folding activity (52-54). Proteins that are predestinated for their transport to the cell surface or extracellular secretion are co-translationally translocated from the cytoplasm into the ER, bound by BiP and are N-terminally glycosylated. N-glycosylated proteins are bound by soluble *CALR* or its membrane-bound partner *CANX* as well as co-chaperones to help in protein folding. Several rounds of binding and releasing of proteins might be necessary to achieve a fully folded protein confirmation and this process is known as the calnexin/calreticulin cycle (55, 56). Only fully folded proteins are guided towards the secretory pathway to traffic via the Golgi complex towards the cell surface. Terminally misfolded proteins on the other hand are labelled for their cytoplasmic export and subsequent degradation via the proteasome complex, a process known as ER-associated degradation (ERAD) (57-59).

The second major role of *CALR* is binding and storage of Ca^{2+} ions in the ER to regulate cellular calcium homeostasis (60-62). Ca^{2+} ions are one of the most important second messengers and their cytoplasmic concentration is therefore tightly regulated. Various external and internal stimuli mediate release of Ca^{2+} from the ER into the cytoplasm via the inositol 1,4,5-triphosphate receptor (IP3R) and in turn activate downstream kinases or other enzymes to induce cellular processes like muscle contraction, cell growth and motility or cytoskeleton rearrangement (63, 64).

ER calcium concentrations are restored by the sarco/endoplasmic reticulum Ca^{2+} ATPase (SERCA), which is pumping Ca^{2+} ions form the cytoplasm back into the ER (65). ER refilling can be supported by the import of extracellular Ca^{2+} through membrane-spanning ion channels in a process called store operated Ca^{2+} entry (SOCE) (66).

Today more than 50 different mutations in the *CALR* gene are known with the vast majority being insertions or deletions. The two most frequent mutations are a 52 bp deletion (p.L367fs*46, type 1) herein termed DEL and a 5 bp (TTGTC) insertion (p.K385fs*47, type 2) termed INS occurring in exon 9 and account for more than 80% of all mutations found (44, 45). Most of the remaining mutations can be classified as type 1-like or type 2-like since all of them introduce a +1 bp frameshift in the open reading frame (ORF) leading to extended translation and formation of a novel C-terminal end (67, 68) **(Figure 2A)**. These mutations are generally found to be pathogenic while non-frameshift mutations most likely represent germline variants and are not identified as pathogenic. Furthermore, *CALR* mutations are almost exclusively heterozygous in MPN patients with some homozygous cases reported (69-71). Although both types of mutations form a common mutant C-terminus and lose the ER retention signal KDEL, DEL mutations cause a loss in nearly all negatively charged amino acids seen in wildtype protein and INS mutations eliminate only half of them, resulting in different biochemical properties (72, 73).

Interestingly mutant *CALR* was found to bind to TpoR in the ER and traffic as a complex via the Golgi apparatus to the cell surface. This binding is dependent on the N-terminal lectin domain of *CALR*. Binding of mutant *CALR* allows thrombopoietin (TPO)-independent dimerization of TpoR at the cell surface and activation of its downstream signaling (mainly JAK-STAT) confirming a gain-of-function (GOF) upon mutation acquisition (74-77) **(Figure 2B)**. Intriguingly, a recent study reports that mutant *CALR* forms homomultimers through its novel C-terminus, which is another prerequisite for TpoR binding and activation (78). Cytokine-independent activation of TpoR signaling leads to increased survival and proliferation of HSCs and megakaryocytes since these cells show highest expression levels of TpoR. The resulting clonal expansion of these cells results in the clinical phenotypes and therefore, the described oncogenic mechanism of mutant *CALR* is thought to be the main contributor for the initiation of MPNs.

Several studies investigated additional effects of *CALR* mutations and found subcellular localization of mutant *CALR* outside of the ER due to its loss of the KDEL sequence. Mutant *CALR* was found to translocate to the nucleus enabling novel interactions with other proteins like Fli-1 and their recruitment to the *MPL* promoter to increase transcription (79). Additionally, mutant *CALR* was found to be either displayed on the cell surface or to be secreted as soluble protein. Cell surface expression of wildtype *CALR* was initially reported to be a so called “eat me” signal that is used to label apoptotic cells for clearance by phagocytes and presents a physiologic process for cellular cleanup (80-83).

It was thought that cell surface mutant *CALR* would no longer act as “eat me” signal and could thereby promote immune evasion of malignant cells. Two studies report conflicting results on this issue as the first group could not find any difference in phagocytosis by macrophages (84), while the second group more recently confirmed inhibition of dendritic cell-mediated phagocytosis in non-MPN cell and mouse models (85). Mutant *CALR* was reported to be secreted in pre-clinical models and importantly was detected in the plasma of MPN patients (86-88). Although, secreted mutant *CALR* was shown to activate TpoR signaling in cell lines, its impact on the pathogenesis of MPNs is still unclear (89).

Furthermore, the impact of *CALR* mutations on the cellular Ca^{2+} signaling was evaluated. While *CALR* wildtype cells show a release of stored Ca^{2+} from the ER upon external stimuli such as TPO, *CALR* mutant cells spontaneously take up extracellular Ca^{2+} via SOCE, leading to abnormal proliferation of megakaryocytes (90). Thus, inhibition of SOCE could provide an option to slow down megakaryocyte growth. In summary, not one but several altered or novel functions of mutant *CALR* will contribute to the aberrant expansion of megakaryocytes and the development of MPNs.

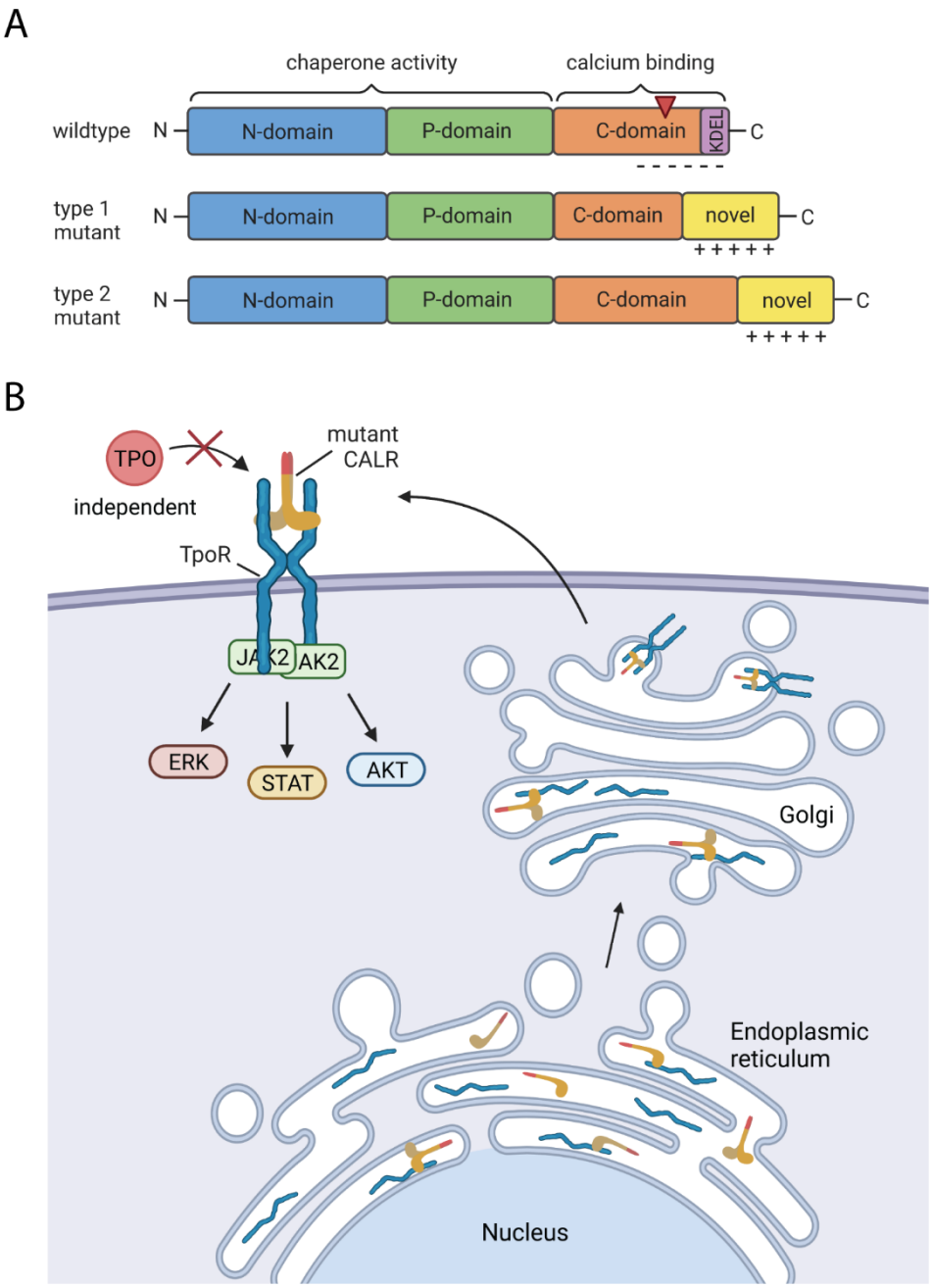

Figure 2. Structure of mutant *CALR* and aberrant activation of TpoR signaling.

(A) *CALR* domain arrangement in wildtype and mutant protein variants. N- and P- domain comprise mainly chaperone function whereas the C-domain has high calcium binding capacity. KDEL is the ER retention signal, and the red triangle shows the mutation hotspot in exon 9. The symbols **–** and **+** delineate negatively and positively charged amino acids respectively. **(B)** Schematic representation of the mechanism-of-action of mutant *CALR*. Mutant *CALR* binds TpoR in the ER and translocate via the Golgi to the cell surface, where an active dimeric complex is formed. Mutant *CALR* consequently activates TpoR downstream signaling via STAT, ERK or AKT.

Meta-analyses investigating the outcomes of MPN patients show differences in *CALR* mutant ET and PMF compared to *JAK2* or *MPL* mutant patients, despite having very similar disease manifestation and clinical parameters. *CALR* mutant patients tend to be younger, which might be one reason for their reduced risk for thrombotic events and for their better OS (91-93). This is especially relevant for PMF, where *CALR* mutations became an independent prognostic factor for OS (94). Comparison of both *CALR* mutation types revealed a higher incidence of type 1 mutations in PMF while type 2 mutations are more common in ET. The clinical parameters and outcomes seem to be similar, however (95, 96).

Today, the only clinically approved targeted therapy for MPN patients is *JAK2* inhibition via ruxolitinib or fedratinib (97-100). It is underwhelming that no *CALR*-specific drug entered the clinics so far, considering that mutant *CALR* provides a promising target due to the neoantigen characteristics of its novel C-terminus (101). Fortunately, first reports suggesting immunogenicity of mutant *CALR* were published recently. Mutant *CALR* specific memory T-cells were detected in healthy individuals but are mostly absent in MPN patients (102, 103). This is mediated by compromising the peptide loading of major histocompatibility complex (MHC) class I and a skewing in its expression towards MHC-I alleles that would not present mutant *CALR,* a phenomenon that can be overcome by peptide cancer vaccines (104, 105).

Additionally, the use of immune checkpoint blockade via PD-1 and CTLA4 could increase T-cell mediated immunity and thereby help to strengthen future immunotherapies (106). Another strategy currently under investigation are monoclonal antibodies targeting the mutant *CALR* neoepitope. First promising results show disruption of mutant *CALR* and TpoR interaction and amelioration in MPN phenotypes *in vivo* (107, 108). Ideally, mutant *CALR*-specific immunotherapies will get approval in the near future, however more therapeutic compounds are needed to broaden clinician's treatment options and provide ideal strategies for individual patient subgroups with distinct molecular background.

4.2 Pre-clinical models of *CALR* mutant MPN

Pre-clinical models are important tools of modern medicine allowing extensive investigation of physiologic and pathophysiologic conditions and drawing meaningful conclusions from these studies for the treatment of patients in the clinic. Immortalized cell lines derived from human or animal tissue for *in vitro* culture are by far the most commonly used models of the last five decades. These cell lines captivate by their unstoppable growth upon sufficient nutrient and growth factor supply, thus providing an almost unlimited source of cells. Despite the majority of cell lines isolated for research being derived from solid cancers, a remarkable repertoire of leukemia-derived cell lines is currently available. Interestingly, some of these leukemic cell lines are dependent on one or more cytokines to promote their continuous growth *in vitro*. These cell lines became of special interest for MPN research since MPN mutations generally confer cytokine independent growth. Today three of these cell lines are commonly used: the murine interleukin 3 (IL-3) dependent Ba/F3 cell line (109), the human granulocyte-macrophage colony-stimulating factor (GM-CSF) dependent erythroleukemic TF-1 cell line (110) and the human erythropoietin (EPO) or TPO dependent megakaryoblastic UT7 cell line (111, 112).

Upon identification of *CALR* mutations in MPN patients, these mutations were introduced in the aforementioned cell lines via lentiviral transduction to study their impact on cell growth and survival. All studies showed cytokine independent growth of the cell lines only when TpoR was expressed, underlining the importance of TpoR signaling (JAK-STAT) activation through binding of mutant *CALR (72, 73, 75, 76)*. In addition, cell lines harboring mutant *CALR* labelled with various C- or N-terminal tags were generated to study protein-protein interactions via immunoprecipitation or mass spectrometry in more detail (78, 79, 113). One study reported the generation of patient derived *CALR* mutant induced pluripotent stem cells (iPSC) that allowed to investigate the megakaryocytic differentiation properties. *CALR* mutant iPSCs showed accelerated and TPO independent differentiation and maturation of megakaryocytes (114).

Despite their unquestionable value for MPN research that led to the discovery of groundbreaking knowledge, transformed cell line models with unphysiological expression of *CALR* do not reflect the phenotypic and molecular characteristics of primary hematopoietic cells. Thus, precisely engineered *CALR* mutant cell models using primary hematopoietic stem and progenitor cells are needed for an unbiased investigation of transforming mechanisms.

One of the biggest challenges in pre-clinical research is to transfer the knowledge gained from *in vitro* studies into *in vivo* applications. Non-human mammalian disease models are indispensable for in depth investigation of findings in living organisms to facilitate this knowledge transfer. Mice became one of the most used model organisms that foster pre-clinical research due to their genetic similarity to humans, their ease in breeding and care and due to the accelerated experiments as a result of their fast metabolism and overall short life expectancy.

In order to generate appropriate disease models in mice, genetic engineering is often required to introduce the disease-causing mutations. Since mouse orthologs of human disease-causing genes were largely unknown in the past, human genes should be transferred into mice to study them *in vivo*. This could either mean to manipulate only somatic cells of the organ/tissue of interest or to modify germline cells which would inflict the whole organism. Somatic cell manipulation requires direct delivery of genetic material to target cells which can be very difficult to reach depending on their tissue localization, a problem still widely discussed in modern gene therapy.

Thus, early reports focused on transduction of hepatic and hematopoietic cells (115, 116). *Ex vivo* retroviral transduction of aspirated BM and subsequent transplantation into recipient mice turned out to be an efficient and versatile tool to generate genetically engineered mice restricted to the hematopoietic system (117, 118). This method was for example used to efficiently generate mice with CML (119).

The journey towards transgenic mice on the other hand started in 1974 when Rudolph Jaenisch and Beatrice Mintz transduced mouse embryos with SV40 virus and realized that the viral DNA was integrated into the germ line and passed onto next generations (120). This finding paved the way for gene transfer into mice and just a few years later, plasmid DNA was already successfully injected into the nucleus of mouse oocytes for genomic integration and birth of transgenic animals by foster mice (121). At this stage DNA integration was still random but the development of transgenic mice moved forward in parallel with the improvements in genetic engineering (see next chapter).

Another milestone for the generation of transgenic mice was the isolation of pluripotent mouse embryonic stem cells (ESC) and their *in vitro* culture, which allowed better and targeted genetic manipulations (122, 123). Genetically modified ESCs are then introduced back into blastocysts to form a transgenic mouse. Today, transgenic mice are regularly generated to study the function of genes and certain mutations thereof or to generate specific disease models.

The issue of tissue-specific expression of transgenes has been achieved via the use of promoters known to be active in certain tissue. However, certain transgenes or genetic perturbations turned out to be embryonically lethal when constitutively expressed in a certain tissue context and prevented the generation of such mice. This limitation was overcome by the use of inducible recombination systems like Cre/loxP (124). This system allows to introduce specific genetic changes via the controlled expression of the Cre recombinase by activation of its promoter through application of drugs like tamoxifen, interferons and tetracyclines. Probably the most widely used inducible recombinase is the Mx1-Cre system, which is induced by interferons but its expression is not restricted to one type of tissue (125). To ensure expression specific to the hematopoietic system, the Cre recombinase is usually controlled by either *Vav* promoter (126, 127) or *Scl* stem cell enhancer elements (128, 129).

The first *CALR* mutant mouse models were reported in 2016 and were based on BM transplantation (72, 73). BM was isolated from young mice, depleted for lineage differentiated cells and transduced with lentiviral vectors containing *CALR* DEL or INS mutant sequences coupled to GFP. Transduced BM cells were transplanted into irradiated recipient mice to generate chimeras that develop MPN. Both models reported a drastic increase in platelets accompanied by increased numbers of megakaryocytes in the BM and spleen resembling the clinical characteristics of ET. Phenotypes were milder in *CALR* INS transduced mice compared to *CALR* DEL. Interestingly, *CALR* DEL transduced mice developed symptoms of post-ET MF after 6 months as seen by BM fibrosis, decrease in cellularity and splenomegaly (73). Using this method, a later study could show that introduction of rare type 1-like and type 2-like mutations resulted in very similar phenotypes as seen with the more common type 1 and type 2 mutations, confirming that their classification is not only structurally adequate but also functionally (130).

These BM transplantation models were followed by a transgenic mouse that expressed DEL mutant human *CALR* at physiological levels in mouse HSCs using a mouse MHC class I promoter. These mice exhibited ET phenotypes similar to the models described above but never progressed to MF and had comparable survival to wildtype mice, indicating that the degree of *CALR* expression influences the disease penetrance. Soon after, mice were engineered to harbor *CALR* mutations using the novel CRISPR/Cas9 technology. First reports focused on the generation of *CALR* DEL mutations as deletions in exon 9 could be mimicked easier using this method. Three different models were generated harboring either 19, 52 or 61 bp deletions in the mouse *CALR* gene (88, 131).

While 52 and 61 bp deletions are generally found in humans, 19 bp deletion is an orthologous frameshift mutation in mouse *CALR*. Unexpectedly, all three models showed only a mild increase in platelets and megakaryocytes with the most pronounced effects seen by the 52 bp deletion (88). Detailed analysis revealed that mouse mutant *CALR* activates mouse TpoR at a lesser extent than human mutant *CALR* and thereby explains the lack in disease penetrance of these murine only models. Even more importantly, it was shown that human TpoR-mediated JAK-STAT signaling is far more activated by both mouse and human mutant *CALR* than mouse TpoR.

These results led to the development of knock-in mouse models with chimeric murine *CALR* that harbors a human mutant *CALR* C-terminus and should thereby more potently activate mouse TpoR (132). Additionally, researchers included a tamoxifen inducible Cre/loxP system to tightly control the expression of mutant *CALR* by administration of tamoxifen. As expected *CALR* mutant mice developed ET-like thrombocytosis with BM and spleen megakaryocyte accumulation. This study compared for the first time the difference in disease penetrance from heterozygous and homozygous mutation genotypes. Interestingly, homozygous mutations drastically elevated platelet levels and led to an additional leukocytosis, which was not seen before in other models. Homozygous *CALR* DEL mutations also strongly induced BM fibrosis and linked splenomegaly in these mice, making them a potent model to study PMF. Nevertheless, the species-specific interaction differences between mutant *CALR* and TpoR are limiting the use of current mouse models to faithfully investigate the pathogenesis of MPN.

Besides fully murine *in vivo* models, the generation of xenografted mice hosting human cells is a valuable option to investigate human cell behavior in a living organism. However, the transplantation of human cells into mice is hampered by the mouse immune system that would efficiently identify human cells as foreign via MHC molecules and eradicate them. Generation of immunocompromised mouse strains to dampen the murine immune response to human cells started with the detection of homozygous severe combined immunodeficiency (SCID) mutations in the *Prkdc* gene in mice (133, 134). These mice have impaired VDJ recombination leading to a deficiency but not absolute lack in B- and T-cells.

Subsequently, these mice were crossed to the non-obese diabetic (NOD) background, which shows a broad repertoire of adaptive and innate immune deficiencies like impaired T- and NK cell function, cytokine production and activity of the complement system, to combine their immunologic phenotypes (135).

NOD-SCID mice were soon used for xenotransplantation of human HSCs (136). Despite improvements in engraftment via intrafemoral injection, human engraftment was limited by remaining NK cell activity (137).

As a consequence, the gene for interleukin 2 receptor gamma (IL2RG) subdomain was depleted from the NOD-SCID background to generate NSG mice with non-functional NK cells (138). IL2RG is a common subdomain of several cytokine receptors and crucial for their activity to mediate maturation and function of immune cells including NK cells. Due to their superior engraftment of human HSCs, NSG mice promptly became the “gold standard” for human hematopoietic xenotransplantation to study normal and malignant hematopoiesis and to generate humanized mouse models (139, 140).

The development of immunocompromised mice for human engraftment did not stop at this point though and even more sophisticated models were generated. Another strain of NSG mice with an additional homozygous missense mutation in the *Kit* gene, encoding the stem cell factor (SCF) receptor, termed NSGW41 was generated (141). This missense mutation leads to a LOF in the SCF receptor, impairing HSC survival and opening stem cell niches in the murine BM. While NSG mice need to be irradiated prior to transplantation to deplete mouse hematopoietic cells and allow engraftment of human HSPCs, NSGW41 mice allow human engraftment without irradiation due to reduced endogenous HSCs (142).

A new era for hematopoietic xenotransplantations with a focus on patient-derived xenografts (PDX) was heralded by the generation of transgenic mouse strains harboring human cytokines. One of these strains is NSG-SGM3 (NSGS) which is expressing human SCF, GM-CSF and IL-3. These mice promote the expansion of human myeloid cells in xenografted mice but more importantly improve engraftment of AML samples that were notoriously difficult to engraft in NSG mice (143, 144). Probably the most sophisticated immunocompromised mouse model for hematopoietic xenotransplantations today is the MISTRG strain (145). This strain is not based on NSG mice but on recombination activating 2 (Rag2) null and IL2RG null immunodeficient mice and has four human cytokine transgenes introduced into the respective mouse gene locus: macrophage colony-stimulating factor (M-CSF), IL-3, GM-CSF and TPO. These cytokines promote the growth of almost the full human myeloid lineage spectrum and thus allow the generation of even better humanized mouse models.

In addition, these mice harbor the human signal regulatory protein alpha (SIRPα) transgene, which is a cell surface receptor expressed on mouse phagocytes. SIRPα is the receptor for the “don’t eat me” signal CD47, which is expressed on many human cancer cells and helps these cells to avoid phagocytosis (146, 147). By providing mouse phagocytes with the human counterpart to CD47, human CD47 expressing cells circumvent phagocytosis in the mouse, which greatly improves engraftment of human HSPCs and patient samples (148, 149).

Xenotransplantation of MPN patient-derived cells presented similarly challenging as other hematological malignancies (150, 151). A few studies however reported successful engraftment of the more aggressive PMF and secondary MF samples in immunocompromised mice that were humanized to some degree. In the first report, humanized BM ossicles were generated in NSG mice to provide a cellular human environment for successful and robust engraftment of MF-derived $CD34^+$ HSPCs. These xenografts exhibited the main clinical phenotype of reticulin fiber myelofibrosis (152). Another group reported the transplantation of MF HSPCs into the novel MISTRG mice, which resulted in robust engraftment in the BM and peripheral blood (PB). However, the prevalence of BM fibrosis remained low in this model (153). In the latest report, MF HSPCs were transplanted intratibial into the murine BM of irradiated NSGS mice to achieve engraftment and myelofibrosis with high degree (154). Despite these improvements on patient-derived samples, transplantation of engineered human HSPCs into these advanced immunocompromised mice to model MPN phenotypes in a genetically defined setting remains untested.

4.3 CRISPR/Cas9-mediated genome engineering

Genetic engineering of prokaryotic and eukaryotic organisms has a long history reaching back into the 1950s when James Watson and Francis Crick first discovered the double helix structure of the DNA (155). This was followed by important milestones that paved the way for molecular cloning, like the isolation of bacterial DNA polymerases (156) and the subsequent first *in vitro* synthesis of DNA (157, 158). However, the discovery and isolation of DNA ligases (159-161) and restriction enzymes (162, 163) in the late 1960s were crucial to generate the first recombinant DNA (rDNA) (164). While the initial steps towards genetic engineering took years, the discovery of the tools needed to generate rDNAs greatly accelerated genetic research, leading to the generation of many transgenic organisms shortly after, having wide ranging impact to human kind like the generation of synthetic human insulin in *E. coli* (165), which reduced the need to slaughter millions of animals to harvest porcine insulin.

Although, the rDNA technology opened the field for genetic engineering, the steps to generate these DNA sequences was still very laborious. Luckily, a simple yet very powerful method developed by Kary Mullis greatly reduced the workload for genetic researchers. The method known as polymerase chain reaction (PCR) allowed rapid amplification of any desired DNA sequences *in vitro* and therefore became an integral part of labs around the world (166). The ease in use and the fast turnaround time are the reasons why PCR is still in use today and is known even outside the scientific community for its diagnostic use to detect viral infections. Despite all improvements of rDNA technology, these methods would only allow the generation of genetically modified organisms by transfection with plasmid or viral vectors providing a template for the expression of a gene of interest but would not allow to make any precise genetic modifications in the host genome itself.

This long-awaited goal was first achieved by the development of zinc finger nucleases (ZFN), which combined the cleavage domain of a restriction enzyme with several zinc finger DNA binding domains, each recognizing a separate 3 bp sequence (167).

Thereby, ZFNs provided for the first time a modular system that allowed to cut DNA in a sequence- and site-specific manner and introduce genetic changes via homologous recombination by providing a DNA repair template (168). A major drawback of ZFNs however was the difficulty to re-design and produce DNA binding domains to efficiently target any genomic site of interest.

This was partly improved by another type of engineered nucleases termed transcription activator-like effector nucleases (TALEN). TALENs use bacterial transcription activator-like effector proteins as DNA binding domains as they show a clear and predictable correlation between amino acid sequences in their variable DNA recognition sites and the binding of specific nucleotides (169-172). Thus, TALENs could be re-designed more rapidly for changing applications, further fostering genetic research. In the meantime, huge sequencing efforts within the human genome project (173, 174) provided sequence information for most parts of the human genome building the basis for identifying coding and non-coding elements in a chromosomal context as well as the identification of genetic variants like cancer driving mutations.

Both generations of nucleases were soon outclassed by the clustered regularly interspaced short palindromic repeats (CRISPR) and CRISPR associated protein (Cas) system. The CRISPR/Cas system was initially found in archaea and bacteria as a defense mechanism against viral infection (175). Infected bacterial cells integrate viral sequences called spacers between short repeat sequences into their genome (176). This array of repeats and spacers is accompanied upstream by several Cas genes encoding bacterial endonucleases and trans-encoded small RNA genes. Once the CRISPR locus gets expressed, the long pre-mature CRISPR RNA (crRNA) is processed by cleavage of spacer and repeat pairs. These mature crRNAs form a duplex with the trans-activating crRNA (tracrRNA) (177) and associate with Cas enzymes to facilitate anti-viral immunity (178). Upon repeated viral infection, crRNAs bind complementary viral sequences, which are cleaved by Cas enzymes to eradicate any foreign DNA (179).

Soon it was recognized that this bacterial defense system could provide a novel tool for genome editing, which was published in two landmark studies in 2012 (180, 181). Since RNA is responsible for sequence-specific DNA binding in this system, laborious engineering of protein domains is dispensable and complementary RNA sequences can be easily and rapidly adapted to any target DNA. Additionally, it was shown that crRNA and tracrRNA can be combined to form a synthetic single guide RNA (sgRNA) simplifying the CRISPR system. Cas9 was found to be a member within the Cas endonuclease family, that can solely cleave DNA without the need for accessory proteins and therefore proofed to be an ideal candidate for this new genome editing tool (182, 183). However, Cas9 is not completely sequence independent, but recognizes a commonly occurring DNA sequence downstream of the crRNA targeting site called protospacer adjacent motive (PAM).

CRISPR/Cas9 rapidly became the dominating technology for genome engineering of eukaryotic organisms (184, 185) allowing targeted and highly specific introduction of double-strand breaks (DSB). Targeting a specific genomic locus requires the design of a sgRNA with 20 nucleotides of “seed sequence” complementary to the target DNA and adjacent to a PAM sequence required by the Cas9. The most commonly used Cas9 is derived from *Streptococcus pyogenes* and requires NGG as PAM where N stands for any nucleotide. The occurrence of such a PAM sequence next to the target region of interest limits the possibilities of DSB sites. When co-expressed in any given cell, Cas9 and sgRNA assemble to an active ribonucleoprotein (RNP) complex searching for complementary DNA sequences in the genome. Upon binding of the sgRNA and unwinding of the genomic DNA, Cas9 cleaves both DNA strands 3 bp upstream of the PAM sequence inducing a DSB with blunt ends **(Figure 3A)**.

DNA damage generally activates cellular repair machineries to safeguard genomic stability. DSBs are repaired by either one of two mechanisms. The first one being the error-prone non-homologous end joining (NHEJ) which is active throughout the cell cycle. NHEJ rejoins the DNA ends of a DSB while removing or adding nucleotides on one or both ends and thereby creating insertions and deletions (INDELs) (186).

The second pathway called homology directed repair (HDR) utilizes homologous DNA sequences from sister chromatids to accurately repair the DSB via homologous recombination (187) **(Figure 3B)**. This pathway is mainly active during the S-phase of the cell cycle, however still at a lesser extent compared to NHEJ the dominating repair pathway in this scenario (188). Both pathways became highly relevant for CRISPR/Cas9-mediated genome engineering. NHEJ is commonly used to generate gene knock-out (KO) for loss-of-function (LOF) studies by targeting early exons of protein coding genes. INDELs generated via NHEJ mostly cause frameshifts in the ORF generating premature stop codons and leading to nonsense-mediated decay (NMD) of the resulting mRNA or expression of truncated and non-functional proteins (189). HDR on the other hand allows knock-in (KI) of genes or any foreign DNA into a desired DNA locus for GOF studies. Providing exogenous DNA flanked by sequences homologous to both ends of the DSB allows its integration via HDR into the host genome. The exogenous DNA intended for the KI can either be i) of a different species to generate transgenic organisms, ii) a modified endogenous sequence to introduce genetic variants like gene mutations or iii) a whole expression cassette including a gene with its own promoter to establish a specific gene expression status, amongst many other possible applications.

It is important to mention that although the CRISPR/Cas9 system enables precise editing of on-target genomic loci, off-target editing at unwanted sites might happen too. This is mainly mediated by sequence similarities between the edited loci enabling complete or partial binding of the sgRNA. Mismatches in the DNA sequence are mainly tolerated at the 5'-end of the sgRNA whereas base matching is very strict at the 3'-end next to the PAM sequence (190). Today, potential off-target sites are predicted by algorithms implemented in sgRNA design tools and allow minimization of off-target editing already at the planning stage (190-192). Additionally, various Cas9 variants have been engineered to reduce off-target activity and increase specificity (193-195) alongside tools to detect and quantify editing at unwanted off-target sites (196-199).

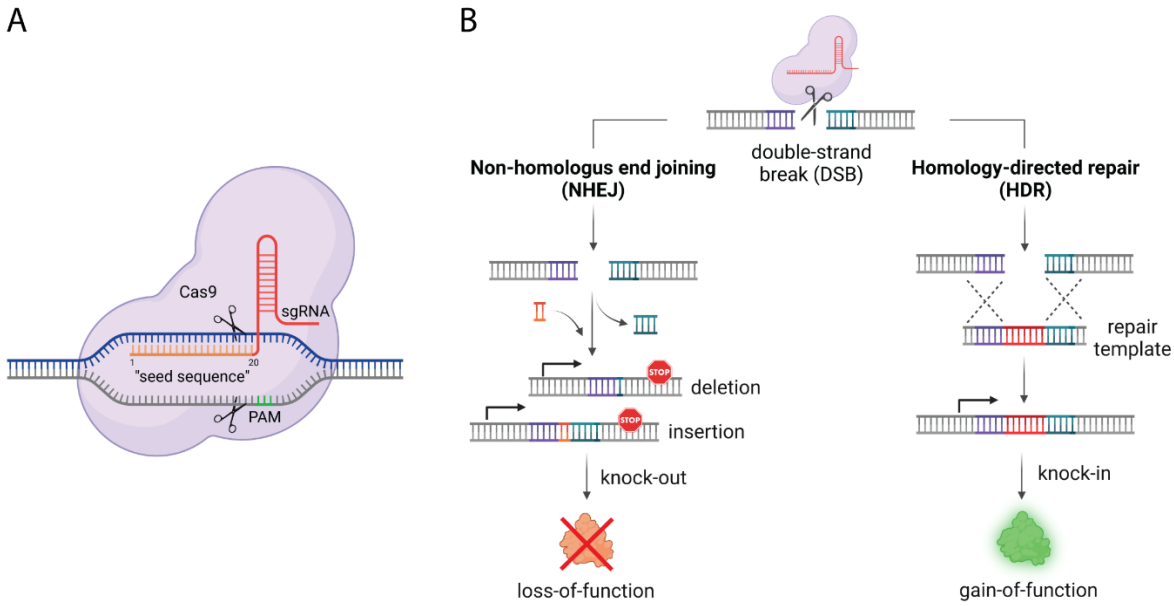

Figure 3. CRISPR/Cas9-mediated genome editing

(A) Depiction of the Cas9-sgRNA complex unwinding a stretch of DNA. Binding of DNA via the "seed sequence" of the sgRNA is followed by DNA cleavage through Cas9 3 base pairs upstream of PAM. **(B)** Schematic overview of the two cellular double-strand break repair pathways that are used for gene knock-out and knock-in.

Initially, CRISPR/Cas9 components were delivered via plasmid vector transfection into cells resulting in expression of sgRNA and Cas9 protein by the cellular gene expression machineries, which takes 8-12 hours but lasts several days as gene expression continues until all remaining plasmid DNA was degraded (200). However, plasmid DNA is not tolerated by all types of cells and can induce substantial toxicity. Retroviral vectors provide an alternative delivery strategy leading to stable integration of the CRISPR components. A strategy mainly used to generate cell lines with either constitutive or inducible expression for CRISPR screens (201, 202). In recent years, the delivery of pre-complexed synthetic sgRNA and Cas9 protein via electroporation/nucleofection proved to be superior for genome editing of primary human cells compared to the aforementioned strategies (203). RNP provides an immediately active complex for rapid editing within a few hours and is less toxic in many cases due to cellular clearance within 48 hours. In addition, the short time window of activity reduces potential off-target editing, which is more frequently seen in stably expressing cells (200, 204).

For efficient HDR-mediated KI upon DSB induction by Cas9, DNA repair templates can be delivered either i) directly as single-stranded oligodeoxynucleotide (ssODN) for short sequence insertions or single nucleotide changes, or ii) in form of a viral vector for long insertions including whole genes or expression cassettes (205-208). Adeno-associated viruses (AAV) became the most prominent choice in this regard due to their single-stranded DNA genome, their very low frequency of integration into the host genome and their broad spectrum of infectivity of human cell types (209, 210).

In recent years, CRISPR/Cas9-mediated genome engineering became essential for hematologic research. Besides modification of T-cells for immunotherapy (T-cell receptor (TCR)-engineered or chimeric antigen receptor (CAR) T-cells) (211, 212), HSCs were in the focus of hematology-related genetic research. HSCs represent the origin for all hematopoietic cells and as such acquisition of genetic perturbations has detrimental effects on their progeny, thus HSCs were found to be at the root of many hematological disorders (213-215). While immortalized cell lines are regularly engineered using CRISPR/Cas9 due to the ability to select for edited clones even at low editing frequencies, primary HSCs do not allow for unlimited clonal expansion and thus require more sophisticated editing strategies.

Nevertheless, several studies reported successful and efficient knock-out of genes in human HSPCs (216, 217) including targeting the transcriptional regulator of fetal hemoglobin *BCL11A* for the treatment of hemoglobinopathies like ß-thalassemia and sickle cell disease (SCD) (218, 219), which led to the first clinical trial of a CRISPR-mediated ex vivo gene correction (220). Similarly, single or multiplexed deletion of hematologic genes is efficiently used to mimic LOF mutations for leukemic cell models (221, 222). Site specific introduction of driver mutations in HSPCs to model leukemic GOF mutations however remains challenging. HDR-mediated knock-in efficiencies are usually low and require enrichment of genetically engineered cells. Therefore, strategies using fluorescent reporters for flow cytometry-based enrichment and tracking were developed (223).

These undebatable advantages of the CRISPR/Cas9 technology over former designer nucleases led us to utilize this technique for the genetic engineering of *CALR* mutations to better characterize their impact on human HSPC biology.

4.4 Rationale and aims of the dissertation

Despite increasing interests in unveiling the pathological mechanisms of mutant *CALR*-driven MPNs and groundbreaking insights in recent years, many questions remain unanswered. It is not fully clear yet, which mechanisms are induced in healthy HSCs upon acquisition of mutations and how these change their survival and differentiation properties to contribute to the myeloproliferative phenotype. In addition, novel therapeutic strategies either directly targeting mutant *CALR* or exploiting specific *CALR* mutant cell characteristics are greatly needed to improve patient outcomes, especially for PMF patients with poor prognosis. To this end, primary HSPC-based models that allow for faithful and prospective investigations are essential. However, current research mainly utilizes transformed and immortalized cell lines that are usually genetically distinct to primary cells and are already biased towards increased proliferation. Additionally, studies using patient material do not allow to draw meaningful conclusions on disease initiating mechanisms due to their retrospective nature.

Based on these limitations and gaps in knowledge, the aims of this dissertation were to 1) generate a novel heterozygous *CALR* mutant MPN cell model by forward engineering healthy primary human HSPCs using the CRISPR/Cas9 technology and to 2) characterize the impact of acquired *CALR* mutations on the phenotype of engineered HSPCs. 3) Engineered *CALR* mutant human HSPCs will be xenotransplanted into immunocompromised mice to investigate their disease-related properties *in vivo* and to generate a humanized *CALR* mutant MPN mouse model. 4) Furthermore, transcriptional profiling of engineered *CALR* mutant HSPCs will be used to gain deeper insights into the molecular changes driving cell transformation. 5) Based on these results, novel therapeutic drug options for *CALR* mutant MPNs will be investigated.

The results of this dissertation will contribute to a better understanding of *CALR* mutant MPNs and will provide disease models with great value for the MPN research community. Lastly, the findings of this work have a high potential for translational impact via the development of novel therapeutic strategies.

5. Material and Methods

The majority of work described here was solely conducted by myself. Experiments that were partly or completely performed by others are designated as such.

5.1 Cell culture

5.1.1 Cell line culture

K562 cells were a gift from the Majeti lab (Stanford, CA, USA) and cultured in high glucose and L-glutamine containing RPMI1640 media (Sigma Aldrich, St. Louis, MO, USA) supplemented with 10% fetal bovine serum (FBS, Pan-Biotech, Aidenbach, Germany) and 1% Penicillin/Streptomycin (P/S, Sigma Aldrich) at 37°C and 5% CO_2 in a humidified incubator. UT7/TPO and TF-1_TpoR cell lines were gifted from the Thomas lab (Adelaide, Australia) and both cultured in high glucose and L-glutamine containing RPMI1640 supplemented with 10% FBS, 1% P/S and 20 ng/ml TPO (PeproTech, Rocky Hill, NJ, USA). HEK293T cells were a gift from the Majeti lab and were cultured in high glucose and L-glutamine containing DMEM media (Sigma Aldrich) supplemented with 10% FBS, 1% P/S. All cell lines were regularly checked for identity via STR profiling and for mycoplasma contamination via PCR.

5.1.2 Primary cell isolation

UCB collection was performed by Bettina Amtmann, trained study nurse at the Department of Obstetrics and Gynecology, Medical University of Graz. PB collection from MPN patients was performed by nurses at the outpatient clinic of the Division of Hematology, Medical University of Graz. CD34+ cell isolation via magnetic beads was performed by Angelika Schlacher and Lisa Auinger at the Division of Hematology, Medical University of Graz.

$CD34^+$ HSPCs were isolated either from umbilical cord blood (UCB) of term deliveries or from peripheral blood (PB) of MPN patients upon routine visits at the outpatient clinic. UCB was collected at the Department of Obstetrics and Gynecology, Medical University of Graz only when an informed consent from donors was received.

The whole procedure was approved by an institutional review board of the Medical University of Graz (IRB approval: 31-322 ex 18/19). PB from ET, PMF and post-ET MF patients was collected at the Division of Hematology, Medical University of Graz upon informed consent from the patients (IRB approval: 30-464 ex 17/18). First, mononuclear cells (MNC) where enriched from whole blood by density gradient separation via centrifugation with Ficoll-Paque® Plus (GE Healthcare, Chicago, IL, USA) for 30 min at 400 g and room temperature, deceleration off. UCB-derived $CD34^+$ HSPCs were then purified via magnetic beads and column-based positive selection using CD34 MicroBeads (Miltenyi Biotech, Bergisch Gladbach, Germany) according to the manufacturer's protocol. Patient PB-derived $CD34^+$ HSPCs were purified from MNCs directly prior to culture via FACS. Thus, MNCs were stained with CD34-FITC, CD45-V500 (Beckman Coulter, Brea, CA, USA) and a lineage marker (Lin) cocktail (CD2, CD3, CD14, CD16, CD19, CD56, all PE-Cy5, Beckman Coulter) before sorting viable Lin^- $CD34^+$ $CD45^{dim}$ cells.

5.1.3 Primary cell culture

$CD34^+$ HSPCs isolated from UCB and having a purity above 90% were either frozen in liquid nitrogen for long-term storage or directly cultured in serum-free stem cell retention media in order to expand prior to genome engineering. Thus, StemSpan™ SFEMII basal media (StemCell Technologies, Vancouver, BC, Canada) was supplemented with the human recombinant cytokines SCF, TPO, FLT3, IL-6 (all 100 ng/ml, PeproTech) and the small molecule stimulators of hematopoiesis UM171 (35 nM, StemCell Technologies) and StemReginin 1 (SR1, 750 nM, PeproTech).

5.2 Design of CRISPR/Cas9-mediated knock-in approach

5.2.1 Guide RNA (gRNA) design

In order to knock-in *CALR* mutations at the endogenous gene locus, we decided to adapt a recently published CRISPR/Cas9-based genome editing strategy (223). The principle of this strategy is to knock-in a mutation-bearing cDNA upstream of the natural mutation hotspot in the genome. To introduce the two most common *CALR* mutations, originally occurring in exon 9, we decided to insert the mutant sequences in the upstream intron 7. Thus, we were looking for possible gRNA sequences in intron 7 using the CRISPOR web tool (www.crispor.tefor.net) (224). A query was started with the last 2000 bp of intron 7 as input and filtering for *Homo sapiens* genome (GRCh38) and *Streptococcus pyogenes* Cas9 with NGG as PAM sequence. Three gRNAs were selected for best predicted on-target (efficiency score) and off-target activity (specificity score).

CALR_I7_gRNA1: 5'-CGCCTGTAATCCTCGCCCAG-3'

CALR_I7_gRNA2: 5'-GAGAATGATGTGAACCCAGG-3'

CALR_I7_gRNA3: 5'-TCAGGAGATCGAGACCACCC-3'

Based on superior on-target activity in an initial test in K562 cells, gRNA 1 was selected for all following experiments in primary cells. Therefore, gRNA 1 was acquired as chemically modified single guide RNA (sgRNA) from Synthego (Redwood City, CA, USA) containing 2'-o-methyl groups at the first and last three bases and 3'-phosphorothioate bonds between the first 3 and the last 2 bases.

5.2.2 AAV donor DNA vector design

We decided to design an AAV vector for the delivery of *CALR* donor DNA to integrate into the site-specific DSB generated by the CRISPR system. Since the gRNA was designed to target intron 7, the *CALR* cDNA comprised only the downstream exons 8 and 9. The cDNA was codon optimized and harbored either the wildtype (WT) sequence or a type 1 (52 bp deletion) or type 2 (5 bp insertion) *CALR* mutation followed by a SV40 poly-adenylation (polyA) signal. To ensure splicing of the cDNA to the endogenous exons 1-7 upon integration, we included a 5' splice acceptor (last 150 bp of intron 7) upstream. The cDNA construct was followed downstream by a spleen focus-forming virus (SFFV) promoter driving constitutive expression of a fluorescent reporter gene (GFP, BFP, or mCherry) that would allow for enrichment of successfully modified cells.

Wildtype cDNA was combined with either GFP or mCherry and mutant cDNA with BFP allowing to distinguish cells with mono- or bi-allelic integration as well as cells with heterozygous or homozygous genotypes by looking at the fluorescent reporter combinations. This whole cassette was flanked by sequence arms homologous to the *CALR* gene sequence next to the DSB to facilitate HDR-mediated integration. The left homology arm (LHA) was 250 bp and the right homology arm (RHA) 400 bp in size.

5.3 Generation of genome editing reagents

5.3.1 gRNA vector cloning

CALR gRNA sequences were cloned into the Cas9-eGFP expressing pX458 vector (#48138, Addgene, Watertown, MA, USA) as previously described (225). Briefly, the 20-nucleotide targeting sequence and its complementary sequence were ordered as single-stranded oligonucleotides (oligos) (IDT, Coralville, IA, USA). Both oligos were phosphorylated and annealed using T4 Polynucleotide Kinase (NEB, Ipswich, MA, USA). Annealed oligos were cloned into BbsI-digested pX458 using Quick Ligation™ Kit (NEB). After transformation into chemically competent *E. coli* (5-alpha, NEB), three individual colonies were picked for amplification in overnight cultures. Plasmid DNA was isolated (Monarch Plasmid Miniprep Kit, NEB) and sanger sequenced (Eurofins Genomics, Ebersberg, Germany) for successful integration of gRNAs. Only correctly cloned vectors were used for genome editing experiments.

5.3.2 AAV vector cloning

LHA, RHA and codon-optimized *CALR* cDNAs (either wildtype or mutant) were ordered as double-stranded DNA (IDT). SFFV promoter, fluorescent protein (GFP, BFP, mCherry), and polyA sequences were PCR-amplified from vectors gifted by the Porteus and Majeti labs (Stanford, CA, USA). All fragments included at each end 40 bp of overlapping sequence to the neighboring fragments of the donor vector and were cloned all in one step into the NotI-digested pAAV-MCS2 vector (#46954, Addgene), containing ITRs from AAV serotype 2 (AAV2), using NEBuilder® HiFi DNA Assembly Mastermix (NEB). Cloned vectors were amplified and sequenced as described above.

5.3.3 Recombinant AAV6 production

Recombinant AAV6 (rAAV6) vectors were produced as described previously.(223) Briefly, $11x10^6$ HEK293T cells were seeded in each of ten 150 mm cell culture dishes. 24 hours later the cells were transfected with 6 µg of the generated AAV donor vector and 22 µg of the AAV helper plasmid pDGM6 (#110660, Addgene), which contains AAV6 cap genes, AAV2 rep genes, and adenovirus 5 helper genes, using polyethylenimine (PEI).
After 72 hours incubation, rAAV6 was purified using the AAVpro® Purification Kit (Takara Bio, Shiga, Japan) according to the manufacturer's protocol. The purified viral vectors were stored in aliquots at -80°C until further use. To ensure high viral titers in each of the rAAV6 preparations, the number of vector genomes per µl was quantified by ddPCR (QX200, Bio-Rad, Hercules, CA, USA).

5.4 Genome editing of human cells

5.4.1 Electroporation and transduction

CRISPR reagents were delivered in form of the directly active and short-lived RNP complex to ensure fast on-target editing with minimum off-target activity. Therefore, Cas9 protein (IDT) and sgRNAs were complexed at a molar ratio of 1:2.5 at 25˚C for 10 min. $CD34^+$ HSPCs were pre-cultured in stem cell retention media for 3 days to increase cell numbers for gene editing and to induce proliferation, which improves HDR-mediated integration. $2x10^5$ - $5x10^6$ HSPCs were then suspended in Human Primary Cell Nucleofection Kit P3 (Lonza, Basel, Switzerland) and electroporated with 230 µg/ml RNP complex using the 4D-Nucleofector® (Lonza, program: DZ-100). Directly after electroporation, cells were transferred to pre-warmed stem cell retention media and diluted to $1x10^6$ cells/ml. Cells were then transduced with AAV6 donor vectors at an MOI of 5,000-10,000 vector genomes/cell. The virus-containing culture media was replaced with fresh growth media after 6-8 h to reduce viral exposure. After a total of 48 hours cells with high fluorescent reporter expression (GFP, BFP or mCherry), indicative of successful integration, were enriched on a FACSAria™ IIIu cell sorter (BD Biosciences, San Jose, CA, USA).

5.4.2 Confirmation of site-specific knock-in

To confirm correct integration of *CALR* cDNA at the endogenous gene locus, DNA was extracted from either $5x10^4$ sort-purified cells or single picked colonies from CFU assays, amplified via PCR and finally sequenced. Therefore, cells were suspended in 25 µl of QuickExtract™ DNA Extraction Solution (Epicentre, Madison, WI, USA), vortexed for 15 sec, incubated at 65°C for 6 min, vortexed again for 15 sec and incubated at 98°C for 2 min. The integration site at intron 7 of the *CALR* gene was amplified via an 'in-out' PCR using a forward primer that binds outside the LHA and a reverse primer that is specific for the integrated cDNA (insert). The sequences of the primers used are listed below.

*CALR*_outside_LHA: 5'-AAGTGATCCGTTCGCCATGAC-3'

*CALR*_WT_insert: 5'-ACGTCCTCTTCCTCGTCCTC-3'

*CALR*_DEL_insert: 5'-CCAACCCTGGAGACACGCTTC-3'

*CALR*_INS_insert: 5'-TCAGTCCATCCCTGCAAGCAC-3'

PCR-amplified sequences were separated via agarose gel electrophoresis, PCR bands were isolated, and Sanger sequenced to confirm error-free and seamless integration at the *CALR* locus.

5.4.3 Immunocytochemical staining

$5x10^4$ genome engineered fluorescent reporter positive cells were spun at 600 g for 3 min onto Super Frost Plus™ glass slides (Thermo Fisher Scientific, Waltham, MA, USA) using cytology funnels. Cytospins were then air dried for 30 min and fixed with absolute methanol for 5 min. Fixed cells were permeabilized with PBS containing 0.1% Triton X-100 (Sigma Aldrich) for 5 min and washed twice with PBS containing 0.01% Tween-20 (Sigma Aldrich). Next, slides were blocked with 5% horse serum (Vector Laboratories, Burlingame, CA, USA) for 1 h at 20°C and stained with mouse anti-mutant *CALR* (CAL2, dianova, Hamburg, Germany) primary antibody at a 1:100 dilution for 1 h at 37°C in a humidified incubator. Stained slides were then washed three times with PBS (Sigma Aldrich) containing 0.01% Tween-20 and stained with ImmPRESS anti-mouse HRP secondary antibody (Vector Laboratories) for 1 hour at 37°C. After another round of washing, cells expressing *CALR* mutant protein were finally stained using a DAB HRP substrate (Vector Laboratories). To improve contrast and to better visualize individual cells, nuclei were counter-stained with DAPI (Sigma Aldrich). Stained cells were evaluated on an upright light microscope (Olympus BX51, Tokyo, Japan).

5.5 Functional characterization of genome-edited cells

5.5.1 Methylcellulose-based colony forming assay (MethoCult™)

Genome engineered fluorescent reporter positive HSPCs were sorted into StemSpan™ SFEMII media (StemCell Technologies), mixed with semi-solid methylcellulose media (MethoCult™ Enriched, StemCell Technologies) and seeded in triplicates into 35 mm culture dishes (300 cells/dish). Culture dishes and dishes filled with sterile water were placed inside 200 mm glass dishes to maintain constant and sufficient humidity throughout the whole culture period. After 14 days of incubation at 37°C, 5% CO_2, colonies were distinguished and counted based on morphologic evaluation (CFU-GM: colony-forming unit granulocyte/macrophage, CFU-M: colony-forming unit monocyte, BFU-E: burst-forming unit erythroid). Colony scoring was performed according to the manufacturer's user manual "Human CFU assays using MethoCult".

5.5.2 Collagen-based megakaryocyte colony forming assay (MegaCult™)

Genome engineered fluorescent reporter positive HSPCs were sorted into MegaCult™-C medium with lipids (StemCell Technologies) containing 10 ng/ml IL-3 and IL-6 and 50 ng/ml TPO (all Peprotech) or without TPO for TPO-independent experiments. Sorted cells were mixed with cold collagen, seeded in quadruplicates into 2-well chamber slides (1800 cells/well, Thermo Fisher Scientific) and incubated for 12 days at 37°C, 5% CO_2. To visualize megakaryocytic colonies, collagen embedded colonies were fixed on the chamber slides and stained for CD41 expression using a mouse anti-human CD41 primary antibody (Biolegend, San Diego, CA, USA) followed by an anti-mouse alkaline phosphatase (AP) secondary antibody (Vector Laboratories). Addition of the AP substrate Vector® Red (Vector Laboratories) stained $CD41^+$ megakaryocyte colonies magenta, whereas $CD41^-$ non-megakaryocytic colonies were stained blue by counter-staining with 0.2% Evans blue (Sigma Aldrich). Based on this high contrast staining, megakaryocyte colonies were quantified using an upright light microscope (Olympus BX51).

5.5.3 Megakaryocyte differentiation

Genome engineered fluorescent reporter positive HSPCs were sorted into StemSpan™ SFEMII media (Stemcell Technologies) supplemented with either 30 ng/ml or 5 ng/ml TPO together with 1 ng/ml SCF, 10 ng/ml IL-6, 10 ng/ml IL-9 (all Peprotech) and 0.4% LDL (Sigma Aldrich) and plated into 48-well plates at a density of $1x10^5$ cells/ml. To minimize additional stress, cells were already split into separate wells for each day of analysis. On day 7, half of the old culture media was replaced with fresh growth media containing the same concentration of cytokines. Cell differentiation and growth was assessed on days 4, 7, and 10, by staining the cells with CD41-APC-Cy7 and CD42b-APC (BioLegend) fluorochrome conjugated antibodies and adding counting beads (CountBright, Thermo Fisher Scientific) prior to measurement on the flow cytometer (CytoFLEX S, Beckman Coulter). Flow cytometry data was analyzed using the FlowJo software v10.8 (FlowJo LLC, Ashland, OR, USA). Based on the megakaryocyte-specific marker expression, we separated early megakaryocytic progenitors ($CD41^+$ $CD42b^-$) and mature platelet-forming megakaryocytes ($CD41^+$ $CD42b^+$).

5.5.4 Inhibitor treatments

Genome engineered fluorescent reporter positive HSPCs were sorted either into StemSpan™ SFEMII media (StemCell Technologies) and admixed with inhibitors or DMSO at the desired concentrations. For pan-myeloid differentiation, cells were then mixed with methylcellulose media (MethoCult™ Enriched, StemCell Technologies) and seeded in triplicates (300 cells each) into 6-well SmartDishes™ (StemCell Technologies). Empty spaces of SmartDishes™ were filled with sterile water and were placed with additional water filled dishes inside 200 mm glass dishes to maintain humidity throughout the 14-day culture at 37°C, 5% CO_2. CFU-GM and BFU-E colony scoring and counting was automatically performed using the STEMvision™ device (StemCell Technologies). For megakaryocytic differentiation, cells were mixed with collagen-based media (MegaCult™-C, StemCell Technologies) and seeded in quadruplicates (1800 cells each) into double chamber slides (Thermo Fisher Scientific). Chamber slides were incubated together with water filled dishes for 12 days at 37°C, 5% CO_2. Collagen-embedded CFU-Mk colonies were fixed and stained for CD41 expression via immunocytochemistry before manual counting.

Bortezomib and HA15 (both MedChemExpress, Monmouth Junction, NJ, USA) were dissolved and pre-diluted in DMSO and final concentrations in the CFU-assays were 2 nM and 5 µM respectively. Colony counts of each inhibitor treated sample were normalized to its respective DMSO treatment control and expressed as fold changes.

5.6 Mouse experiments

5.6.1 Xenotransplantation

We performed xenotransplantations of genome engineered human HSPCs into immunocompromised mice to evaluate their *in vivo* characteristics and disease initiating potential. All animal experiments performed in this study were conducted in accordance with the regulations of the Institutional Animal Care and Use Committee at Medical University of Graz, Austria and approved by the Austrian Ministry for Science (GZ: BMWFW-66.010/0018-V/3b/2018). Additionally, to minimize laboratory animal distress and suffering, current FELASA guidelines were strictly followed. NSG breeder mice were purchased from Jackson laboratories (Bar Harbor, ME, USA) whereas NSGW41 mice were a gift from Claudia Waskow (Leibniz Institute on Aging, Jena, Germany). All mice were bred in house at the Biomedical Research Facility of the Medical University of Graz and housed in individually ventilated cages under specific pathogen-free (SPF) conditions due to their compromised immune system. 24 h prior to transplantation, 8- to 12-week-old NSG mice were sub-lethally irradiated with 100 rad of x-rays (RS2000 x-ray Irradiator, Rad Source Technologies, Buford, GA, USA) to deplete the murine BM and improve engraftment of human cells.

To minimize handling-induced reduction in stemness, we transplanted a mix of unsorted fluorescent reporter positive (CRISPR-modified) and reporter negative (unmodified) HSPCs as early as 8 h after nucleofection and AAV6 transduction. $5x10^5$ cells of this mix were intrafemorally transplanted into irradiated NSG mice. To investigate a potential competitive growth advantage of *CALR* mutant cells, we sort-purified reporter positive (CRISPR-modified) human HSPCs 48 h post nucleofection and mixed *CALR* mutant and wildtype cells at a 1:1 ratio. $1x10^5$ cells of this mix were intrahepatically transplanted into 48 hour-old new-born NSGW41 mice.

To perform secondary transplantations, NSG mice were sacrificed 24 weeks after primary transplantation and all major bones (femur, tibia, humerus, ulna, radius, pelvis, spine) were collected and crushed using mortar and pestle to extract all the BM. After density gradient separation, $hCD45^+$ cells were enriched from MNCs using magnetic beads and columns (Miltenyi). 0.5-1.0x10^6 freshly enriched $hCD45^+$ cells were intrafemorally transplanted into 8- to 12-week-old sub-lethally irradiated NSG mice.

5.6.2 Human cell engraftment check

Engraftment of human cells in the murine BM was evaluated after 8 (short-term), 16, and 24 weeks (long-term) via flow cytometry. Murine BM was aspirated from the transplanted femur and excessive red blood cells were lysed with RBC lysis buffer (eBioscience, San Diego, CA, USA) for 10 min at 20°C. Remaining cells were stained with fluorochrome-conjugated antibodies for 30 min at 4°C. mTer119-BUV661, mCD45-APC-Cy7, hCD45-BB700, CD33-PE (BD Biosciences, San Jose, CA, USA), CD19-SB600 (eBioscience), CD41-PE-Cy7 (BioLegend) were used at a 1:50 dilution, while SYTOX Red (Invitrogen, Carlsbad, CA, USA) was added at a 1:1000 dilution directly before measurement to assess viability. Stained cells were acquired on a 5-laser flow cytometer (CytoFLEX LX, Beckman Coulter) and all flow cytometry data was analyzed using FlowJo v10.8 (FlowJo LLC).

5.6.3 Immunohistochemical staining

Mouse tissue embedding, sectioning and IHC staining was performed by MTAs and pathologic evaluation of the stainings was done by Prof. Dr. Christine Beham-Schmid at the Diagnostic and Research Institute of Pathology, Medical University of Graz.

At time of sacrifice, spleens and transplanted femurs were collected from NSG mice and fixed in 4% formalin for at least 48 h. Spleen size and weight were measured prior to fixation. After fixation, femurs were first decalcified, femurs and spleens were then dehydrated and embedded in paraffine. Formalin-fixed paraffine-embedded (FFPE) tissues were sectioned to 5 µm thickness using a rotary microtome (HM340E, Thermo Fisher Scientific) and fixed on Super Frost Plus™ glass slides (Thermo Fisher Scientific). Next, sections were de-paraffinized using xylene (Sigma Aldrich) and re-hydrated by decreasing ethanol (Sigma Aldrich) concentrations.

To block endogenous peroxidase activity, sections were incubated in 3% H_2O_2 (Sigma Aldrich). Unspecific binding was prevented by blocking slides with 5% horse serum (Vector Laboratories) for 1 h at 20°C. Sections were stained with primary antibodies against human CD45 (Abcam, Cambridge, UK) and mutant *CALR* (Dianova) at a 1:50 dilution for 1h at 20°C in a humidified chamber. Stained slides were then washed three times with PBS and stained with either anti-rabbit or anti-mouse HRP secondary antibodies (Abcam) at a 1:1000 dilution for 1 hour at 20°C. After another round of washing, tissues were stained using a DAB HRP substrate (Abcam). To better visualize individual cells, nuclei were counter-stained with hematoxylin. Stained tissues were imaged on an upright light microscope with attached camera (Olympus BX51, Tokyo, Japan).

5.7 Molecular characterization of genome-engineered cells

5.7.1 RNA sequencing and gene expression analysis

RNA sequencing including library preparation and parts of the data analysis was conducted at the Biomedical Sequencing Facility (BSF), Research Center for Molecular Medicine (CeMM). In-depth bioinformatical data analysis was supported by Dr. Slave Trajanoski at the Core Facility Computational Bioanalytics, Medical University of Graz.

To reveal early *CALR* mutation-induced changes in human HSPCs, we performed bulk RNA sequencing of genome engineered cells. $2x10^5$ sort purified fluorescent reporter positive (heterozygous *CALR* mutant or wildtype) UCB-derived HSPCs from three individual donors were cultured for two additional days in stem cell retention media before isolation of total RNA using the Monarch Total RNA Miniprep Kit (NEB). RNA concentration was measured by the Qubit 2.0 Fluorometric Quantitation system (Thermo Fisher Scientific) while RNA quality was assessed using the Experion Automated Electrophoresis System (Bio-Rad). When RNAs passed the first quality check, RNA-seq library preparation was performed using the TruSeq Stranded mRNA LT sample preparation kit (Illumina, San Diego, CA, USA). Library quality control (QC) was performed similar to the total RNA QC and if satisfactory, sample libraries were pooled at equimolar amounts for sequencing. Sequencing was performed on a HiSeq 3000 instrument (Illumina) with 50-base-pair, single-end sequencing. Raw sequencing data is available through NCBI's Gene Expression Omnibus (GEO) under accession number GSE195705 (https://www.ncbi.nlm.nih.gov/geo/query/acc.cgi?acc=GSE195705).

Next, NGS reads were mapped to the reference genome GRCh38 using “Spliced Transcripts Alignment to a Reference” (STAR) and the “basic” Ensembl transcript annotation version e100 (April 2020). Mapped NGS reads were counted with the Bioconductor (v3.12) GenomicAlignments (v1.26.0) package via the summarizeOverlaps function in Union mode and differential gene expression was evaluated by the Bioconductor DESeq2 (v1.30.0) package. Volcano plots and heatmaps were generated via the Bioconductor packages ggplot2 (3.3.3), EnhancedVolcano (1.8.0) and ComplexHeatmap (2.6.2).

To identify differentially regulated cellular pathways, we performed gene set enrichment analysis (GSEA) from normalized read counts calculated by the DESeq2 package (GSEA v.4.1.0, BROAD Institute, Cambridge, MA, USA). Gene sets were derived from the Molecular Signatures Database (MSigDB v7.4). Enrichment plots and the normalized enrichment score (NES) were reported for gene sets with false discovery rate (FDR) < 0.25. Furthermore, for an even more detailed analysis, significantly differentially expressed genes (DEG) with padj < 0.05 from the DESeq2 package were used for a pathway enrichment analysis using the Enrichr webtool (maayanlab.cloud/Enrichr). Enriched terms and their combined enrichment score (log p-value from Fisher exact test multiplied with the z-score of the deviation from the expected rank) were reported from the Bioplanet 2019 and Reactome 2016 gene set databases. Finally, the top 10 common DEGs from DEL vs. WT and INS vs. WT expression analyses were used for a STRING protein interaction network analysis (STRING v11.5, Elixir, Hinxton, Cambridgeshire, UK). We generated an interaction plot considering only interactions with high evidence (interaction score > 0.7) and max. 10 interaction partners per protein. The clustering of proteins was performed using the MCL method with an inflation parameter of 3.

5.7.2 RT-qPCR

To confirm the differential expression of genes identified in the RNA-seq experiments, total RNA from UCB-derived HSPC of three independent donors, engineered to harbor wildtype or mutant *CALR* sequences, was extracted using the Monarch Total RNA Miniprep Kit (NEB) according to the manufacturer’s protocol. Total RNA was reverse transcribed into cDNA using the LunaScript® RT SuperMix Kit (NEB). Gene expression was quantified via qPCR using a dye-based Luna® Universal qPCR Master Mix (NEB) on a QuantStudio™ 5 Real-Time PCR system (Applied Biosystems) using the primers listed in the table below.

All genes were measured in technical duplicates and *HPRT1*, *GUSB*, and *GAPDH* were used as housekeeping genes (HKG). Gene expression in *CALR* mutant samples was normalized to the average of all three HKGs and to wildtype samples via the ΔΔCT method, resulting in mean fold changes.

Table 1: RT-qPCR primer list

Gene	**Primer sequence 5' – 3'**
PRKCZ	Fwd: CAACTGCAAACTGCTGGTCC Rev: AGGCATGACAGAATCCATATGCT
CRELD2	Fwd: CAAGTACGAGTCCAGCGAGAT Rev: TGGAGAGCAGCACACTTTCA
MANF	Fwd: GTCACATTCTCACCAGCCACT Rev: GGCCCCGATATAGTAGCACAAC
HSPA5	Fwd: CATCAACGAGCCTACGGCA Rev: AGACACATCGAAGGTTCCGC
PDIA3	Fwd: CACGGACGACAACTTCGAGA Rev: TGGCAGTGCAATCAACCTTTG
PDIA4	Fwd: CTCCAGAACCCAGGAAGAAATTG Rev: TTCTCATACTCGGGGGCAAG
HSP90B1	Fwd: CCAGCAGAAAAGAGGCTGAAT Rev: ATTCGGGAAGGGCCTGAATAC
DNAJB11	Fwd: GGTGCTGCTTATGAGGTTCTGT Rev: GTCTTGCTGACGAGGGGTTC
HYOU1	Fwd: AACCTGAGAAAGTAGAGACTGGA Rev: CTTTCTGTTCAGGTTCTGCTCC
SDF2L1	Fwd: TGTCCAACAACCAGGAGGTGAG Rev: AGCAGCGCACTGTCCATAG
CALR	Fwd: GATCCCACAGACTCCAAGCC Rev: GGCTTCCACTCACCCTTGTA
HPRT1	Fwd: TGAGGATTTGGAAAGGGTGT Rev: GAGCACACAGAGGGCTACAA
GUSB	Fwd: GAAAATATGTGGTTGGAGAGCTCATT Rev: CCGAGTGAAGATCCCCTTTTTA
GAPDH	Fwd: GTCTCCTCTGACTTCAACAGCG Rev: ACCACCCTGTTGCTGTAGCCAA

5.7.3 Western Blot

$3x10^6$ TF-1_TpoR cells were directly lysed in 300 µl Laemmli buffer (Bio-Rad, Hercules, CA, USA) containing 10% β-mercaptoethanol by sonication for 3-5 min at 20°C. Fully lysed samples were boiled at 95°C for 5 min before loading of protein lysate onto 4-20% polyacrylamide gels (Mini-PROTEAN® TGX™, Bio-Rad) for electrophoresis. Size-separated proteins were then transferred onto PVDF membranes (Bio-Rad) via a semi-dry transfer (Trans-Blot® Turbo™, Bio-Rad). Membranes were blocked with 5% BSA (Pan-Biotech, Aidenbach, Germany) prior to antibody incubation to reduce background staining. All primary antibodies were used at 1:1000 dilutions in 5% BSA and incubated over-night at 4°C. Primary antibodies against CALR (#12238), β -Actin (#4970), p-STAT1 (#9167), p-STAT3 (#9145), p-AKT (#4060), p-ERK1/2 (#4370), STAT1 (#9172), STAT3 (#4904), STAT5 (#94205), AKT (#4691), and ERK1/2 (#9102) were purchased from Cell Signaling Technology (Danvers, MA, USA), against p-STAT5 (#611965) was purchased from BD Biosciences, and against Vinculin (#ab129002) from Abcam (Cambridge, UK). Secondary HRP-linked antibodies against rabbit (#7074) and mouse (#7076, Cell Signaling Technology) were used at 1:5000 dilutions in 5% BSA and incubated for 1h at 20°C. Antibody-labelled proteins were detected using ECL substrates (Bio-Rad) on a ChemiDoc imaging system (Bio-Rad).

5.8 Statistical analyses

All statistical analyses were performed using PRISM 9 (Graphpad Software, San Diego, CA, USA). Statistical significance of *in vitro* experiments was evaluated by either one-way ANOVA with Dunnett's multiple comparison correction (bar graphs) or two-way ANOVA with Dunnett's multiple comparison correction (line graphs). Results of *in vivo* studies were tested for statistical significance using an un-paired student's t-test (two-sided) with Welch's correction for end point analyses or two-way ANOVA with Sidak's multiple comparison correction for repeated comparisons of subsequent time points. All data was checked for normal distribution prior to statistical testing. If similarity of variances between groups was not given, Geisser-Greenhouse correction was used. Experimental results with p-values < 0.05 were considered statistically significant. The degree of significance was reported using asterisks (* $p < 0.05$, ** $p < 0.01$, *** $p < 0.001$). All graphs depicted here show the mean ± standard error of mean (SEM) of independent biological replicates. Bar graphs additionally show individual values of biological replicates.

6. Results

The following results from genome engineering *CALR* mutations in human CD34$^+$ HSPCs and their characterization *in vitro* and *in vivo* have been published in:

Foßelteder et al. Human gene-engineered calreticulin mutant stem cells recapitulate MPN hallmarks and identify targetable vulnerabilities. Leukemia 2023.

See Appendix

6.1 Development and proof of a site-specific genomic knock-in strategy for *CALR* mutations.

In order to improve current *CALR* mutant MPN models, we first aimed to introduce the two most common *CALR* mutations into the endogenous gene locus of primary human HSPCs and thereby conserve the cell intrinsic regulation of gene expression to mimic the natural acquisition of mutations as close as possible. To this end, we decided to use the powerful CRISPR/Cas9 gene editing tool. Specifically, we aimed to target intron 7 of the *CALR* gene, which lies upstream of the mutational hotspots in exon 9 and introduce a cDNA comprising exons 8 and 9 with either wildtype or mutant sequences. Thus, we designed three gRNAs targeting intron 7, cloned them into a gRNA and Cas9 expressing plasmid vector (pX458) and nucleofected these vectors into the CML-derived cell line K562, which was used to initially test all our genome editing reagents (**Figure 4A**).

Genome editing analysis via the ICE analysis webtool (Synthego) from sequenced DNA 48 hours post nucleofection showed highest DNA cutting efficiency for gRNA 1 (**Figure 4B**). Based on that, gRNA1 was used for all further experiments and enabled the design of vectors to deliver the donor DNA for genomic integration of *CALR* mutations. AAV6 has been shown to efficiently transduce hematopoietic stem cells (226) and has enough packaging capacity (~4.7 kb) to cover all necessary sequences. Thus, our donor DNA vector was based on an AAV vector backbone (pAAV-MCS) and included a codon-optimized *CALR* cDNA comprising exons 8 and 9 with either wildtype, type 1, or type 2 mutant sequences (**Figure 4C**). The cDNA was preceded by a splice acceptor to ensure proper splicing of the introduced exons 8 and 9 to the endogenous exons 1-7, generating a full length *CALR* transcript.

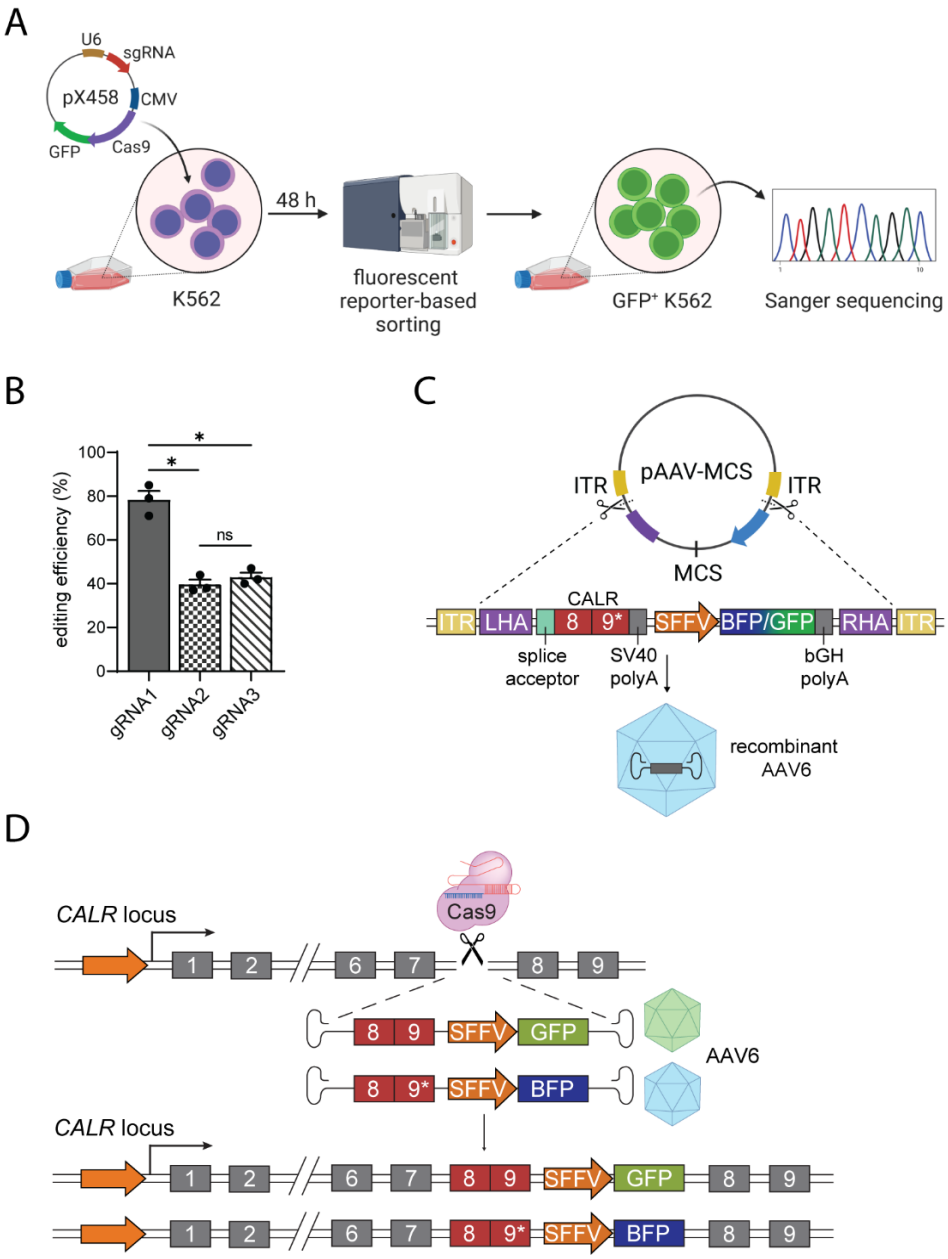

Figure 4. gRNA selection and AAV donor DNA design.

(A) Workflow for testing the editing efficiency of gRNAs in K562 cells. **(B)** Bar graph showing editing efficiency of three pre-selected gRNAs. **(C)** DNA donor vector design for AAV6-mediated transfer. ITR sequences represent inverted tandem repeats at both ends of the AAV genome. LHA and RHA are left and right homology arms respectively and are matching the double-strand break ends in the *CALR* locus. The red blocks indicate codon optimized *CALR* cDNA comprising exons 8 and 9. Asterisks mark mutation bearing exon 9. SFFV is a constitutively active spleen focus-forming virus promoter driving the expression of green and blue fluorescent proteins GFP, BFP). **(D)** Scheme showing the biallelic knock-in of *CALR* wildtype and mutant cDNA (exons 8 and 9) coupled with distinct fluorescent reporter proteins (GFP/BFP).

Although, genome editing efficiencies improved constantly in recent years, knock-in of longer DNA stretches via HDR has remained challenging, resulting in overall low number of cells with correct insertion. To overcome this issue, we decided to adopt a recently published approach to co-integrate fluorescent reporter genes, allowing flow cytometry-based enrichment and tracking of correctly edited cells (223). Therefore, the *CALR* cDNA in our vector was followed by a SFFV promoter driving constitutive expression of a fluorescent reporter protein (either GFP, BFP, or mCherry). Additionally, mutant and wildtype *CALR* sequences were linked to a unique fluorescent protein allowing to distinguish mutational status via flow cytometry. This donor DNA cassette was flanked by homology arms allowing HDR-mediated integration into the DSB site generated by Cas9 (**Figure 4D**).

Co-delivery of CRISPR reagents (Cas9 and sgRNA) and AAV6 into K562 cells **(Figure 5A)** revealed successful integration and generation of a mixed population with different editing outcomes i) no integration of any donor DNA but most likely introduction of INDELs by Cas9 (**Figure 5B, lower left gate**), ii) integration of a single donor DNA (mono-allelic) (**Figure 5B, upper left and lower right gates**), and iii) integration of both donor DNAs (bi-allelic) (**Figure 5B, upper right gate**). Flow cytometry-based sorting of cells allowed purification of all reporter positive cell populations. (**Figure 5C**). Bi-allelic integration of mutant or wildtype cDNAs coupled to distinct fluorescent reporters allows for the unambiguous generation of homozygous or heterozygous genotypes and these data suggest that this knock-in strategy is feasible to use in primary human HSPCs.

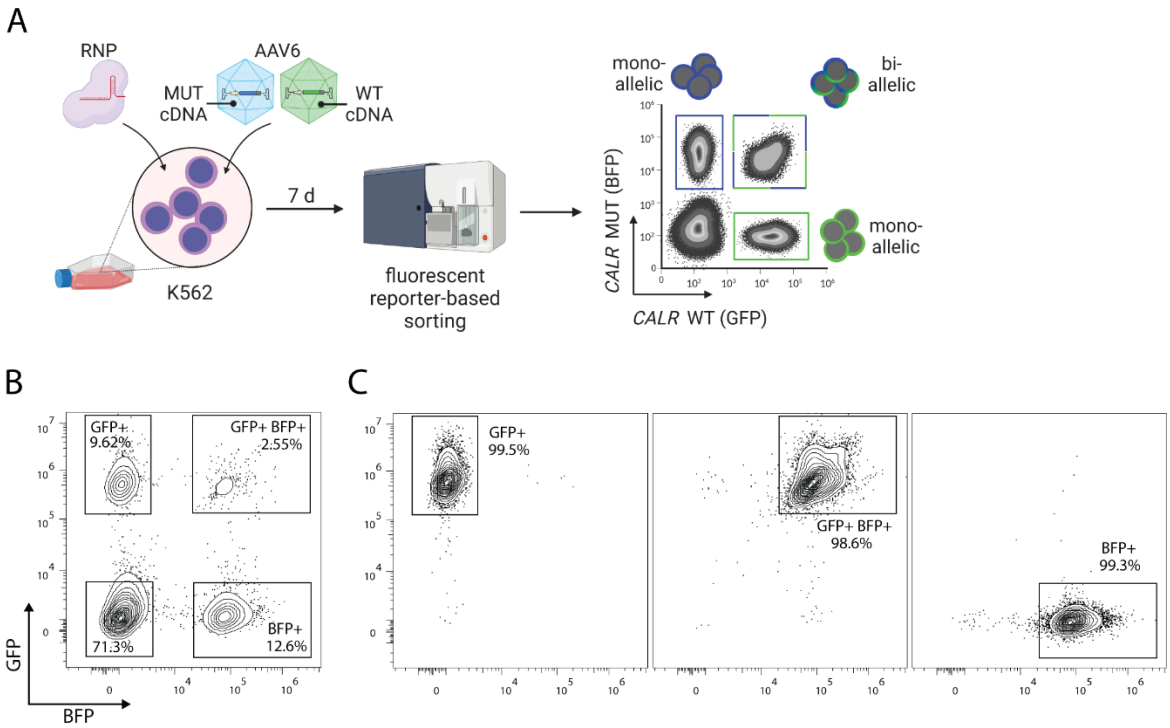

Figure 5. Introduction of *CALR* mutations and purification of successfully modified reporter positive cells via FACS.

(A) Workflow for CRISPR/Cas9 and AAV6-mediated knock-in of *CALR* mutations in K562 cells with subsequent purification of successfully modified cell populations. **(B)** FACS plot depicting a mixture of cell populations and their respective proportions 7 days after genetic modification. **(C)** FACS plots showing sort-purified and reporter positive cell populations.

6.2 Generation of *CALR* mutant primary human HSPCs.

Since our knock-in strategy proved to be successful in K562 cells, we applied this strategy to generate *CALR* mutant $CD34^+$ HSPCs derived from human UCB (**Figure 6A**). In case of a single AAV transduction and mono-allelic integration, we achieved 25-38% on-target integration (**Figure 6B**). Whereas dual transduction and bi-allelic integration resulted in 2.5-4.5% of HSPCs with a successful knock-in (**Figure 6C**). Mono-allelic integration of *CALR* mutant cDNA is sufficient to generate a heterozygous genotype, as the coding sequence of the second endogenous wildtype allele is not disturbed by our intron-targeting approach. Mono-allelic integration is therefore preferred for downstream experiments with a need for high numbers of primary cells.

To ensure, the knock-in was site-specific and error-free, we performed sequencing of the *CALR* gene locus and mRNA. We detected seamless and sequence specific integration at the desired gene locus and correct splicing of the introduced cDNA to the endogenous upstream exons (**Figure 7A-B**). Additionally, mRNA sequencing confirmed the heterozygous genotype as both wildtype and mutant transcripts were detected simultaneously. Finally, to fully prove the successful generation of *CALR* mutant HSPCs, we performed immunocytochemistry (ICC) on engineered HSPCs using a mutation-specific antibody targeting the novel c-terminal domain. Engineered *CALR* mutant HSPCs showed mainly ER located expression of mutant protein, while it was absent in wildtype controls (**Figure 8A**) and size differences of DEL and INS mutant proteins further confirmed mutation type-specific expression (**Figure 8B**). Furthermore, undisturbed regulation of gene expression was confirmed via immunoblotting of total *CALR* protein. Our genetic modification did not alter *CALR* gene expression (**Figure 8C**).

In summary, these data show that our CRISPR/Cas9 and AAV6-based knock-in strategy can reliably generate heterozygous *CALR* mutant primary human HSPCs which provide a useful tool for further functional and mechanistic studies.

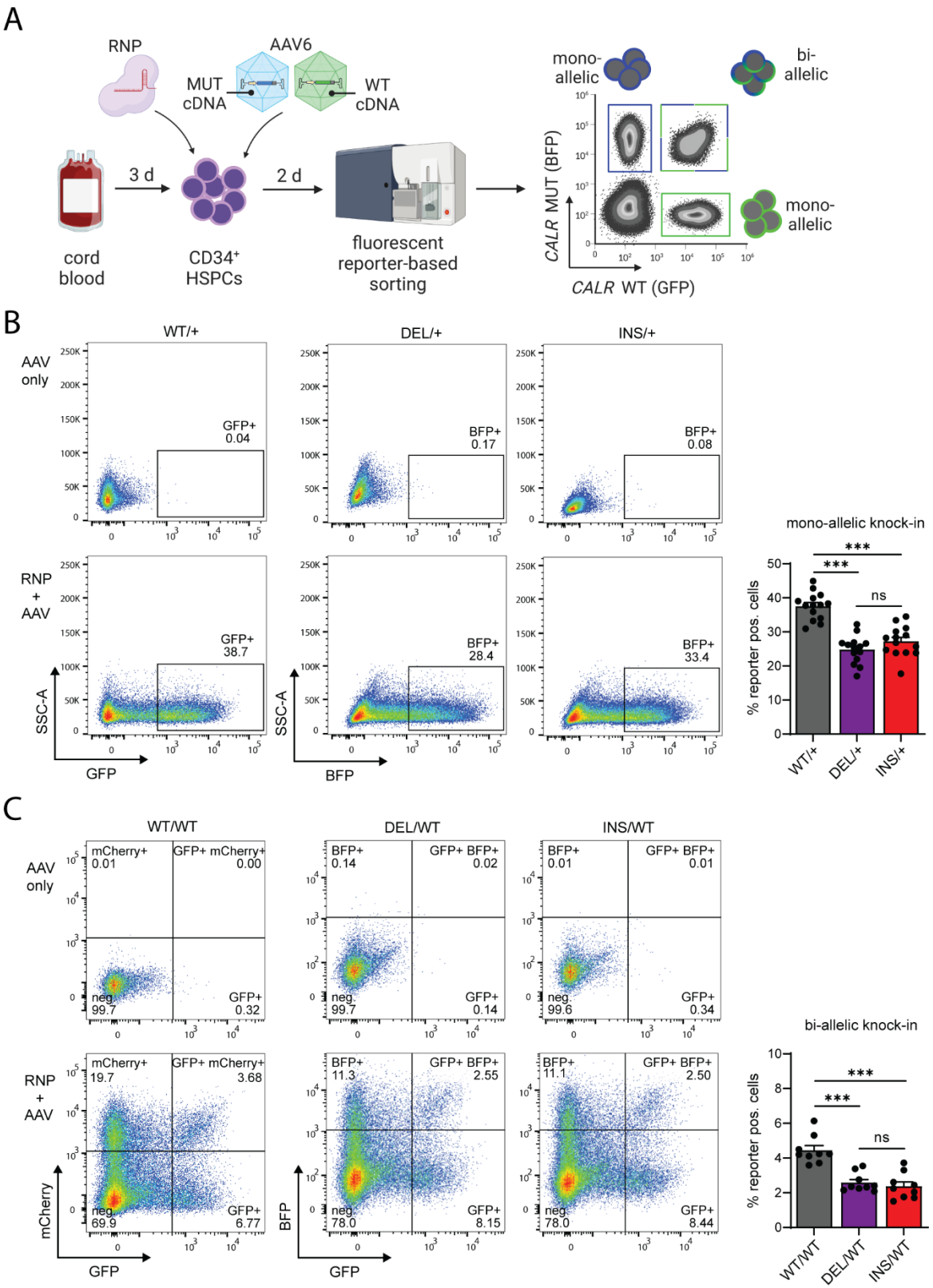
A
RNP
AAV6
MUT cDNA
WT cDNA
3 d
2 d
cord blood
CD34+ HSPCs
fluorescent reporter-based sorting
mono-allelic
bi-allelic
mono-allelic
CALR MUT (BFP)
CALR WT (GFP)
B
WT/+
DEL/+
INS/+
AAV only
RNP + AAV
GFP+ 0.04
BFP+ 0.17
BFP+ 0.08
GFP+ 38.7
BFP+ 28.4
BFP+ 33.4
SSC-A
GFP
BFP
mono-allelic knock-in
% reporter pos. cells
***
***
ns
WT/+
DEL/+
INS/+
C
WT/WT
DEL/WT
INS/WT
AAV only
RNP + AAV
mCherry+ 0.01
GFP+ mCherry+ 0.00
neg. 99.7
GFP+ 0.32
BFP+ 0.14
GFP+ BFP+ 0.02
neg. 99.7
GFP+ 0.14
BFP+ 0.01
GFP+ BFP+ 0.01
neg. 99.6
GFP+ 0.34
mCherry+ 19.7
GFP+ mCherry+ 3.68
neg. 69.9
GFP+ 6.77
BFP+ 11.3
GFP+ BFP+ 2.55
neg. 78.0
GFP+ 8.15
BFP+ 11.1
GFP+ BFP+ 2.50
neg. 78.0
GFP+ 8.44
mCherry
GFP
BFP
bi-allelic knock-in
% reporter pos. cells
***
***
ns
WT/WT
DEL/WT
INS/WT

Figure 6. Mono- and bi-allelic integration of *CALR* mutations in UCB-derived CD34$^+$ HSPCs. **(A)** Workflow for CRISPR/Cas9 RNP and AAV6-mediated knock-in of *CALR* mutations in UCB-derived HSPCs and the subsequent purification of successfully modified reporter positive cells. **(B-C)** FACS plots from one representative experiment showing the fluorescent reporter expression after mono- (B) or bi-allelic (C) knock-in of *CALR* cDNA. AAV only transductions were performed to determine the background reporter expression without genomic integration for setting the sorting gates. Bar graphs report editing efficiencies of 14 (mono-allelic) and 9 (bi-allelic) independent biologic replicates. Reproduced with modifications from (1) with permission via the CC BY license (https://creativecommons.org/licenses/by/4.0/).

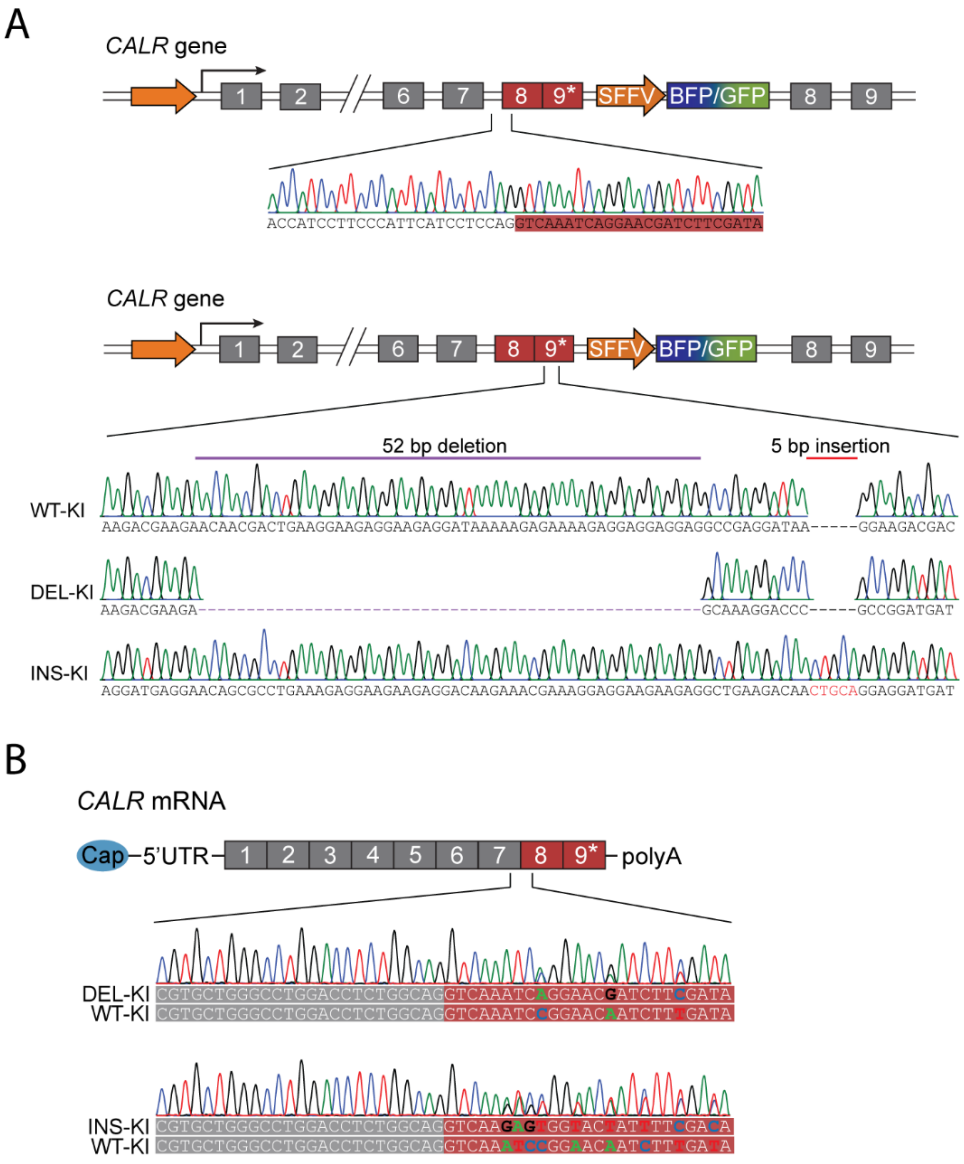

Figure 7. Confirmation of site-specific integration of *CALR* mutations.

(A) Sanger sequencing of the 5' integration site (top) confirms seamless integration and identifies wildtype or mutant sequences in *CALR* exon 9 (bottom). **(B)** Confirmation of correct splicing of endogenous exons to the integrated cDNA via sequencing of reverse transcribed mRNA. Sequences reveal heterozygous expression of mutant and wildtype transcripts as indicated by double base calls at several positions. Reproduced with modifications from (1) with permission via the CC BY license (https://creativecommons.org/licenses/by/4.0/).

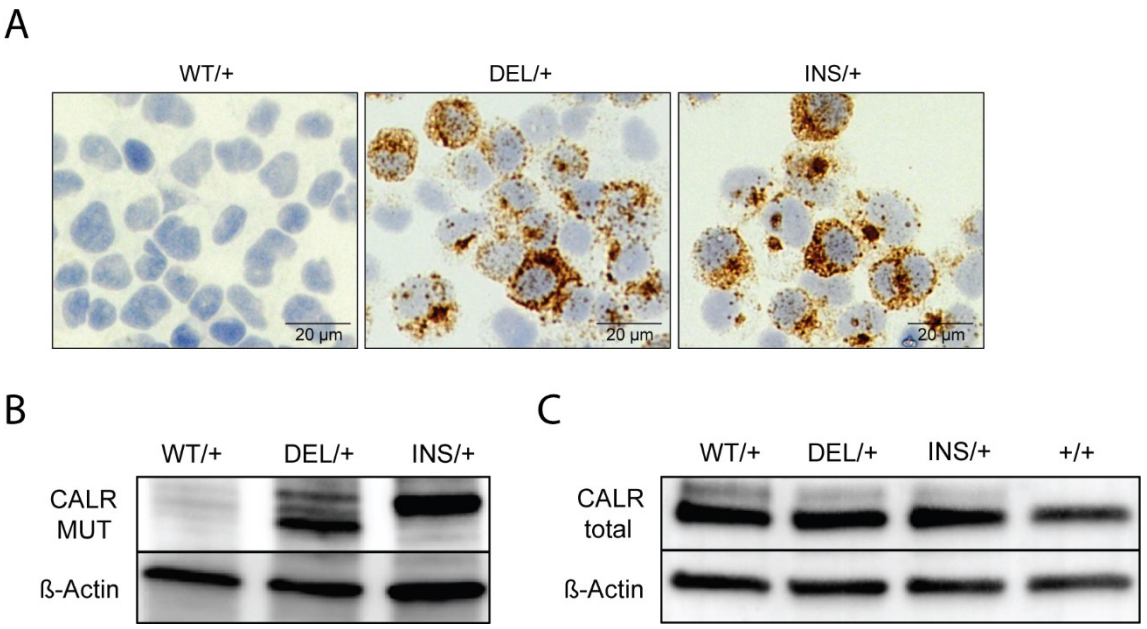

Figure 8. Confirmation of mutant *CALR* expression.

(A-B) Expression of mutant *CALR* protein in engineered HSPCs detected via immunocytochemistry (A) and immunoblotting (B) using a mutation-specific antibody (CAL2, Dianova). **(C)** Total *CALR* protein expression is unchanged between engineered wildtype (WT/+), engineered mutant (DEL/+, INS/+) and unmodified (+/+) genotypes as analyzed by immunoblotting. Reproduced with modifications from (1) with permission via the CC BY license (https://creativecommons.org/licenses/by/4.0/).

6.3 *CALR* mutant HSPCs exhibit TPO-independent growth and megakaryocytic differentiation.

To confirm the activity of mutant *CALR* protein in our engineered cells, we tested if *CALR* mutant cells show TPO-independent growth promoted by *MPL*-mediated intracellular signaling. To this end, we introduced *CALR* mutations or wildtype control into *MPL* expressing TF-1 cells (TF-1_TpoR). Indeed, *CALR* mutant cells proliferated in absence of TPO, which was mediated by activated *MPL* signaling as seen by phosphorylation of downstream signaling mediators STAT1/3/5, AKT and ERK1/2 (**Figure 9A-B**).

To characterize *CALR* mutant HSPCs in a prospective manner and to elucidate phenotypic changes induced upon mutation acquisition that potentially contribute to disease initiation, we performed several cellular assays. It is known from *CALR* mutant MPN patients, that HSPCs alter their differentiation towards the myeloid lineage and specifically towards megakaryocytes (227). Thus, we started with a methylcellulose-based colony-forming unit (CFU) assay (228) to assess the multilineage differentiation properties of *CALR* mutant HSPCs. Type 1 and type 2 mutant HSPCs showed a 1.5-fold increase in erythroid colonies (BFU-E) and a concomitant decrease in myeloid colonies (CFU-GM), suggesting *CALR* mutant HSPCs shift their differentiation towards the megakaryocyte-erythroid lineage upon mutation acquisition (**Figure 9C**). Correct integration of *CALR* mutations was confirmed via ‘in-out’ PCR in individual single cell-derived colonies (**Figure 9D**).

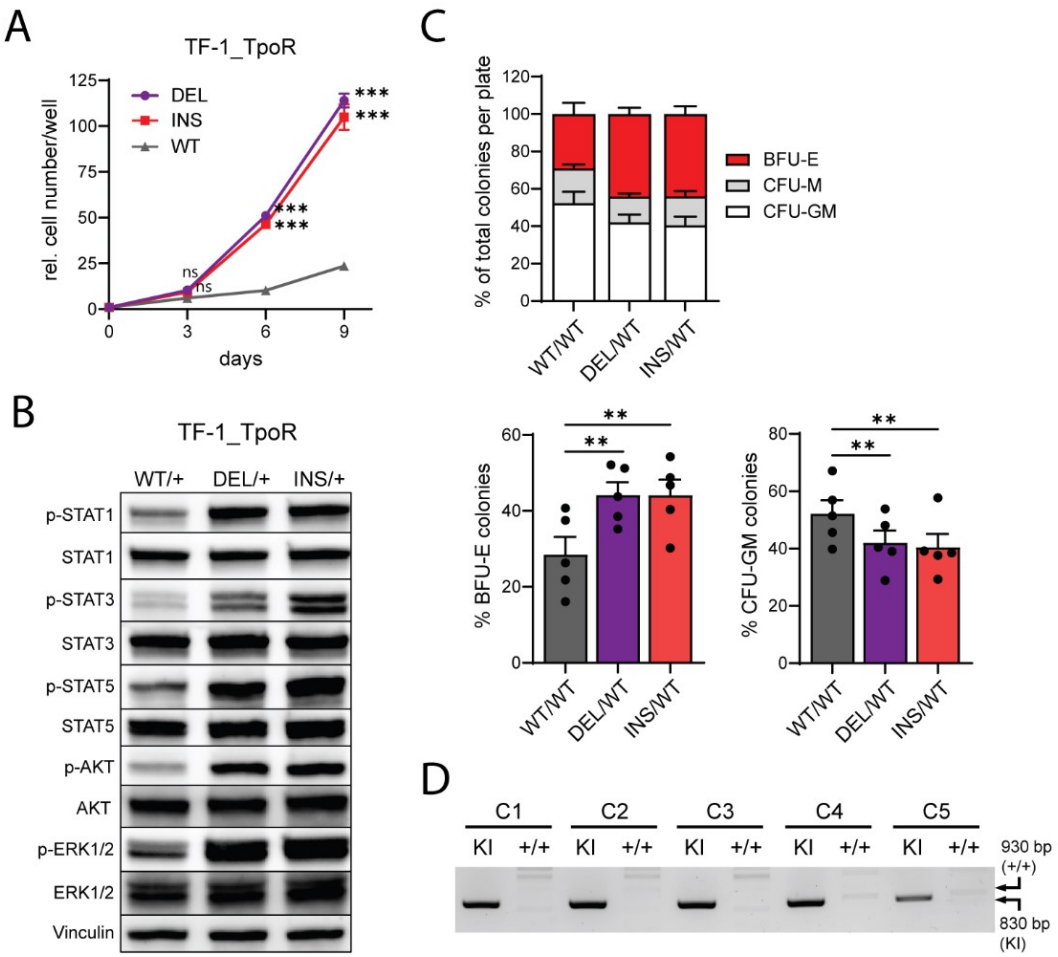

Figure 9. *CALR* mutations induce TPO-independent growth via activation of TpoR signaling pathways.

(A) TPO-independent growth of *CALR* mutant TF-1_TpoR cells *in vitro*. **(B)** Detection of increased TpoR downstream signaling of mutant cells via phospho-specific Western Blot. **(C)** Multi-lineage differentiation of *CALR* mutant HSPCs was assessed in methylcellulose-based CFU assays. Total colony distribution (top) and percentages of BFU-E and CFU-GM colonies (bottom) are shown in bar graphs (n=5). **(D)** 'In-out' PCR of five randomly picked colonies (C1-5) from methylcellulose-based CFU assays to confirm successful knock-in of *CALR* mutations. Bands in KI lanes show integration of *CALR* cDNA while the absence of bands in +/+ lanes indicates all alleles have been targeted. Reproduced with modifications from (1) with permission via the CC BY license (https://creativecommons.org/licenses/by/4.0/).

To investigate megakaryocytic differentiation in more detail and since methylcellulose-based CFU assays do not foster megakaryocyte growth, we performed a collagen-based megakaryocyte-specific CFU assay (229). Under standard conditions using near-saturating concentrations of TPO (50 ng/ml), *CALR* mutant HSPCs showed only a modest increase in megakaryocyte colonies (**Figure 10A, left**). However, when cells were plated in absence of TPO, *CALR* mutant HSPCs formed 2-fold more megakaryocyte colonies compared to wildtype controls (**Figure 10A, right**), confirming TPO-independent differentiation and growth solely induced by *CALR* mutations.

These results were underlined by data from a liquid culture megakaryocytic differentiation. Culture with 30 ng/ml TPO resulted in increased growth only for *CALR* INS cells (**Figure 10B, left**), while megakaryocytic differentiation was very efficient but unchanged between genotypes, with > 90% of cells expressing CD41 and CD42b megakaryocyte cell surface markers (**Figure 10C, top**). However, when TPO was reduced to 5 ng/ml, *CALR* mutant cells showed clearly better survival and differentiation. While wildtype cells could barely survive under these conditions, mutant cells turned TPO-independent and outgrew after an initial drop in viability within the first four days (**Figure 10B, right**). The majority (> 80%) of *CALR* mutant cells formed mature megakaryocytes expressing CD41 and CD42b cell surface markers, while only half of the wildtype cells showed this phenotype (**Figure 10C, bottom**).

In presence of high TPO levels, cells of each genotype formed large megakaryocytes (> 40 µm) which presented multilobulated nuclei (**Figure 11A, top**), whereas at low TPO concentrations, only *CALR* mutant cells were capable of forming cells with megakaryocyte phenotypes (**Figure 11A, bottom**). The functionality of these megakaryocytes was underlined by the formation of cellular protrusions that would eventually shed platelets in the surrounding media (**Figure 11B**). These data underline that acquisition of *CALR* mutations can solely transform healthy HSPCs and that mutant *CALR* mainly drives the TPO-independent growth and megakaryocyte biased differentiation.

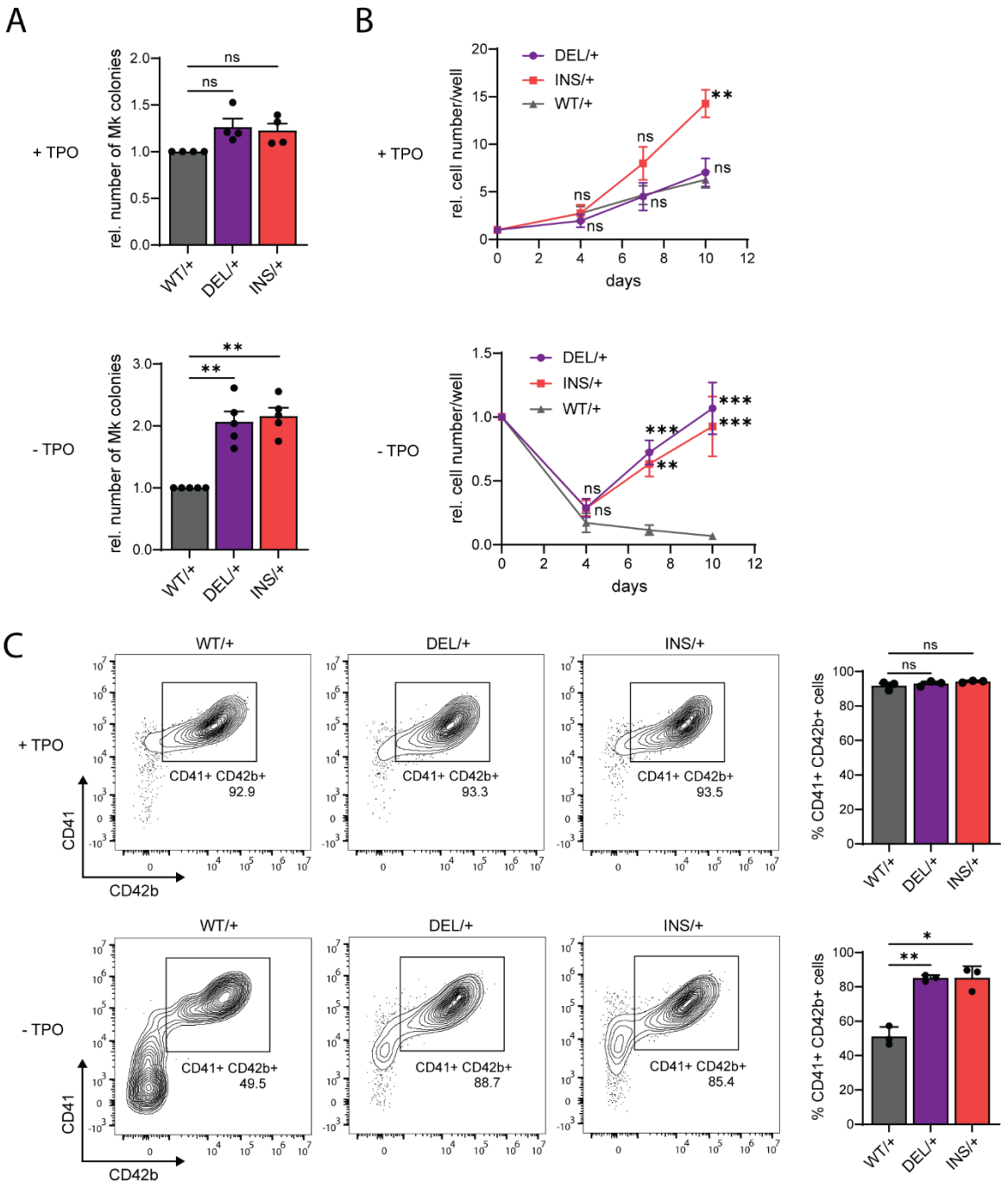

Figure 10. *CALR* mutant HSPCs show TPO-independent megakaryocytic differentiation. (A) Megakaryocyte-directed differentiation of engineered HSPCs in a collagen-based colony-forming assay in presence (left) and absence (right) of TPO (n=5). **(B)** Megakaryocytic liquid culture differentiation with 30 ng/ml (left) and 5 ng/ml (right) of TPO (n=3). **(C)** Flow cytometric assessment of liquid culture differentiation via CD41 and CD42 cell surface marker expression at 30 ng/ml (top) and 5 ng/ml (bottom) TPO. Reproduced with modifications from (1) with permission via the CC BY license (https://creativecommons.org/licenses/by/4.0/).

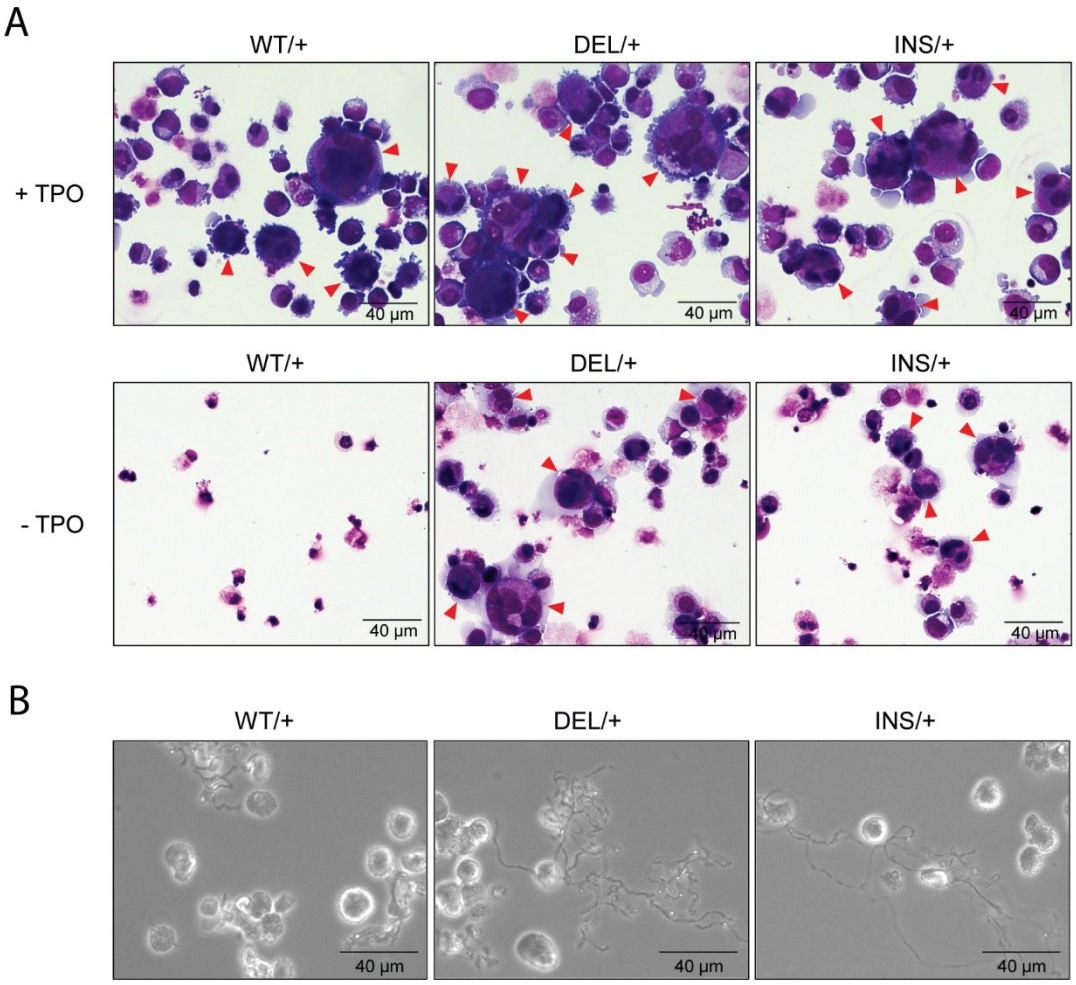

Figure 11. *CALR* mutant HSPCs form platelet shedding megakaryocytes.

(A) Micrographs of Pappenheim stained cells after 10 days of liquid culture differentiation. Red arrows indicate megakaryocytes with large multilobulated nuclei. **(B)** Micrographs from megakaryocyte liquid cultures showing the formation of cellular protrusions indicative of platelet shedding. Reproduced with modifications from (1) with permission via the CC BY license (https://creativecommons.org/licenses/by/4.0/).

6.4 Genome-engineered *CALR* mutant human HSPCs robustly engraft in NSG mice and exhibit a growth advantage *in vivo*.

Current pre-clinical *in vivo* MPN models are mostly murine only and lack a meaningful human cellular context. Therefore, we sought to investigate the potential of our genome engineered *CALR* mutant HSPCs to engraft in the murine BM and their ability to initiate MPN-like phenotypes in those mice. For this purpose, we used immunocompromised NSG mice, which were shown to support human HSPC engraftment (230) and engineered wildtype *and CALR* type 2 (INS) mutant human HSPCs via single AAV6 transduction (mono-allelic knock-in) to maximize the number of correctly modified cells for xenotransplantation.

Genome editing efficiencies of human HSPCs prior to transplantation were 40% and 26% for wildtype and INS cells respectively (**Figure 12B**). We transplanted an unpurified mixed population of CRISPR-modified and unmodified human HSPCs from three independent UCB donors intrafemorally into sub-lethally irradiated NSG mice (at least 2 mice per donor and genotype) (**Figure 12A**). Transplantation shortly after genetic modification and without additional stress induced by flow cytometric cell sort should preserve stemness and engraftment potential of HSPCs.

Constitutive expression of fluorescent reporter proteins allowed specific tracking of CRISPR-modified cells at any time without the need of prior purification (**Figure 12C**). Human cell engraftment was evaluated via flow cytometric analysis of aspirated murine BM after 8, 16 and 24 weeks. Mice transplanted with *CALR* INS HSPCs showed significantly higher human engraftment ($hCD45^+$ cells in murine BM) at the initial time of analysis (8 weeks) and persisted throughout the experiment (**Figure 12E**). Importantly, *CALR* INS cells outcompeted their unmodified counterparts between 8 and 16 weeks as seen by a 2-fold increase in BFP^+ cells within the engrafted $hCD45^+$ cells (**Figure 12F**). *CALR* wildtype cells, however showed no competitive growth advantage and were outperformed by the co-transplanted unmodified cells as seen by the decrease in GFP^+ cells.

To confirm that mutant *CALR* is expressed in engrafted genome engineered human cells and could therefore drive their pathogenic phenotype, we performed ICC on hCD45^{+} BFP^{+} and hCD45^{+} GFP^{+} cells aspirated and sort-purified from murine BM. Indeed, only *CALR* INS mutant BFP^{+} cells showed expression of mutant *CALR* protein as expected (**Figure 12D**).

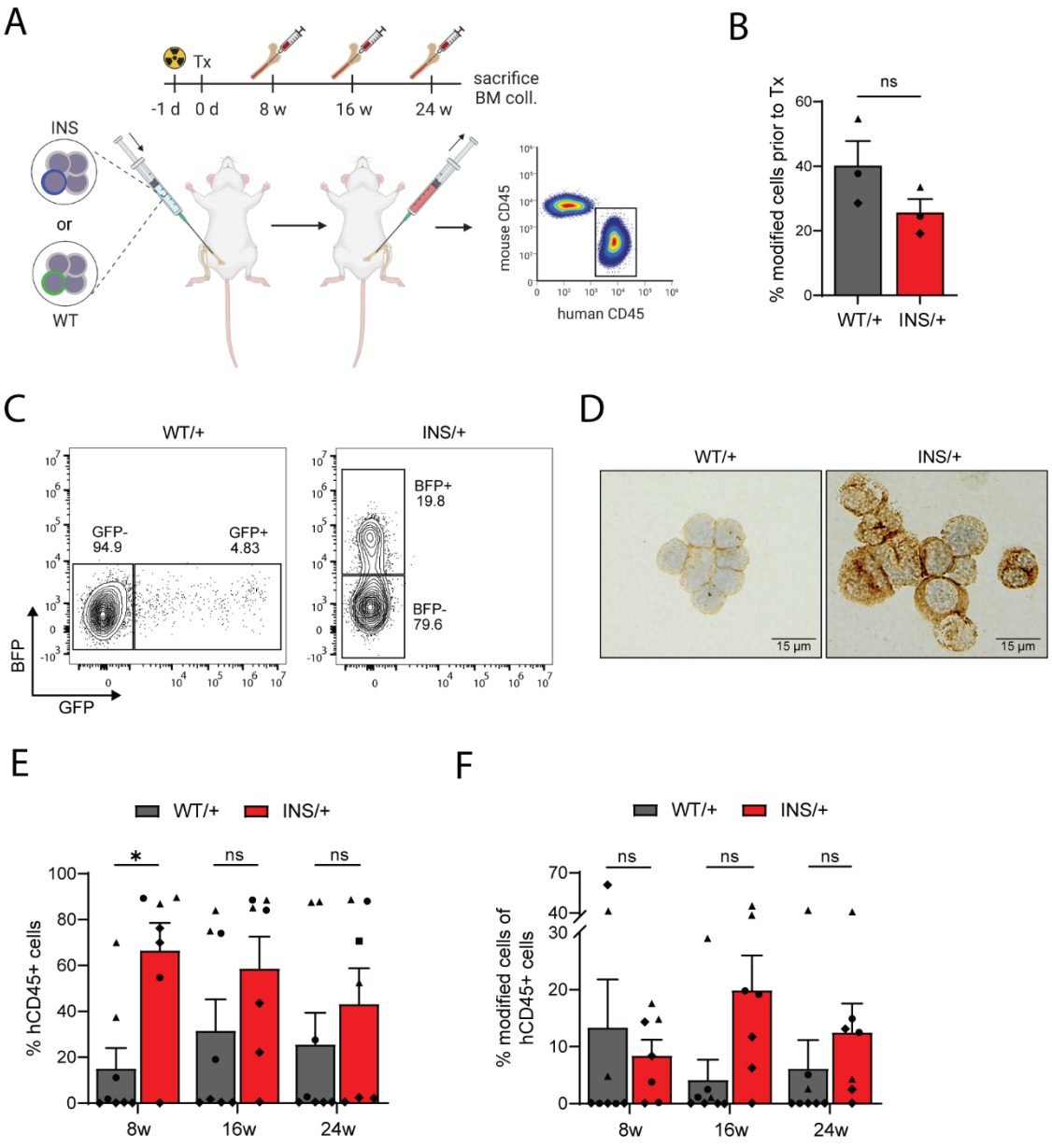

Figure 12. Engraftment of human *CALR* mutant HSPCs in xenotransplanted NSG mice. (A) Schematic overview of xenotransplantation experiments. *CALR* wildtype or INS genome engineered but unsorted human HSPCs were intrafemorally transplanted into sub-lethally irradiated NSG mice. Human engraftment was evaluated from consecutive BM aspirations via flow cytometry before mice were sacrificed after 24 weeks. **(B)** Percentage of correctly modified human HSPCs via mono-allelic knock-in prior to transplantation (n=3). **(C)** Representative FACS plots depicting the tracking of fluorescent reporter positive human cells in the murine BM. **(D)** Confirmation of mutant *CALR* protein expression in xenografted hCD45$^+$ cells via immunocytochemistry. **(E)** Total human engraftment (% hCD45$^+$ cells) in the murine BM was assessed after 8, 16 and 24 weeks (n=7 mice from 3 independent UCB donors). **(F)** Percentage of reporter positive modified *CALR* wildtype or INS cells within hCD45$^+$ cells. Symbols (●, ▲, ♦) in bar graphs depict individual donors. Reproduced with modifications from (1) with permission via the CC BY license (https://creativecommons.org/licenses/by/4.0/).

We could confirm the *in vivo* competitive growth advantage of *CALR* mutant cells in a second xenotransplantation model, which allowed direct comparison of CRISPR-modified cells. Therefore, we transplanted 1:1 mixed sort-purified fluorescent reporter positive *CALR* wildtype (GFP$^+$) and INS mutant (BFP$^+$) HSPCs intrahepatically into newborn NSGW41 mice (**Figure 13A**). These mice harbor a loss-of-function *Kit* mutation that opens the HSC niche in the murine BM for engraftment of human HSPCs without the need of pre-conditioning via irradiation (142). Engrafted *CALR* INS cells clearly outgrew wildtype cells by more than 3-fold at 16 weeks post-transplant (**Figure 13B-C**).

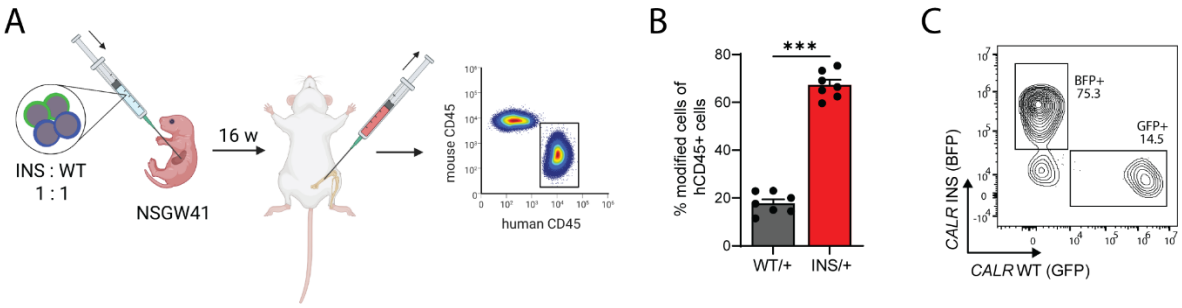

Figure 13. *CALR* mutant cells outgrow wildtype cells in a competitive *in vivo* setting.
(A) Competitive xenotransplantation of engineered and sort-purified *CALR* wildtype and INS HSPCs into the liver of new-born NSGW41 mice (n=7). **(B)** Engraftment of human genome engineered cells (% modified cells within hCD45$^+$ cells) in the murine BM was evaluated after 16 weeks via flow cytometry. **(C)** FACS plot showing the distribution of engrafted *CALR* wildtype and INS cells of one representative mouse. Reproduced with modifications from (1) with permission via the CC BY license (https://creativecommons.org/licenses/by/4.0/).

6.5 *CALR* mutant human HSPCs show increased megakaryopoiesis and initiate MPN-like phenotypes *in vivo*.

CALR INS mutant cells engrafted in NSG mice showed increased myeloid lineage skewing as seen by an increased ratio of myeloid (CD33$^+$) to lymphoid (CD19$^+$) cells (**Figure 14A**). Furthermore, we found significantly more CD41$^+$ megakaryocyte progenitors in *CALR* INS transplanted mice (**Figure 14B**), resembling the megakaryocyte-biased differentiation we observed *in vitro*. At time of sacrificing (24 weeks post-transplant) *CALR* INS transplanted mice presented with increased spleen size and weight (**Figure 14C**), a clinical hallmark often seen in MPN patients. Immunohistochemical (IHC) analysis of the mouse spleens revealed that human cell engraftment was not restricted to the BM but extended also into secondary hematopoietic organs (**Figure 15**). Strikingly, two out of six (2/6) mice receiving *CALR* INS HSPCs showed extreme splenomegaly, which was not seen in any (0/5) of wildtype transplanted mice (**Figure 14C**). This splenomegaly was accompanied by clinical grad 2 fibrosis in the BM as seen by reticulin fiber staining (**Figure 14D**) and together closely resemble clinical phenotypes of MF patients.

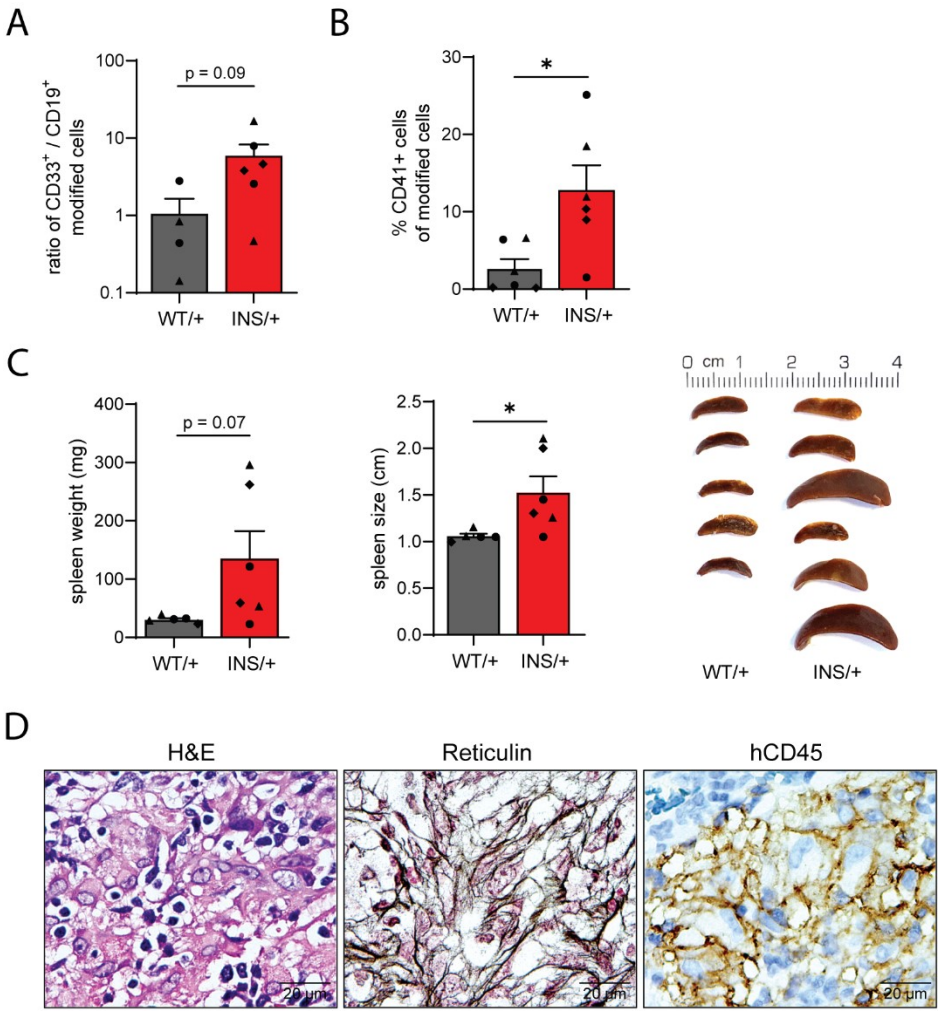

Figure 14. *CALR* mutant cells induce splenomegaly and BM fibrosis in xenografted NSG mice.

(A) Ratio of myeloid ($CD33^+$) to lymphoid ($CD19^+$) cells shown for reporter$^+$ $hCD45^+$ engrafted human cells 16 weeks post-transplant. **(B)** Percentage of $CD41^+$ megakaryocyte progenitors within engrafted reporter$^+$ $hCD45^+$ cells after 16 weeks. **(C)** Weight and size of mouse spleens at time of sacrifice 24 weeks post-transplant. Symbols (●, ▲, ♦) in bar graphs depict individual donors. **(D)** Representative micrographs of a sectioned and stained femur showing fibrosis upon human cell engraftment as seen by reticulin fiber deposition. Reproduced with modifications from (1) with permission via the CC BY license (https://creativecommons.org/licenses/by/4.0/).

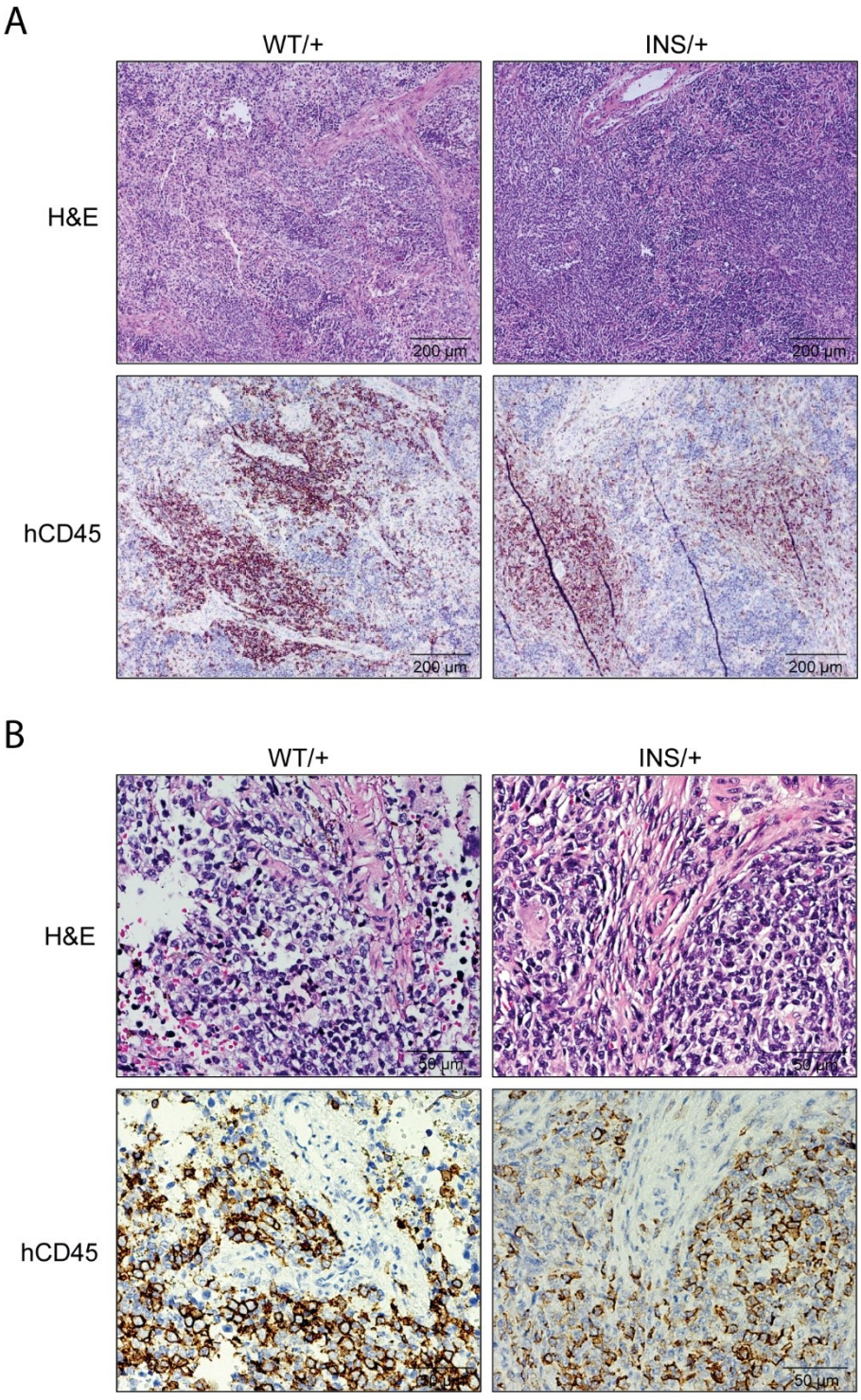

Figure 15. Human cells populate mouse spleens in xenografted NSG mice.

(A-B) Representative micrographs of H&E and hCD45 stained sections of mouse spleens. Low (A) and high (B) magnification images are depicted for better evaluation of tissue morphology. Reproduced with modifications from (1) with permission via the CC BY license (https://creativecommons.org/licenses/by/4.0/).

Lastly, to investigate the repopulating potential of our genome engineered human HSPCs, we performed secondary transplantation into NSG mice. To this end, we purified hCD45^{+} cells from the BM of primary recipients and transplanted them intrafemorally into sub-lethally irradiated secondary recipients (**Figure 16A**). We found low but detectable human engraftment in the BM of secondary recipients after 8 weeks. Importantly, CRISPR-modified (GFP/BFP^{+}) cells retained some of their repopulating potential with a trend to better engraftment in *CALR* INS recipient mice (**Figure 16B-C**).

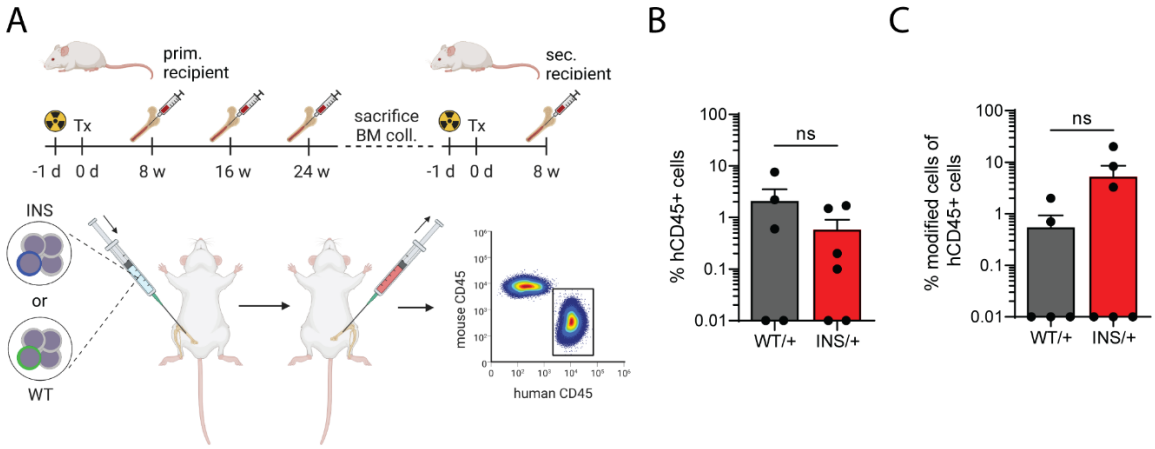

Figure 16. Genome engineered human HSPCs partly retain repopulating potential in vivo.
(A) Transplantation of hCD45^{+} enriched BM from primary recipient NSG mice after 24 weeks into secondary recipients. (n=6 mice from 3 independent UCB donors). **(B)** Total human engraftment (% hCD45^{+} cells) in the murine BM 8 weeks post-transplant. **(C)** Engraftment of human genome engineered cells (% modified cells within hCD45^{+} cells) in the murine BM 8 weeks after secondary transplantation. Reproduced with modifications from (1) with permission via the CC BY license (https://creativecommons.org/licenses/by/4.0/).

In conclusion, these *in vivo* experiments show that we can reliably generate a trackable humanized *CALR* mutant mouse model, that transfers established *in vitro* phenotypes to *in vivo* and extends those by clinical phenotypes of MPN patients.

6.6 *CALR* mutations induce compensatory chaperone expression in human HSPCs through unfolded protein response.

Three years after the first description of *CALR* mutations in MPN, the main oncogenic mechanism of mutant *CALR* driving MPN pathogenesis was discovered (72, 75, 77). Cytokine-independent activation of *MPL* signaling through direct binding of mutant *CALR* explained the exaggerated growth of megakaryocytes which is strongly dependent on TPO. Nevertheless, we sought to explore additional mutant *CALR*-induced mechanisms that contribute to the pathogenesis of MPNs.

To this end, we performed RNA-sequencing of sort-purified genome engineered *CALR* wildtype and mutant human HSPCs from three independent UCB donors. To capture cellular mechanisms induced early upon mutation acquisition, we extracted RNA already four days after CRISPR/Cas9 and AAV6-mediated knock-in (**Figure 17A**). RNA-sequencing revealed differential expression (padj < 0.05) of 104 and 29 genes in *CALR* DEL and INS cells compared to wildtype controls respectively (**Figure 17B-C**). A significant proportion of deregulated genes are shared by both mutation types, however INS cells show downregulation of 35 genes when directly compared to DEL, pointing towards mutation type-specific differences. Interestingly, the vast majority of genes is upregulated in *CALR* mutant cells, indicating an induction of certain pathways.

Clustering of individual samples based on differential gene expression underlined these results, where samples clustered based on their genotype with greater similarity between mutant cells than to wildtype (**Figure 18**). We confirmed the upregulation of the top ten differentially expressed genes (DEGs) that were common between both mutation types via RT-qPCR (**Figure 19A**). Additionally, we could show that these genes are upregulated in MPN patient-derived $CD34^+$ HSPCs with more pronounced effects in DEL samples (**Figure 19B**). Patient demographics are listed in **Table 2**. Furthermore, we compared the DEGs from our UCB-derived dataset to previously published data from single cell RNA-sequencing of ET and MF patient-derived $CD34^+$ HSPCs. Six of our top ten (6/10) DEGs were overlapping with the published dataset further validating the data from our genome engineered cells (**Figure 19C**).

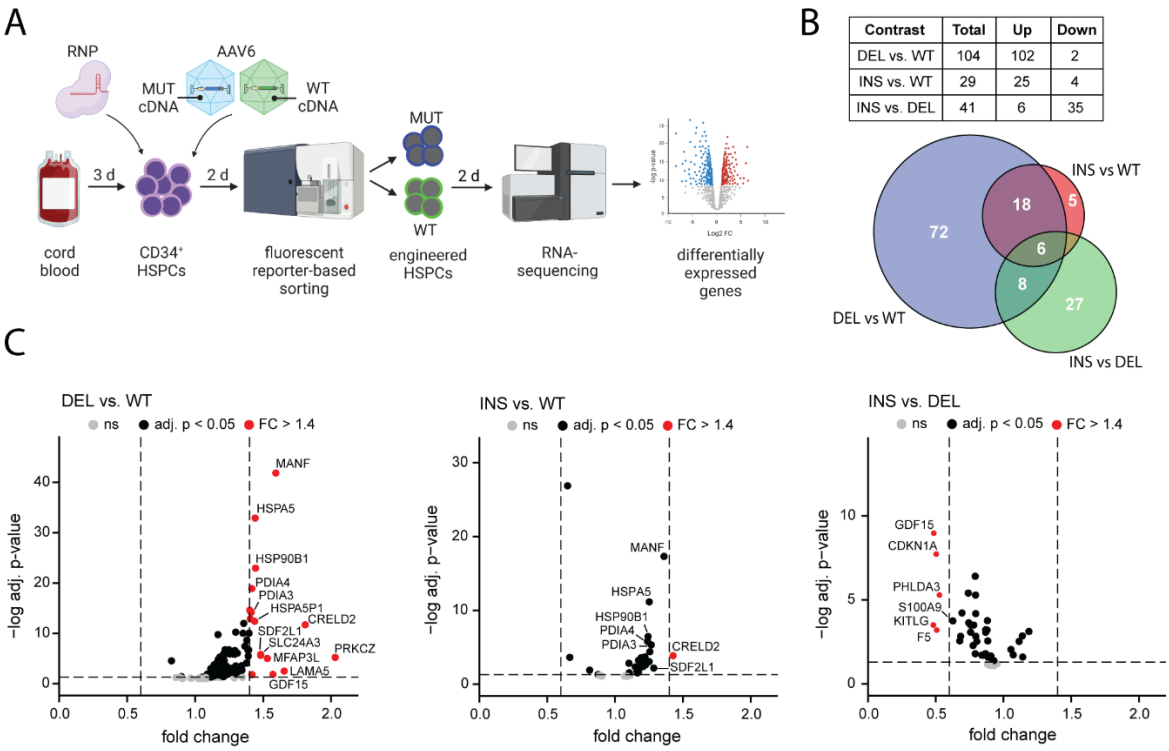

Figure 17. Transcriptional profiling of *CALR* mutant human HSPCs.

(A) Workflow of genome engineering of human HSPCs and subsequent RNA-sequencing (n=3 independent UCB donors). **(B)** (Top)Table reporting the total number of deregulated genes and up- or down-regulated genes for multiple comparisons. (Bottom) Venn diagram showing the overlap of deregulated genes between genotypes. **(C)** Volcano plots showing up- or down-regulated genes in *CALR* mutant HSPCs. Black dots represent significantly deregulated genes while red dots additionally have a fold change > 1.4. Reproduced with modifications from (1) with permission via the CC BY license (https://creativecommons.org/licenses/by/4.0/).

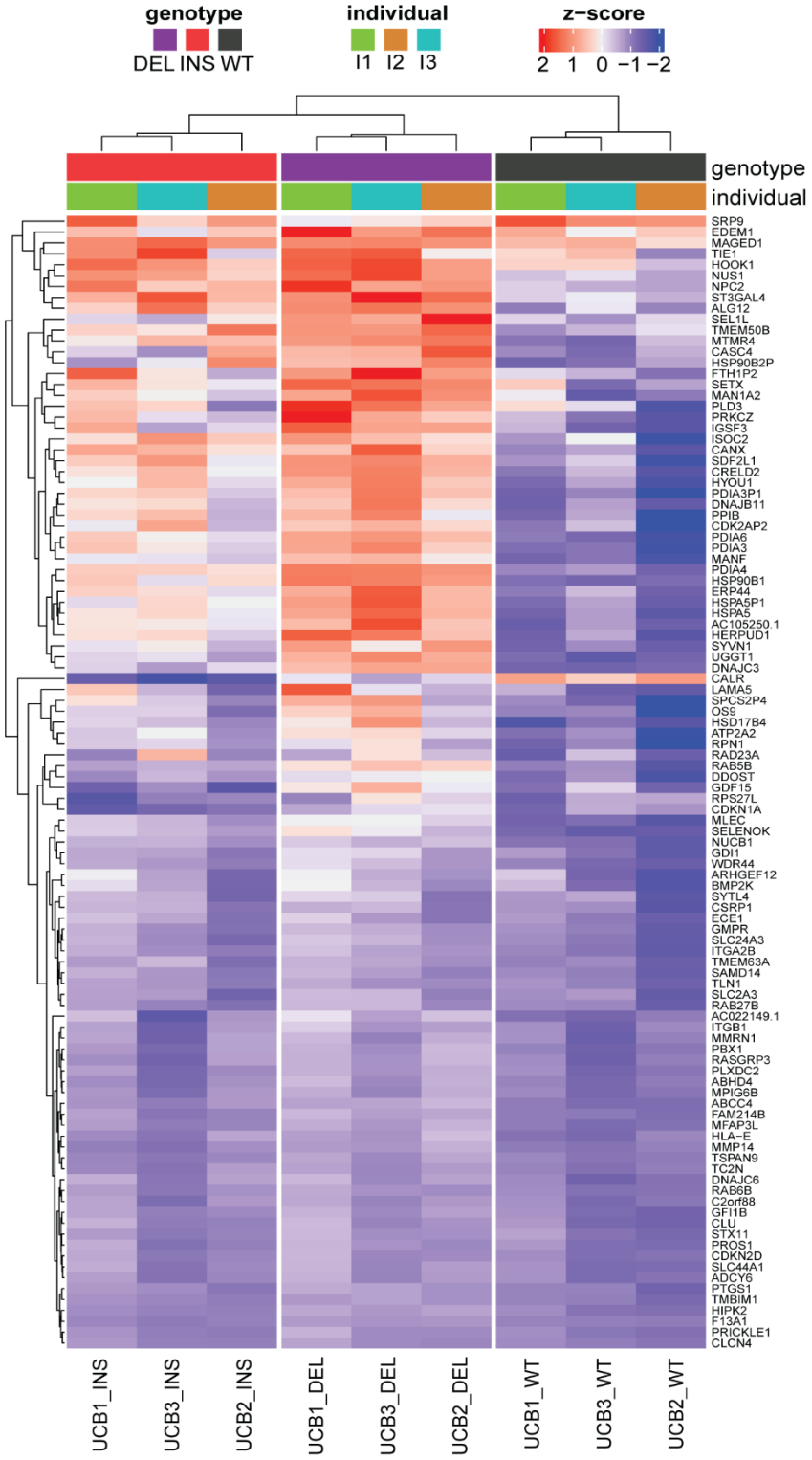

Figure 18. Clustering of *CALR* mutant human HSPCs based on their gene expression profile. Clustering of samples is shown on top and clustering of genes left of the heatmap. Heatmap coloring reports z-scores (degree of differential expression) of individual genes. Reproduced with modifications from (1) with permission via the CC BY license (https://creativecommons.org/licenses/by/4.0/).

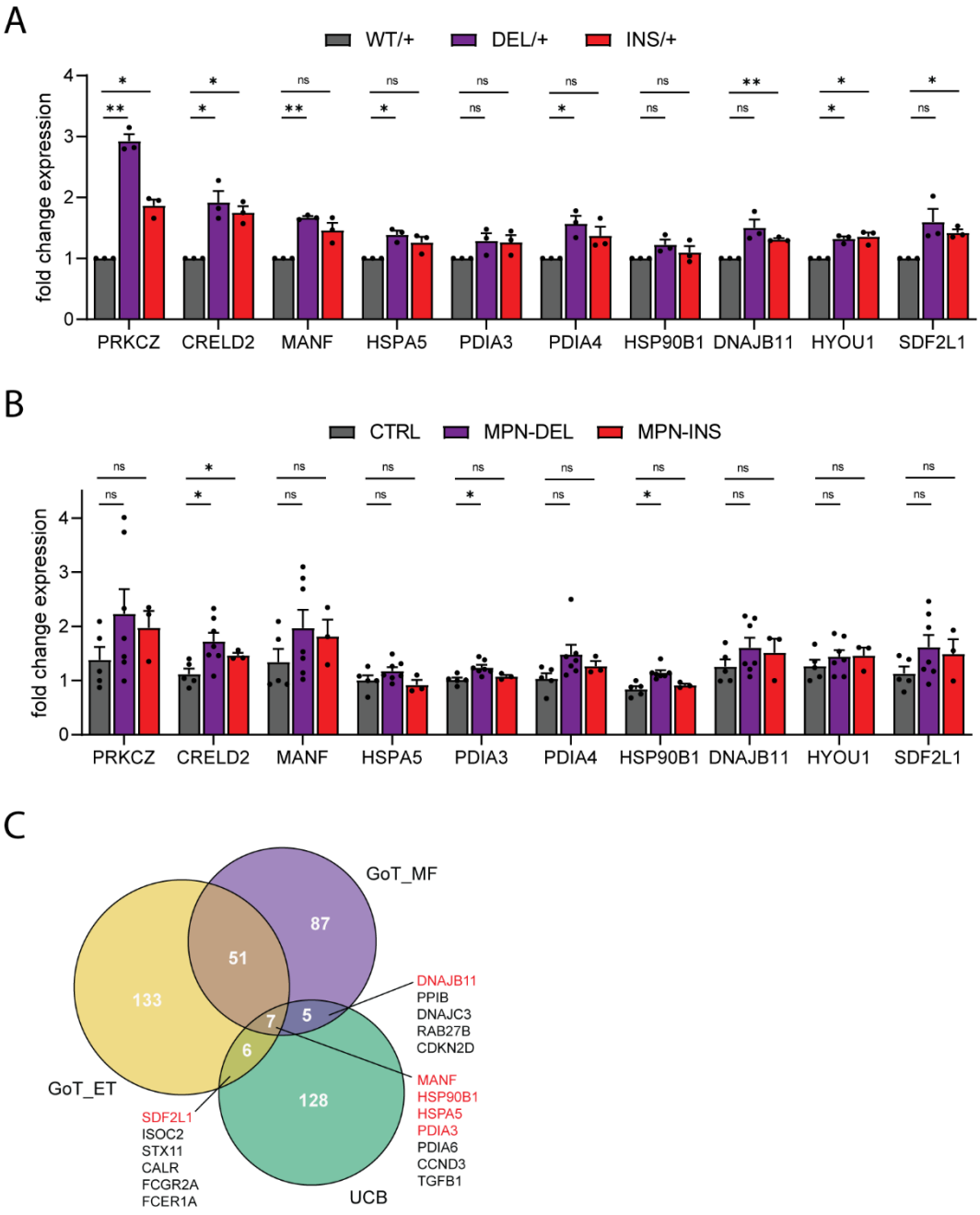

Figure 19. Validation of DEGs from transcriptional profiling results.

(A) Confirmation of up-regulation of top 10 differentially expressed genes (DEG) via qRT-PCR in UCB-derived HSPCs (n=3). **(B)** Expression of the top 10 DEGs detected via RNA-Seq was confirmed via qRT-PCR in MPN patient-derived HSPCs (n=7 MPN-DEL, n=3 MPN-INS) compared to healthy controls (n=5 CTRL). **(C)** Venn diagram showing the overlap of deregulated genes between the dataset of this work and previously published data from patient-derived CD34⁺ HSPCs (231). Reproduced with modifications from (1) with permission via the CC BY license (https://creativecommons.org/licenses/by/4.0/).

Table 2: Summary of *CALR* mutant MPN patient demographics.

This table contains relevant clinical information of all *CALR* MUT MPN patients, of which $CD34^+$ HSPCs were used for RT-qPCR. Reported blood parameters were analyzed at time of diagnosis. *CALR* driver mutations and further leukemia-associated co-mutations were detected via next-generation sequencing of PB-derived cells. Dx = diagnosis, Hb = hemoglobin levels, Plt = platelet counts, WBC = white blood cell counts, PB blasts = peripheral blood $CD34^+$ blasts, ET = essential thrombocythemia, PMF = primary myelofibrosis, p-ET MF = post-essential thrombocythemia myelofibrosis

Patient ID	Sample ID	Diagnosis (Dx)	Age at Dx	Sex	CALR mutation	Co-mutations	Spleen size (cm)	Hb (g/dl)	Plt ($x10^9$/L)	WBC ($x10^9$/L)	PB blasts (%)
LB-MUG-035	9703	PMF	55.2	F	c.1099_1150del (p.L367fs*46)	-	22	11.2	341	8.98	3
LB-MUG-010	9793	p-ET MF	40.7	F	c.1099_1150del (p.L367fs*46)	NRAS c.G35A (p.G12D), ASXL1 c.2467delT (p.L823*)	20	12.2	437	12.06	1
LB-MUG-004	9800	p-ET MF	60.2	F	c.1154_1155ins TTGTC (p.K385fs*47)	ASXL1 c.1772dupA (p.Y591*), PTPN11 c.A922G (p.N308D)	N/A	10.0	321	6.65	1
LB-MUG-332	10049	p-ET MF	63.4	F	c.1154_1155ins TTGTC (p.K385fs*47)	ASXL1 c.1772dupA (p.Y591_Q592delinsX)	28	11.0	724	14.13	1
LB-MUG-230	10059	PMF	74.5	M	c.1099_1150del (p.L367fs*46)	SF3B1 c.G1998T (p.K666N)	25	11.3	253	12.60	1
LB-MUG-005	9549	PMF	29.0	M	c.1099_1150del (p.L367fs*46)	MPL c.T1543A (p.W515R)	13	14.1	516	10.02	1
LB-MUG-372	9567	ET	40.4	F	c.1154_1155ins TTGTC (p.K385fs*47)	N/A	12	14.2	1557	10.33	1
LB-MUG-338	9731	ET	50.0	M	43 bp deletion	N/A	N/A	13.4	1136	7.00	1
LB-MUG-067	9581	PMF	64.6	F	c.1119_1139delins GCTTTGCGTTTCTT (p.D373_E380delins ELCVSWfs)	NRAS c.T190A (p.Y64N)	18	12.6	390	17.81	3
LB-MUG-159	9910	p-ET MF	58.8	F	c.1099_1150del (p.L367fs*46)	-	N/A	7.9	319	4.78	2

To investigate the DEGs in more detail, we performed gene set enrichment analysis (GSEA). The most prominently enriched signature in both types of mutation was associated with megakaryocyte progenitors, indicating the priming of HSPCs towards megakaryocyte differentiation as an early event in the transformation of healthy cells. (**Figure 20A**). We performed additional enrichment analysis on only significantly upregulated genes in *CALR* mutant cells using the Enrichr tool (Ma'ayan lab) to get a closer look at induced pathways.

The enrichment profile of *CALR* DEL and INS HSPCs was very similar with a strong enrichment for ER stress-related signatures like activation of chaperones through unfolded protein response (UPR) as well as protein processing signatures like ER quality control (ERQC) and protein folding associated terms (N-glycan trimming and Calnexin/Calreticulin cycle) (**Figure 20C-D**). While DEL mutant cells seem to activate UPR via the IRE1α-XBP1 axis, INS mutant cells primarily activate ATF6.

We could also gain additional insights into broader cellular functions deregulated in *CALR* mutant HSPCs. DEL mutant cells show enrichment for platelet associated terms and increased cytosolic Ca^{2+} levels, while being depleted for rRNA processing and transcription related terms (**Figure 20E**). INS mutant cells on the other hand are enriched for Golgi to ER retrograde transport and depleted for translation elongation amongst others (**Figure 20F**).

Having found a lot of ER-located processes involved in protein processing, we sought to investigate their relationship. A protein network analysis of our top ten DEGs using STRING revealed a highly interactive network, with a core of ER-resident chaperones (some of which are part of the Calnexin/Calreticulin cycle) that is interacting with UPR mediators and proteins involved in peptide loading of MHC class I molecules (**Figure 20B**). In summary, these transcriptional data suggest that *CALR* mutant cells upregulate ER-resident chaperones through UPR, most likely as a compensatory mechanism due to reduced chaperone activity of mutant *CALR*, especially of type 1.

The transcriptional profiling data generated from our genome engineered HSPCs allowed us to also uncover *CALR* mutation type-specific differences. INS cells were enriched for cell proliferation-related terms including DNA elongation, mRNA splicing, separation of sister chromatids and cholesterol biosynthesis when directly compared to DEL cells (**Figure 20G**). This was accompanied by less activation of chaperones via UPR and depleted p53 signaling pathways when compared to DEL cells (**Figure 20H**).

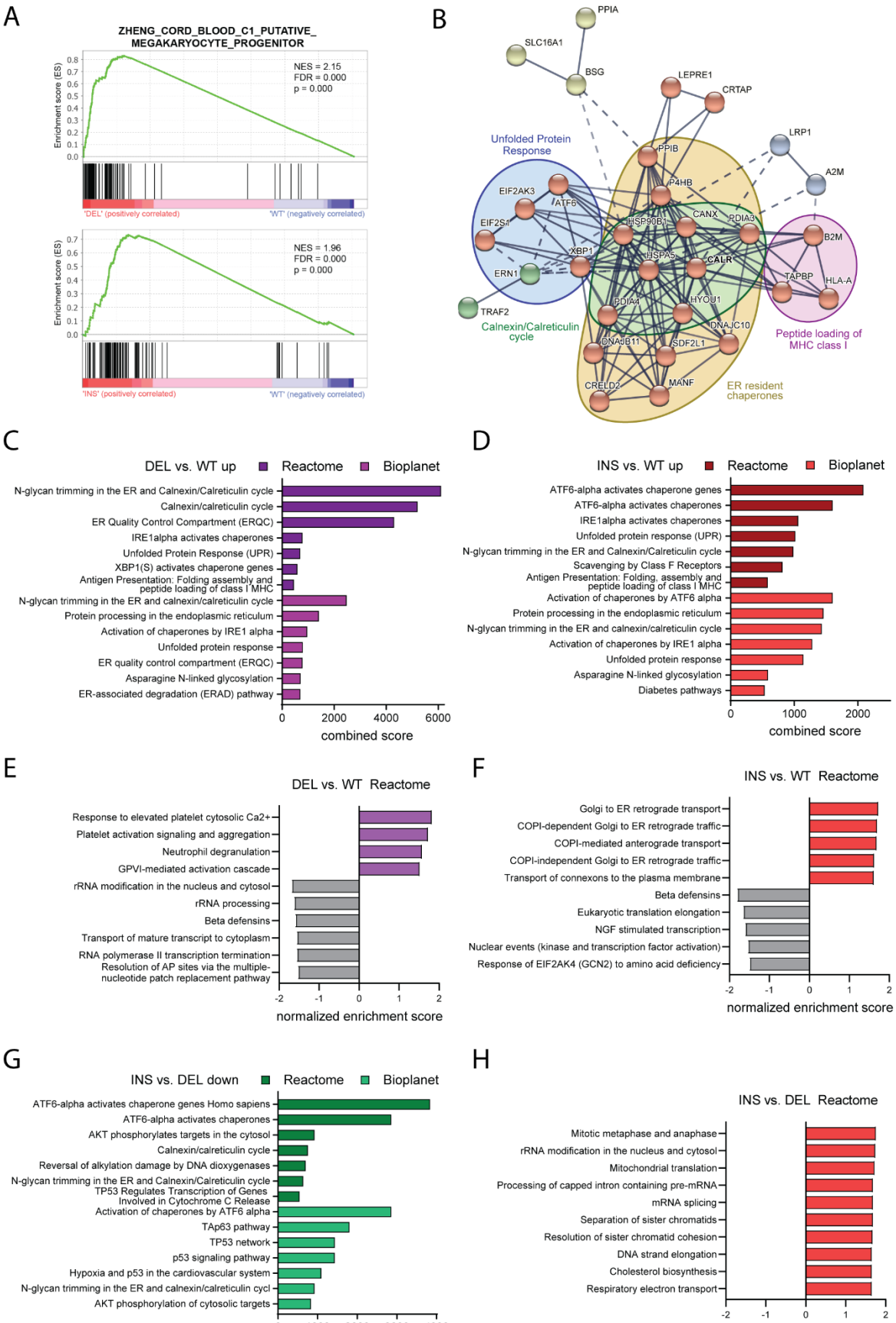
A
ZHENG_CORD_BLOOD_C1_PUTATIVE_
MEGAKARYOCYTE_PROGENITOR
NES = 2.15
FDR = 0.000
p = 0.000
Enrichment score (ES)
'DEL' (positively correlated)
'WT' (negatively correlated)
NES = 1.96
FDR = 0.000
p = 0.000
'INS' (positively correlated)
'WT' (negatively correlated)
B
PPIA
SLC16A1
BSG
LEPRE1
CRTAP
LRP1
A2M
Unfolded Protein Response
PPIB
P4HB
EIF2AK3
ATF6
EIF2S1
HSP90B1
CANX
PDIA3
B2M
XBP1
HSPA5
CALR
ERN1
TAPBP
HLA-A
TRAF2
PDIA4
HYOU1
DNAJC10
Calnexin/Calreticulin cycle
DNAJB11
SDF2L1
Peptide loading of MHC class I
CRELD2
MANF
ER resident chaperones
C
DEL vs. WT up
Reactome
Bioplanet
N-glycan trimming in the ER and Calnexin/Calreticulin cycle
Calnexin/calreticulin cycle
ER Quality Control Compartment (ERQC)
IRE1alpha activates chaperones
Unfolded Protein Response (UPR)
XBP1(S) activates chaperone genes
Antigen Presentation: Folding assembly and peptide loading of class I MHC
N-glycan trimming in the ER and calnexin/calreticulin cycle
Protein processing in the endoplasmic reticulum
Activation of chaperones by IRE1 alpha
Unfolded protein response
ER quality control compartment (ERQC)
Asparagine N-linked glycosylation
ER-associated degradation (ERAD) pathway
0
2000
4000
6000
combined score
D
INS vs. WT up
Reactome
Bioplanet
ATF6-alpha activates chaperone genes
ATF6-alpha activates chaperones
IRE1alpha activates chaperones
Unfolded protein response (UPR)
N-glycan trimming in the ER and Calnexin/Calreticulin cycle
Scavenging by Class F Receptors
Antigen Presentation: Folding, assembly and peptide loading of class I MHC
Activation of chaperones by ATF6 alpha
Protein processing in the endoplasmic reticulum
N-glycan trimming in the ER and calnexin/calreticulin cycle
Activation of chaperones by IRE1 alpha
Unfolded protein response
Asparagine N-linked glycosylation
Diabetes pathways
0
1000
2000
combined score
E
DEL vs. WT Reactome
Response to elevated platelet cytosolic Ca2+
Platelet activation signaling and aggregation
Neutrophil degranulation
GPVI-mediated activation cascade
rRNA modification in the nucleus and cytosol
rRNA processing
Beta defensins
Transport of mature transcript to cytoplasm
RNA polymerase II transcription termination
Resolution of AP sites via the multiple-nucleotide patch replacement pathway
-2
-1
0
1
2
normalized enrichment score
F
INS vs. WT Reactome
Golgi to ER retrograde transport
COPI-dependent Golgi to ER retrograde traffic
COPI-mediated anterograde transport
COPI-independent Golgi to ER retrograde traffic
Transport of connexons to the plasma membrane
Beta defensins
Eukaryotic translation elongation
NGF stimulated transcription
Nuclear events (kinase and transcription factor activation)
Response of EIF2AK4 (GCN2) to amino acid deficiency
-2
-1
0
1
2
normalized enrichment score
G
INS vs. DEL down
Reactome
Bioplanet
ATF6-alpha activates chaperone genes Homo sapiens
ATF6-alpha activates chaperones
AKT phosphorylates targets in the cytosol
Calnexin/calreticulin cycle
Reversal of alkylation damage by DNA dioxygenases
N-glycan trimming in the ER and Calnexin/Calreticulin cycle
TP53 Regulates Transcription of Genes Involved in Cytochrome C Release
Activation of chaperones by ATF6 alpha
TAp63 pathway
TP53 network
p53 signaling pathway
Hypoxia and p53 in the cardiovascular system
N-glycan trimming in the ER and calnexin/calreticulin cycl
AKT phosphorylation of cytosolic targets
0
1000
2000
3000
4000
combined score
H
INS vs. DEL Reactome
Mitotic metaphase and anaphase
rRNA modification in the nucleus and cytosol
Mitochondrial translation
Processing of capped intron containing pre-mRNA
mRNA splicing
Separation of sister chromatids
Resolution of sister chromatid cohesion
DNA strand elongation
Cholesterol biosynthesis
Respiratory electron transport
-2
-1
0
1
2
normalized enrichment score

Figure 20. *CALR* mutant HSPCs induce chaperone expression through unfolded protein response. (A) Gene set enrichment analysis (GSEA) showing strong enrichment in megakaryocyte progenitor signatures for DEL (top) and INS (bottom) HSPCs. Normalized enrichment score (NES), false discovery rate (FDR) and p-value are depicted. **(B)** Protein interaction network analysis was performed from the top 10 upregulated genes in *CALR* mutant HSPCs using STRING. Bold lines indicate high evidence for interaction while dotted lines indicate low evidence. Node (protein) clustering was performed using the MCL method. Colored circles grouping proteins with similar function were manually annotated. **(C-D)** Enrichment analysis (maayanlab.cloud/Enrichr) of significantly upregulated genes (padj < 0.05) from DEL vs. WT (C) and INS vs. WT (D) comparisons was performed and the top 7 enriched terms from the Reactome and Bioplanet gene set databases reported. **(E-F)** Forest plots showing enriched and depleted terms from the Reactome database for DEL vs. WT (E) and INS vs. WT (F) comparisons. **(G-H)** Enrichment analysis specifically reporting enriched and depleted terms in INS compared to DEL cells. Reproduced with modifications from (1) with permission via the CC BY license (https://creativecommons.org/licenses/by/4.0/).

6.7 Proteasome and BiP inhibition induce synthetic lethality in *CALR* MUT HSPCs.

The compensatory upregulation of ER-resident chaperones in *CALR* mutant cells revealed by our RNA-seq data suggests that these cells rely on the expression and activity of induced chaperones to cope with unfolded protein-mediated ER stress and thereby maintaining cell survival. Thus, we reasoned that inhibition of these chaperones or induction of additional ER stress could be novel therapeutic approaches to exploit mutation-specific vulnerabilities. We used HA15 (232) to selectively inhibit BiP (HSPA5), a key chaperone in the ER and amongst the highest upregulated genes in *CALR* mutant HSPCs, and Bortezomib, a proteasome complex inhibitor clinically approved for the treatment of multiple myeloma (233).

To investigate the effect of both inhibitors on HSPCs as well as various lineage-primed progenitors, we treated *CALR* mutant and wildtype HSPCs in methylcellulose-based pan-myeloid and collagen-based megakaryocytic CFU assays (**Figure 21A**). Bortezomib and HA15 significantly reduced the number of CFU-GM and BFU-E colonies in DEL mutant samples compared to DMSO controls (**Figure 21B**). While Bortezomib showed minor toxicity on wildtype and INS mutant cells at 2 nM concentration, DEL mutant cells were preferentially killed.

A similar but less pronounced effect was seen with HA15 at 5 µM. Both inhibitors, however showed increased efficacy in reducing CFU-Mk colonies of DEL and INS mutant samples (**Figure 21C**). Surprisingly, INS mutant samples showed similar sensitivity to inhibitor treatment compared to DEL counterparts in this assay. These results suggest that type 1 and type 2 *CALR* mutant HSPCs can be specifically targeted and irradicated by therapeutic intervention in ER stress response mechanisms and that chaperone and proteasome inhibitors could provide novel therapeutic strategies for MPN patients.

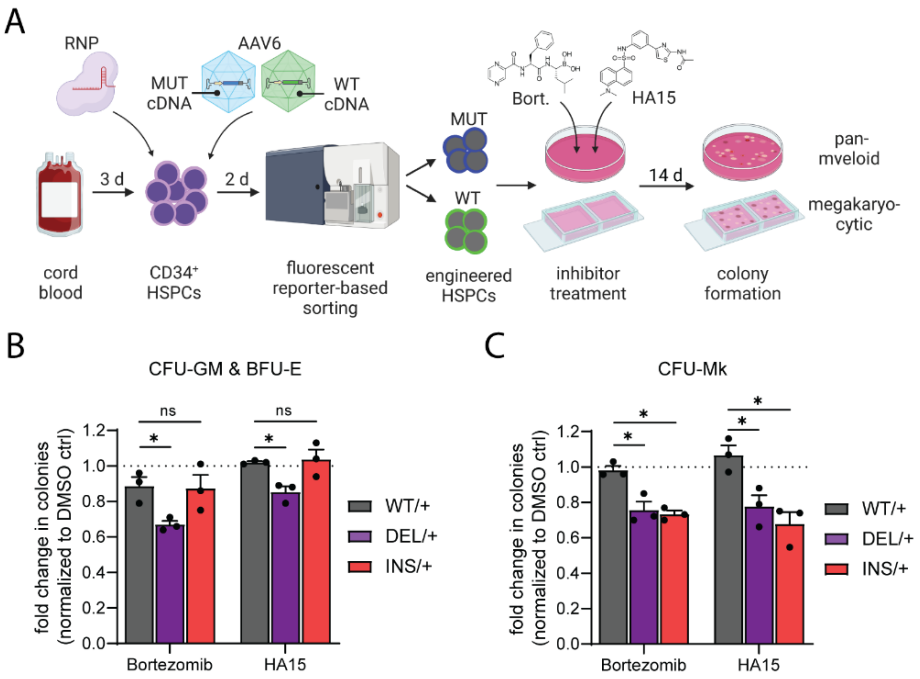

Figure 21. BiP and proteasome inhibition induce synthetic lethality in *CALR* mutant HSPCs. **(A)** Worklfow for genome engineering *CALR* mutant HSPCs and treatment of sort-purified HSPCs with proteasome and BiP inhibitors in semisolid methylcellulose- and collagen-based CFU assays. **(B-C)** Fold change in combined CFU-GM and BFU-E colonies (B) and CFU-Mk colonies (C) after 12-14 days of culture (n=3). Treatment with 5 µM HA15 and 2 nM Bortezomib. Colony counts were normalized to DMSO controls. Reproduced with modifications from (1) with permission via the CC BY license (https://creativecommons.org/licenses/by/4.0/).

In summary, based on the findings of this study we propose a mechanism for the mutant *CALR*-induced cellular changes and how targeted inhibition might harness these to induce mutation-specific cell death.

In *CALR* wildtype cells nascent protein folding in the ER is ensured by an ensemble of chaperones lead by calreticulin as part of the calnexin/calreticulin cycle (**Figure 22, top left panel**). Cells are kept in a steady state by exporting fully folded proteins via the secretory pathway and discarding un-/misfolded proteins via proteasomal degradation Unfolded proteins are generally bound by the key ER-resident chaperone BiP. In steady state conditions unfolded protein levels are low and BiP mainly stays bound to the UPR mediators ATF6, IRE1 and PERK, preventing their activation.

In *CALR* mutant cells however, protein folding is less efficient due to reduced chaperone function of mutant *CALR* protein (**Figure 22, top right panel**). Thus, un-/misfolded protein levels increase and are bound by BiP for transfer to proteasomal degradation. Sequestration of BiP by unfolded proteins away from UPR mediators activates the UPR pathway, ultimately leading to a compensatory induction of chaperone expression to cope with the increased ER stress.

The increased ER stress in *CALR* mutant cells can be harnessed to selectively eradicated these cells via synthetic lethality (**Figure 22, bottom left panel**). Selectively inhibiting BiP via HA15 prevents binding of un-/misfolded proteins leading to a toxic accumulation of these proteins. Similarly, inhibition of the proteasome complex via Bortezomib prevents removal of terminally unfolded proteins leading to an overloading of the ER. Both scenarios result in activation of apoptosis as the cell is unable to handle the excessive ER stress via UPR.

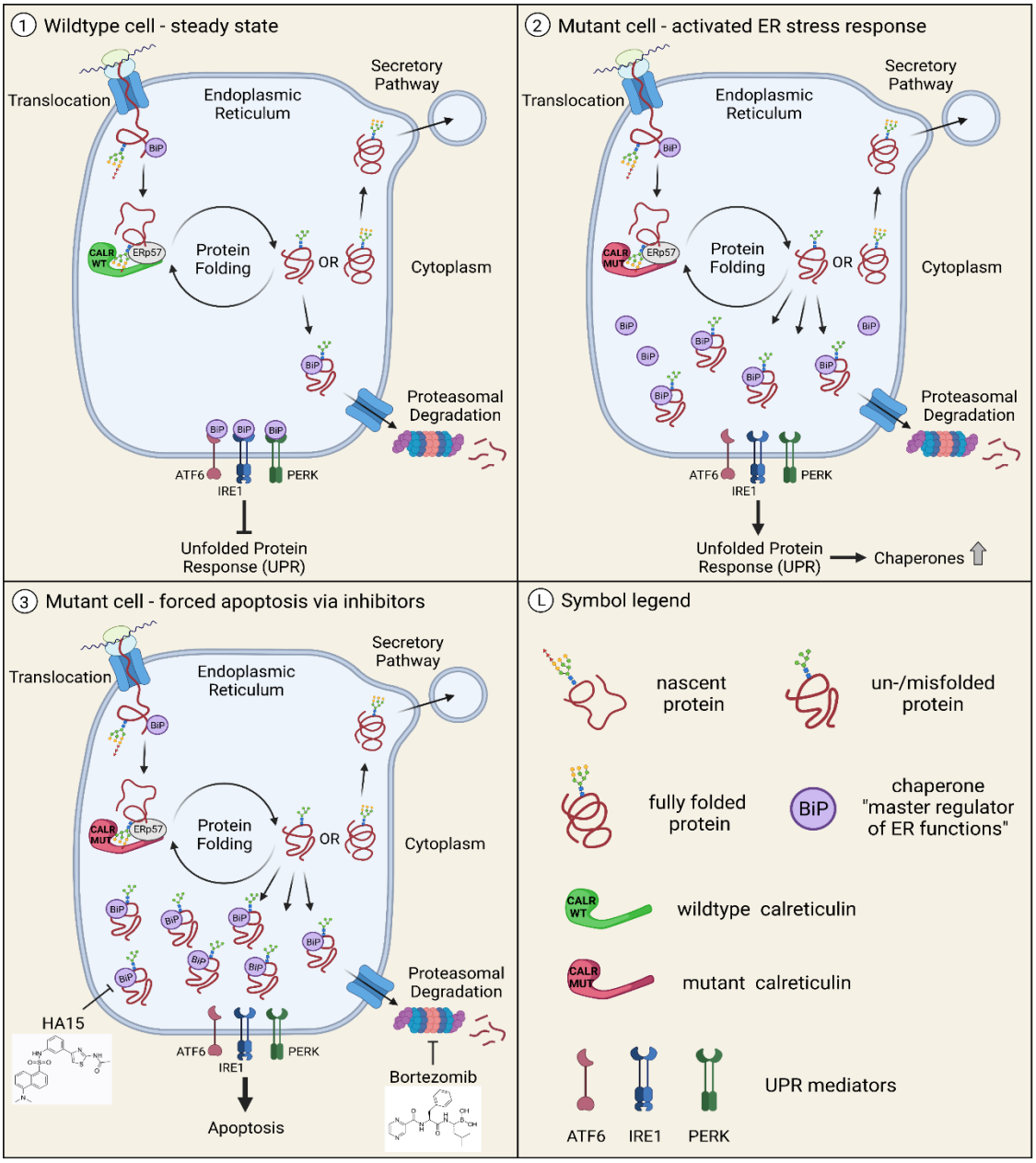

Figure 22. Intracellular mechanisms mediating sensitivity of *CALR* mutant cells to Bortezomib and HA15.

Schematic summary of intracellular mechanisms induced upon *CALR* mutation acquisition and interference via targeted inhibition. Proposed mechanisms are based on the findings of this work and published literature. Top left panel shows *CALR* wildtype cells with physiologic steady state protein folding. *CALR* mutant cells induce chaperone expression via unfolded protein response due to lack in chaperone activity (top right panel). Targeted inhibition of BiP and proteasome results in accumulation of unfolded proteins and ultimately leading to cellular apoptosis (bottom left panel). Reproduced with modifications from (1) with permission via the CC BY license (https://creativecommons.org/licenses/by/4.0/).

7. Discussion

Mutations in the *CALR* gene are major drivers of MPNs, which have been discovered nearly a decade ago. However, the intracellular and pathophysiological changes leading to the development of MPNs are just partly resolved until now. This lack in knowledge is reflected in the unavailability of targeted therapies for *CALR* mutant MPN patients. This thesis aimed to improve prospective investigations by providing a novel human *CALR* mutant cell model and to unveil some of the *CALR* mutation-induced mechanisms, enabling the identification of potential therapeutic targets. To this end, we 1) generated *CALR* mutant human HSPCs using a sophisticated CRISPR/Cas9-based knock-in approach, 2) characterized phenotypic changes of these cells such as TPO-independent growth and megakaryocyte differentiation and 3) xenotransplanted them into immunocompromised mice to investigate their disease-related phenotypes *in vivo*. 4) Transcriptional profiling of engineered *CALR* mutant HSPCs allowed us to identify molecular changes and specific vulnerabilities of mutant cells resulting in 5) the pre-clinical testing of novel potential therapeutic agents.

7.1 Generation of *CALR* mutant HSPCs

CALR mutant cells models have been available since the first description of *CALR* mutations in MPNs (44, 45). These initial studies used murine Ba/F3 cells that were transduced with lentiviral vectors to express human mutant *CALR*. Although, these cell lines helped to gain basic knowledge about mutant *CALR,* their condition is far off the pathophysiologic state of human MPNs. Human cell lines with *CALR* mutations were generated in recent years (76, 234), however these cell lines are usually of malignant origin or transformed to exhibit malignant properties like unrestricted proliferative capacity. These traits in combination with ectopic expression of *CALR* upon lentiviral transduction present biases that prevent the investigation of processes induced by *CALR* mutations in an isolated fashion. Thus, we developed a novel strategy to endogenously express heterozygous *CALR* mutations in otherwise healthy primary human HSPCs to more faithfully and prospectively investigate MPN development.

The CRISPR/Cas9 technology allowed us to introduce site-specifically the two most common *CALR* mutations at the endogenous gene locus via the HDR mechanism. We adapted a recently published approach combining CRISPR/Cas9 with rAAV6-mediated donor DNA delivery, which proofed successful for genome engineering of primary human HSPCs (208, 235). While gene knock-outs became very efficient, genome-wide scalable and broadly available, precise knock-ins especially of larger sequences remain challenging (236). This effect is multiplied by the challenges of editing primary human HSPCs. Low editing efficiencies require enrichment or purification of successfully modified cells. Using cell lines, this can be achieved via clonal expansion and selection of correctly modified clones. Primary cells, however, cannot be expanded *ex vivo* for extended periods, but more importantly, primary human HSPCs will lose their stem cell properties and start to differentiate *in vitro*, limiting their use for functional assays following genome engineering (237).

To overcome these challenges, we simultaneously introduced a fluorescent reporter controlled by an SFFV promoter downstream of *CALR* allowing to purify correctly modified cells via FACS or to track them in xenografted mice. A similar approach based on TALENs has been recently published for the knock-in of the complete *CD40L* coding sequence into the genome of T-cells from inherited X-linked hyperimmunoglobulin M syndrome patients (238). The *CALR* coding sequence comprising exons 1-9 exceeds the 4.7 kb cargo capacity of AAV6 preventing the replacement of the whole *CALR* gene. Since *CALR* mutations occur in exon 9 towards the end of the gene, we introduced a cDNA comprised of only exons 8 and 9 harboring either wildtype or mutant sequences.

Additionally, while CRISPR/Cas9-mediated introduction of DSBs is very efficient, HDR-mediated knock-in of foreign DNA is rather inefficient and often outcompeted by the NHEJ mechanism creating INDELs (188, 239). To prevent disruption of the reading frame of *CALR* alleles where the DSB is not repaired via HDR but NHEJ, we decided to target the non-coding sequence of intron 7. This knock-in strategy required the splicing of the exogenous exons 8 and 9 to the upstream endogenous exons 1-7 for the expression of a full-length transcript. We ensured the splicing process by introducing a splice-acceptor including the 3' splice site, the branch point and the polypyrimidine tract upstream of the exogenous exons.

Sanger sequencing of gDNA and mRNA confirmed that fluorescent reporter expression reliably indicates successful knock-in of exogenous cDNA through our genome editing approach. Furthermore, mRNA sequencing confirmed that *CALR* alleles without HDR-mediated integration are not disrupted and lead to wildtype *CALR* expression necessary for a heterozygous genotype and its phenotypic consequences. Lastly, our genome-engineered *CALR* mutant HSPCs retain endogenous regulation of gene expression and do not show overexpression of *CALR*, therefore clearly improving current cell models generated via lentiviral transduction.

7.2 TPO-independent growth mediated by *CALR* mutations

The pathology of *CALR* mutant MPNs including ET and PMF implies dysregulation of the megakaryocyte lineage which are found abnormally increased in the BM of patients (24, 31). Megakaryopoiesis in the BM is strongly dependent on the presence of TPO, which binds the TpoR (*MPL*) and induces differentiation and growth signaling. Early cell line models reported TPO-independent growth upon introduction of *CALR* mutations revealing first insights into their oncogenic effect on human hematopoiesis (72, 75, 76).

Interestingly, TPO-independence is conferred via the unphysiological binding of mutant *CALR* to the TpoR and subsequent activation of its downstream signaling via JAK-STAT, PI3K-AKT and MAPK pathways. Thus, TpoR expression is required for the oncogenic function of mutant *CALR*. TpoR is expressed in HSPCs and increases during megakaryocyte differentiation, while being absent on other myeloid lineages, suggesting an outgrowth of megakaryocytes by selectively boosting their proliferation. We could functionally validate our CRISPR/Cas9 and AAV6-mediated approach to introduce *CALR* mutations with preserved endogenous expression by reproducing previously published findings showing that a TPO-dependent cell line would become TPO-independent through activation of TpoR signaling upon *CALR* mutation acquisition.

Although, the oncogenic effect of CALR mutations was described for cell lines, their impact on the behavior of healthy HSPCs has not been investigated yet due to the lack of suitable models. Our engineered HSPCs allowed for the first time to investigate the cellular responses induced by *CALR* mutations in a prospective manner.

To avoid missing any additional consequences besides dysregulated megakaryopoiesis we performed a standard myeloid colony forming assay (Methocult™). We observed increased erythroid and decreased granulocytic-monocytic colonies, which suggests shifted differentiation of HSPCs towards megakaryocyte-erythroid progenitors. In Methocult™-assays, the absence of TPO and high concentrations of other cytokines including EPO prevent the formation of megakaryocyte colonies and favor erythroid colonies. Thus, a specific collagen-based assay excluding EPO was necessary to investigate megakaryopoiesis.

We observed clearly increased TPO-independent megakaryocyte colony formation of engineered *CALR* mutant cells in assays lacking TPO, confirming that healthy HSPCs were transformed solely by acquisition of *CALR* mutations isolated from other confounding factors. However, in the presence of TPO (50 ng/ml) *CALR* mutant cells exhibited only mildly increased megakaryopoiesis. Megakaryocyte differentiation assays generally use near saturating and unphysiological concentrations of TPO to maximize the megakaryocyte output, which potentially masks any mutant *CALR* mediated effect. Reducing the TPO concentration is therefore crucial in the context of MPN research.

In addition, liquid cultures allowed us to perform terminal megakaryocyte differentiation and to examine the growth characteristics of *CALR* mutant cells in more detail. Similar to the results from the colony assay, megakaryocyte differentiation was unchanged but very efficient (>90% $CD41^+$ $CD42b^+$ cells) in presence of 30 ng/ml TPO. However, we observed a proliferative advantage of INS mutant cells, which was not seen in the colony assay, suggesting a potential TPO hypersensitivity of these cells. Again, only lowering the TPO concentrations to 5 ng/ml – a concentration insufficient to support megakaryocyte growth and differentiation – revealed TPO-independent survival and growth advantage as well as the superior megakaryocyte differentiation of *CALR* mutant cells in continuous cultures.

Interestingly, HSPCs were dependent on TPO signaling for their survival irrespective of the *CALR* mutation status during the first days of differentiation, suggesting that *CALR* mutant HSPCs do not immediately become TPO-independent and transcriptional changes or external factors priming HSPCs towards megakaryocyte progenitors might be necessary. In summary, our engineered *CALR* mutant primary human HSPCs reproduce previously reported phenotypes of cell lines *in vitro* and allow further investigations to unravel the full pathogenesis of MPNs.

7.3 Xenografts of *CALR* mutant HSPCs and *in vivo* MPN phenotypes

In vivo MPN models are based on transgenic mice expressing either human mutant *CALR*, mouse orthologs or chimeras of both (88, 131, 240, 241). These mice develop robust ET phenotypes including thrombocytosis and megakaryocyte hyperplasia in the BM. Recent studies showed that more advanced symptoms like splenomegaly and BM fibrosis were only seen in mice with homozygous *CALR* mutations suggesting that disease penetrance is dependent on the mutant allele burden (132, 241). However, virtually all patients harbor heterozygous mutations, underlining the importance of developing mouse models that better mimic clinical characteristics. Most importantly, mouse models lack the human cellular context responsible for human MPN pathogenesis. In that respect, recent studies reported variable binding affinities between mutant *CALR* and TpoR of different species origin (131). Specifically, human mutant *CALR* shows greater binding by the human TpoR than the murine receptor, potentially explaining the homozygous genotype necessary in mouse models to achieve sufficient cell activation to develop advanced MPN symptoms. Due to these reasons we decided to perform xenotransplantations of our engineered heterozygous *CALR* mutant HSPCs into immunocompromised mice to generate a novel humanized *in vivo* MPN model.

One of the main challenges of primary cell xenotransplantation, either healthy or patient-derived, is to achieve engraftment with high human chimerism to draw meaningful conclusions. Despite the heterogenous nature of primary cells, we observed mainly high engraftment of human cells. Engraftment of human cells in the murine BM is mainly facilitated by long- and short-term HSCs, which represent only a small fraction of cells within the $CD34^+$ population (242). Prolonged ex vivo cultures and additional manipulations like electroporation and viral transduction reduce stemness and promote cellular differentiation, thereby reducing the fraction of engraftable cells (243). Thus, to maximize the number of cells with remaining repopulating potential, we minimized the culture period and avoided additional manipulations by transplanting HSPCs as early as eight hours post genetic modification and without reporter positive cell sorting. Correctly modified and fluorescent reporter expressing cells could be successfully tracked in the murine BM via flow cytometry.

Although NSG mice support human cell engraftment in the BM, circulation of mature human cells in the periphery is generally low. NSG mice efficiently remove human mature blood cells including erythrocytes, and platelets (244). Our focus was therefore on tracking BM changes as well as organ-specific or whole organism-comprising disease phenotypes. INS mutant cells seemed to outgrow wildtype cells over time in the NSG mouse BM although statistical significance was not reached. Additionally, by using new-born NSGW41 mice, which i) do not need irradiation prior to hematopoietic xenotransplantation (245) and ii) can be successfully engrafted with significantly lower numbers of human HSPCs, we were able to perform competitive transplant experiments with sort-purified, genome-engineered wildtype and mutant cells. Here, INS mutant cells showed a strong growth advantage over wildtype cells strengthening the characteristics we have seen *in vitro*.

Xenotransplantations of healthy UCB-derived $CD34^+$ cells usually result in predominantly B-lymphoid-biased engraftment in NSG mice. INS mutant cells however, showed a myeloid lineage skewing with an increase in $CD33^+$ cells. Importantly, we also found increased $CD41^+$ megakaryocyte progenitors in INS mutant cells. These results not only correlated with our *in vitro* data but also with previously published data from mouse models and with clinical findings in MPN patients. Further MPN disease hallmarks such as splenomegaly and BM fibrosis also developed in mice transplanted with INS mutant cells. These hallmarks are only partially penetrant in our xenografted mice and seem to be restricted to highly engrafted mice. Therefore, we hypothesize that a sufficient human cell number is required to initiate pathogenic fibrotic processes in the murine BM. Nevertheless, this is the first human model reporting the development of major clinical MPN hallmarks *in vivo* on a heterozygous mutational background.

Lastly, we performed secondary transplantations of BM engrafted human cells to assess if the genome engineered HSPCs retained self-renewal capacity and if disease hallmarks would be serially propagated. Similar to previously published data on xenotransplantations of healthy and patient-derived HSPCs (153, 154, 246, 247), secondary engraftment was detectable in a fraction of the mice but remained low (<10% $hCD45^+$ cells). Consequently, disease phenotypes were not propagated to secondary recipients, a goal which remains out of reach for most xenotransplantations. Yet, the *in vivo* models described here provide a suitable basis for further studies investigating either the pathomechanism of *CALR* mutant MPNs or for testing of potential therapeutic compounds in a humanized *in vivo* setting. Since our *in vivo* data is restricted to INS mutant cells it would be also necessary to evaluate the characteristics and disease initiating properties of DEL mutant cells in a mouse xenotransplantation setting.

NSG mice are the gold standard for hematopoietic xenotransplantations, however alternative mouse strains are available including the transgenic NSGS mice, which express the human cytokines SCF, IL-3 and GM-CSF and as a result predominantly favor myeloid engraftment (143). While these mice are beneficial for the engraftment of AML cells with granulocytic and monocytic background, they do not provide a suitable basis for *CALR* mutant MPN modeling. The expression of human IL-3 and GM-CSF diminishes megakaryopoiesis of transplanted human cells thereby preventing the pathogenic processes leading to MPN symptoms (144).

Recently, another transgenic mouse strain named MISTRG was developed expressing even more human cytokines including TPO, the main driver of megakaryopoiesis (145). A recent study reported successful engraftment of primary and secondary MF patient-derived cells in the murine BM of MISTRG mice, where these mice provided superior engraftment over NSG mice with high human chimerism in both BM and PB (153). While human megakaryocyte formation was observable in the BM, fibrosis was only detected in a limited number of mice. Nevertheless, we believe that this novel strain of immunocompromised mice could improve the xenografts of our genome engineered HSPCs and thereby promote disease phenotypes. Although MISTRG mice are currently not available to a broader scientific community, this newer mouse model will most likely further improve our *in vivo* MPN model in the future.

7.4 Early transcriptional rewiring of *CALR* mutant HSPCs

CALR mutations attribute a new function to the *CALR* protein. TPO-independent activation of the TpoR downstream signaling pathways is now considered the primary oncogenic mechanism of *CALR* mutant MPN (227). However, under physiological conditions, *CALR* has many important cellular functions that are unrelated to TpoR signaling, such as mediating folding of nascent proteins in the ER and maintaining cellular calcium homeostasis (50). How these functions are affected by mutations is scarcely investigated and currently poorly understood.

To get a broad overview of cellular changes induced by *CALR* mutations, we performed transcriptional profiling of engineered HSPCs in a prospective manner. We decided to uncover early mutation-induced reprogramming of HSPCs to find novel mechanisms directly caused by mutation acquisition and that are responsible for the fate of these cells. The results from RNA sequencing showed that the transcriptional profile of HSPCs is only moderately changed, which could be due to the early time point of analysis or due to the lower expression of *CALR* in HSPCs compared to mature cells like megakaryocytes (248). Nevertheless, we observed mainly increased expression of genes in *CALR* mutant cells indicating an activation of certain pathways.

Substantial overlap of induced genes between both mutation types additionally suggests activation of a common pathway between these two. Importantly, upregulation of the most prominently induced genes could be validated in HSPCs of MPN patients from our cohort and matches a recently published dataset of patient-derived HSPCs (231), suggesting that the findings from this experiment have great relevance for clinical applications. We observed megakaryocyte lineage priming of HSPCs as an early event, suggesting that aberrant expansion of megakaryocytes is initiated prior to differentiation and not simply a result of increased activation of TpoR signaling through increased TpoR and *CALR* expression in these cells. This transcriptional rewiring resembles data from K562 cells and transgenic mice (234, 249) and could explain the megakaryocyte skewing and expansion in the BM of our xenotransplanted mice and in MPN patients.

Genes induced in *CALR* mutant cells were enriched in signatures including N-glycan trimming of glycosylated proteins, calnexin/calreticulin cycle and activation of chaperones through UPR (IRE1 and ATF6). Since *CALR* has important chaperoning function in the ER, these transcriptional changes suggest a partial or complete loss of chaperone activity in mutant *CALR* and thus a compensatory upregulation of alternative chaperones to maintain proper protein folding and prevent induction of apoptosis through excessive unfolded proteins. Immediate upregulation of chaperones in HSPCs upon introduction of *CALR* mutations indicates a strong dependency of cells on unconfined protein folding and ER stress containment for their survival and therefore represent vulnerabilities for potential therapeutic targeting.

In-depth analysis showed that the upregulated genes form a tightly interacting network of various chaperones around *CALR* that are in contact with UPR mediators and thereby provide multiple targets to potentially interfere with protein folding. Interference with proteins of the heat shock family (HSP) could be readily achieved by available small molecule inhibitors and therefore depict preferential targets, while others would need gene therapy approaches for perturbation and thus present second line targets. Recent studies similarly reported N-glycosylation and UPR via the IRE1α/XBP1 pathway as therapeutic vulnerabilities in type 1 *CALR* mutant murine Ba/F3 cells and used the KIRA8 IRE1α/XBP1 inhibitor to selectively kill these cells (250, 251).

Despite many commonalities between type 1 and type 2 *CALR* mutations, we could for the first time elaborate in more detail on transcriptional differences induced by these mutation types. The main difference we observed, was a less pronounced induction of chaperones in INS mutant compared to DEL mutant HSPCs, which could be explained by no or only a modest loss in chaperone activity of INS mutant *CALR*. INS mutations lead to no loss of amino acids compared to DEL mutations and thus impairment of protein function would be lower, however this remains to be confirmed. Interestingly, INS mutant cells showed less activity of the p53 signaling network with concomitantly increased proliferative signatures including mitotic phases and sister chromatid separation, mRNA processing and cholesterol biosynthesis when compared to *CALR* mutant cells. These transcriptional changes underline the proliferative phenotype we observed in continuous liquid cultures of megakaryocyte directed differentiation and could explain increased platelet counts in *CALR* type 2 mutant ET patients (252). Future studies should focus on identifying more details of *CALR* mutation specific differences, which could help in the understanding of differential clinical phenotypes of MPN patients.

7.5 Pharmaceutical targeting of *CALR* mutant cells

Based on the transcriptional profiling results, we reasoned that interfering with the cellular capability to cope with ER stress, mainly in form of unfolded proteins, could be used to selectively target *CALR* mutant cells. To this end we harnessed the concept of synthetic lethality. Since *CALR* mutant cells seem to face increased ER stress via attenuated *CALR* chaperoning activity, which they compensate by upregulation of other chaperones, inhibiting these compensatory mechanisms could overstrain the cells and stop them in their cell cycle or even drive them into apoptosis.

We decided to target BiP (HSPA5), which is a major chaperone in the ER responsible for binding of nascent proteins and acting as an ER stress sensor for the activation of UPR (253), and additionally one of the strongest upregulated chaperones in our dataset. We used the selective inhibitor HA15, which hasn't been tested yet in human hematopoietic cells, however a recent study reported induction of ER stress followed by cellular apoptosis in lung cancer cells (254). HA15 treatment reduced colony counts of our genome engineered *CALR* DEL and INS mutant HSPCs by 20-30% while keeping wildtype cells unaffected. We believe that *CALR* mutant cells rely on BiP activity to bind and stabilize nascent and unfolded proteins as well as to guide terminally misfolded proteins to the ERAD pathway. Thus, blocking of BiP potentially leads to accumulation and aggregation of unfolded proteins that cannot be resolved in time and will eventually cause cell death.

Additionally, we tested an alternative therapeutic approach, which was not based on direct inhibition of upregulated chaperones in the ER. Cellular protein homeostasis comprises biosynthesis of proteins, their proper folding in the ER prior to membrane trafficking and degradation of terminally un- or misfolded proteins through the proteasome (59). Thus, we reasoned that *CALR* mutant cells would not only depend on compensatory chaperone expression, but also on efficient protein degradation via the proteasome. When we used the proteasome inhibitor Bortezomib on *CALR* mutant HSPCs in a clonogenic assay, we indeed saw a decrease in colonies of up to 30%. The results of this thesis suggest, that *CALR* mutant cells are more sensitive towards Bortezomib since these cells show already increased ER stress through unfolded proteins and cannot cope with additional stress through blockade of the ERAD pathway. Thereby, *CALR* mutant cells get overloaded with unfolded proteins, which in turn triggers apoptosis. Bortezomib is already approved for clinical use in multiple myeloma (233) and would therefore present a candidate drug for rapid translation to MPN patients.

Interestingly, we observed differential sensitivities of *CALR* mutant cells to both inhibitors in pan-myeloid and megakaryocytic colony assays. Colony formation of DEL mutant cells was attenuated in the pan-myeloid as well as the megakaryocytic assay, whereas INS mutant cells were affected only in the megakaryocytic assay. This differential sensitivity of *CALR* mutation types could be explained by the differences in their gene expression. DEL mutant cells show stronger induction of compensatory chaperones compared to INS and might therefore be more amenable to inhibition of induced genes and pathways. In contrast, INS mutant cells seem to show sensitivity to these inhibitors only in megakaryocytes where *CALR* expression is increased (248) and transcriptional changes will be more pronounced.

We are aware that further *in vitro* experiments are needed to elucidate the exact mechanisms by which HA15 and Bortezomib selectively act on *CALR* mutant cells and how their activity is affected by differential gene expression in DEL and INS mutant cells. Additionally, drug combination studies of these two inhibitors should be performed to investigate any synergistic effects upon interfering with protein folding (chaperones) and protein degradation (proteasome). Furthermore, to validate the results of this thesis and to proceed towards a clinical use, studies on MPN patient-derived cells and *in vivo* mouse studies are necessary. Ideally, immunocompromised mice with xenotransplanted human *CALR* mutant cells should be used to find optimal inhibitor concentrations for *in vivo* use and to monitor human cell survival under controlled treatment conditions.

In this thesis, we described the generation of a novel *CALR* mutant humanized MPN model enabling prospective investigations *in vitro* and *in vivo* and shed light on molecular consequences upon *CALR* mutation acquisition that helped to identify novel targeted therapeutic strategies. The results of this work will help to advance future MPN research and close the gap towards targeted therapies for *CALR* mutant patients.

8. Bibliography

1. Foßelteder J, Pabst G, Sconocchia T, Schlacher A, Auinger L, Kashofer K, et al. Human gene-engineered calreticulin mutant stem cells recapitulate MPN hallmarks and identify targetable vulnerabilities. Leukemia. 2023.
2. Bennett JH. Case of hypertrophy of the spleen and liver, in which death took place from suppuration of the blood. Edinburgh Med Sug J. 1845;64:413-23.
3. Heuck G. Zwei Fälle von Leukämie mit eigenthümlichem Blut- resp. Knochenmarksbefund. Archiv für pathologische Anatomie und Physiologie und für klinische Medicin. 1879;78(3):475-96.
4. Vaquez H. Sur une forme spéciale de cyanose s' accompagnant d'hyperglobulie excessive et persistante. CR Soc Biol (Paris). 1892;44:384-8.
5. Osler W. Chronic cyanosis, with polycythæmia and enlarged spleen: a new clinical entity. The American Journal of the Medical Sciences (1827-1924). 1903;126(2):187.
6. Epstein E, Goedel A. Hemorrhagic thrombocythemia with a cascular, sclerotic spleen. Virchows Arch. 1934;293:233-48.
7. Dameshek W. Some speculations on the myeloproliferative syndromes. Blood. 1951;6(4):372-5.
8. Tefferi A. The history of myeloproliferative disorders: before and after Dameshek. Leukemia. 2008;22(1):3-13.
9. Barbui T, Thiele J, Gisslinger H, Kvasnicka HM, Vannucchi AM, Guglielmelli P, et al. The 2016 WHO classification and diagnostic criteria for myeloproliferative neoplasms: document summary and in-depth discussion. Blood cancer journal. 2018;8(2):15-.
10. Swerdlow SH, Campo E, Harris NL, Jaffe ES, Pileri SA, Stein H, et al., editors. WHO Classification of Tumours of Haematopoietic and Lymphoid Tissues. Geneva, Switzerland: WHO Press; 2008.
11. Khoury JD, Solary E, Abla O, Akkari Y, Alaggio R, Apperley JF, et al. The 5th edition of the World Health Organization Classification of Haematolymphoid Tumours: Myeloid and Histiocytic/Dendritic Neoplasms. Leukemia. 2022;36(7):1703-19.
12. Rowley JD. A New Consistent Chromosomal Abnormality in Chronic Myelogenous Leukaemia identified by Quinacrine Fluorescence and Giemsa Staining. Nature. 1973;243(5405):290-3.
13. Shtivelman E, Lifshitz B, Gale RP, Canaani E. Fused transcript of abl and bcr genes in chronic myelogenous leukaemia. Nature. 1985;315(6020):550-4.

14. Shallis RM, Zeidan AM, Wang R, Podoltsev NA. Epidemiology of the Philadelphia Chromosome-Negative Classical Myeloproliferative Neoplasms. Hematol Oncol Clin North Am. 2021;35(2):177-89.
15. Hultcrantz M, Ravn Landtblom A, Andréasson B, Samuelsson J, Dickman PW, Kristinsson SY, et al. Incidence of myeloproliferative neoplasms – trends by subgroup and age in a population-based study in Sweden. Journal of Internal Medicine. 2020;287(4):448-54.
16. Verstovsek S, Yu J, Scherber RM, Verma S, Dieyi C, Chen C-C, et al. Changes in the incidence and overall survival of patients with myeloproliferative neoplasms between 2002 and 2016 in the United States. Leukemia & Lymphoma. 2022;63(3):694-702.
17. Lin Q, Mao L, Shao L, Zhu L, Han Q, Zhu H, et al. Global, Regional, and National Burden of Chronic Myeloid Leukemia, 1990-2017: A Systematic Analysis for the Global Burden of Disease Study 2017. Front Oncol. 2020;10:580759.
18. Spivak JL. Myeloproliferative Neoplasms. The New England journal of medicine. 2017;376(22):2168-81.
19. Spivak JL. Polycythemia Vera. Current Treatment Options in Oncology. 2018;19(2):12.
20. Tefferi A, Vannucchi AM, Barbui T. Polycythemia vera treatment algorithm 2018. Blood cancer journal. 2018;8(1):3.
21. Vannucchi AM, Kiladjian JJ, Griesshammer M, Masszi T, Durrant S, Passamonti F, et al. Ruxolitinib versus Standard Therapy for the Treatment of Polycythemia Vera. New England Journal of Medicine. 2015;372(5):426-35.
22. Burgstaller S, Buxhofer-Ausch V, Sliwa T, Beham-Schmid C, Gastl G, Geissler K, et al. Austrian recommendations for the management of polycythemia vera. Wiener klinische Wochenschrift. 2018;130(17):535-42.
23. Szuber N, Mudireddy M, Nicolosi M, Penna D, Vallapureddy RR, Lasho TL, et al. 3023 Mayo Clinic Patients With Myeloproliferative Neoplasms: Risk-Stratified Comparison of Survival and Outcomes Data Among Disease Subgroups. Mayo Clinic Proceedings. 2019;94(4):599-610.
24. Tefferi A, Pardanani A. Essential Thrombocythemia. The New England journal of medicine. 2019;381(22):2135-44.
25. Tefferi A, Vannucchi AM, Barbui T. Essential thrombocythemia treatment algorithm 2018. Blood cancer journal. 2018;8(1):2.
26. Rumi E, Cazzola M. How I treat essential thrombocythemia. Blood. 2016;128(20):2403-14.

27. Cortelazzo S, Finazzi G, Ruggeri M, Vestri O, Galli M, Rodeghiero F, et al. Hydroxyurea for Patients with Essential Thrombocythemia and a High Risk of Thrombosis. New England Journal of Medicine. 1995;332(17):1132-7.
28. Silver RT, Kiladjian J-J, Hasselbalch HC. Interferon and the treatment of polycythemia vera, essential thrombocythemia and myelofibrosis. Expert review of hematology. 2013;6(1):49-58.
29. Buxhofer-Ausch V, Heibl S, Sliwa T, Beham-Schmid C, Wolf D, Geissler K, et al. Austrian recommendations for the management of essential thrombocythemia. Wiener klinische Wochenschrift. 2021;133(1):52-61.
30. Guglielmelli P, Pacilli A, Rotunno G, Rumi E, Rosti V, Delaini F, et al. Presentation and outcome of patients with 2016 WHO diagnosis of prefibrotic and overt primary myelofibrosis. Blood. 2017;129(24):3227-36.
31. Tefferi A. Primary myelofibrosis: 2021 update on diagnosis, risk-stratification and management. American journal of hematology. 2021;96(1):145-62.
32. Jeryczynski G, Thiele J, Gisslinger B, Wölfler A, Schalling M, Gleiß A, et al. Pre-fibrotic/early primary myelofibrosis vs. WHO-defined essential thrombocythemia: The impact of minor clinical diagnostic criteria on the outcome of the disease. American journal of hematology. 2017;92(9):885-91.
33. Krauth M-T, Burgstaller S, Buxhofer-Ausch V, Gastl G, Geissler K, Keil F, et al. Ruxolitinib therapy for myelofibrosis in Austria. Wiener klinische Wochenschrift. 2018;130(17):495-504.
34. Talpaz M, Kiladjian J-J. Fedratinib, a newly approved treatment for patients with myeloproliferative neoplasm-associated myelofibrosis. Leukemia. 2021;35(1):1-17.
35. Sliwa T, Beham-Schmid C, Burgstaller S, Buxhofer-Ausch V, Gastl G, Geissler K, et al. Austrian recommendations for the management of primary myelofibrosis, post-polycythemia vera myelofibrosis and post-essential thrombocythemia myelofibrosis: an expert statement. Wiener klinische Wochenschrift. 2017;129(9):293-302.
36. Martínez-Cuadrón D, Megías-Vericat JE, Serrano J, Martínez-Sánchez P, Rodríguez-Arbolí E, Gil C, et al. Treatment patterns and outcomes of 2310 patients with secondary acute myeloid leukemia: a PETHEMA registry study. Blood advances. 2022;6(4):1278-95.
37. Kang MG, Choi HW, Lee JH, Choi YJ, Choi HJ, Shin JH, et al. Coexistence of JAK2 and CALR mutations and their clinical implications in patients with essential thrombocythemia. Oncotarget. 2016;7(35):57036-49.

38. Boddu P, Chihara D, Masarova L, Pemmaraju N, Patel KP, Verstovsek S. The co-occurrence of driver mutations in chronic myeloproliferative neoplasms. Annals of hematology. 2018;97(11):2071-80.
39. Mead AJ, Mullally A. Myeloproliferative neoplasm stem cells. Blood. 2017;129(12):1607-16.
40. Kralovics R, Passamonti F, Buser AS, Teo SS, Tiedt R, Passweg JR, et al. A gain-of-function mutation of JAK2 in myeloproliferative disorders. The New England journal of medicine. 2005;352(17):1779-90.
41. Levine RL, Wadleigh M, Cools J, Ebert BL, Wernig G, Huntly BJ, et al. Activating mutation in the tyrosine kinase JAK2 in polycythemia vera, essential thrombocythemia, and myeloid metaplasia with myelofibrosis. Cancer Cell. 2005;7(4):387-97.
42. Pikman Y, Lee BH, Mercher T, McDowell E, Ebert BL, Gozo M, et al. MPLW515L is a novel somatic activating mutation in myelofibrosis with myeloid metaplasia. PLoS medicine. 2006;3(7):e270.
43. Pardanani AD, Levine RL, Lasho T, Pikman Y, Mesa RA, Wadleigh M, et al. MPL515 mutations in myeloproliferative and other myeloid disorders: a study of 1182 patients. Blood. 2006;108(10):3472-6.
44. Klampfl T, Gisslinger H, Harutyunyan AS, Nivarthi H, Rumi E, Milosevic JD, et al. Somatic mutations of calreticulin in myeloproliferative neoplasms. The New England journal of medicine. 2013;369(25):2379-90.
45. Nangalia J, Massie CE, Baxter EJ, Nice FL, Gundem G, Wedge DC, et al. Somatic CALR mutations in myeloproliferative neoplasms with nonmutated JAK2. The New England journal of medicine. 2013;369(25):2391-405.
46. Kaifie A, Kirschner M, Wolf D, Maintz C, Hänel M, Gattermann N, et al. Bleeding, thrombosis, and anticoagulation in myeloproliferative neoplasms (MPN): analysis from the German SAL-MPN-registry. Journal of hematology & oncology. 2016;9(1):18.
47. Titmarsh GJ, Duncombe AS, McMullin MF, O'Rorke M, Mesa R, De Vocht F, et al. How common are myeloproliferative neoplasms? A systematic review and meta-analysis. American journal of hematology. 2014;89(6):581-7.
48. Grinfeld J, Nangalia J, Green AR. Molecular determinants of pathogenesis and clinical phenotype in myeloproliferative neoplasms. Haematologica. 2017;102(1):7-17.
49. Gelebart P, Opas M, Michalak M. Calreticulin, a Ca2+-binding chaperone of the endoplasmic reticulum. The international journal of biochemistry & cell biology. 2005;37(2):260-6.

50. Michalak M, Corbett EF, Mesaeli N, Nakamura K, Opas M. Calreticulin: one protein, one gene, many functions. Biochemical Journal. 1999;344(2):281-92.
51. Kozlov G, Pocanschi CL, Rosenauer A, Bastos-Aristizabal S, Gorelik A, Williams DB, et al. Structural Basis of Carbohydrate Recognition by Calreticulin *. Journal of Biological Chemistry. 2010;285(49):38612-20.
52. Kozlov G, Muñoz-Escobar J, Castro K, Gehring K. Mapping the ER Interactome: The P Domains of Calnexin and Calreticulin as Plurivalent Adapters for Foldases and Chaperones. Structure. 2017;25(9):1415-22.e3.
53. Frickel E-M, Riek R, Jelesarov I, Helenius A, Wüthrich K, Ellgaard L. TROSY-NMR reveals interaction between ERp57 and the tip of the calreticulin P-domain. Proceedings of the National Academy of Sciences. 2002;99(4):1954-9.
54. Ellgaard L, Frickel E-M. Calnexin, calreticulin, and ERp57. Cell Biochemistry and Biophysics. 2003;39(3):223-47.
55. Caramelo JJ, Parodi AJ. Getting In and Out from Calnexin/Calreticulin Cycles. Journal of Biological Chemistry. 2008;283(16):10221-5.
56. Ellgaard L, Helenius A. A Chaperone System for Glycoprotein Folding: The Calnexin/Calreticulin Cycle. In: Eggleton P, Michalak M, editors. Calreticulin: Second Edition. Boston, MA: Springer US; 2003. p. 19-29.
57. Meusser B, Hirsch C, Jarosch E, Sommer T. ERAD: the long road to destruction. Nature Cell Biology. 2005;7(8):766-72.
58. Hwang J, Qi L. Quality Control in the Endoplasmic Reticulum: Crosstalk between ERAD and UPR pathways. Trends in biochemical sciences. 2018;43(8):593-605.
59. Nishikawa S-i, Brodsky JL, Nakatsukasa K. Roles of Molecular Chaperones in Endoplasmic Reticulum (ER) Quality Control and ER-Associated Degradation (ERAD). The Journal of Biochemistry. 2005;137(5):551-5.
60. Michalak M, Groenendyk J, Szabo E, Gold LI, Opas M. Calreticulin, a multi-process calcium-buffering chaperone of the endoplasmic reticulum. The Biochemical journal. 2009;417(3):651-66.
61. Opas M, Dziak E, Fliegel L, Michalak M. Regulation of expression and intracellular distribution of calreticulin, a major calcium binding protein of nonmuscle cells. Journal of Cellular Physiology. 1991;149(1):160-71.
62. Smith MJ, Koch GL. Multiple zones in the sequence of calreticulin (CRP55, calregulin, HACBP), a major calcium binding ER/SR protein. The EMBO Journal. 1989;8(12):3581-6.
63. Clapham DE. Calcium Signaling. Cell. 2007;131(6):1047-58.

64. Carafoli E. Calcium signaling: A tale for all seasons. Proceedings of the National Academy of Sciences. 2002;99(3):1115-22.
65. Wuytack F, Raeymaekers L, Missiaen L. Molecular physiology of the SERCA and SPCA pumps. Cell Calcium. 2002;32(5):279-305.
66. Ambudkar IS, de Souza LB, Ong HL. TRPC1, Orai1, and STIM1 in SOCE: Friends in tight spaces. Cell Calcium. 2017;63:33-9.
67. Eder-Azanza L, Navarro D, Aranaz P, Novo FJ, Cross NCP, Vizmanos JL. Bioinformatic analyses of CALR mutations in myeloproliferative neoplasms support a role in signaling. Leukemia. 2014;28(10):2106-9.
68. Lasho TL, Finke CM, Tischer A, Pardanani A, Tefferi A. Mayo CALR mutation type classification guide using alpha helix propensity. American journal of hematology. 2018;93(5):E128-E9.
69. Theocharides APA, Lundberg P, Lakkaraju AKK, Lysenko V, Myburgh R, Aguzzi A, et al. Homozygous calreticulin mutations in patients with myelofibrosis lead to acquired myeloperoxidase deficiency. Blood. 2016;127(25):3253-9.
70. Stengel A, Jeromin S, Haferlach T, Meggendorfer M, Kern W, Haferlach C. Detection and characterization of homozygosity of mutated CALR by copy neutral loss of heterozygosity in myeloproliferative neoplasms among cases with high CALR mutation loads or with progressive disease. Haematologica. 2018.
71. Rizvi Q, Zaidi U, Shahid S, Ahmed S, Shamsi T. Homozygous CALR Mutation in Primary Myelofibrosis and Its Effect on Disease Phenotype: A Case Report and Review of the Literature. Case reports in hematology. 2019;2019:1430170.
72. Elf S, Abdelfattah NS, Chen E, Perales-Paton J, Rosen EA, Ko A, et al. Mutant Calreticulin Requires Both Its Mutant C-terminus and the Thrombopoietin Receptor for Oncogenic Transformation. Cancer discovery. 2016;6(4):368-81.
73. Marty C, Pecquet C, Nivarthi H, El-Khoury M, Chachoua I, Tulliez M, et al. Calreticulin mutants in mice induce an MPL-dependent thrombocytosis with frequent progression to myelofibrosis. Blood. 2016;127(10):1317-24.
74. Pecquet C, Chachoua I, Roy A, Balligand T, Vertenoeil G, Leroy E, et al. Calreticulin mutants as oncogenic rogue chaperones for TpoR and traffic-defective pathogenic TpoR mutants. Blood. 2019;133(25):2669-81.
75. Chachoua I, Pecquet C, El-Khoury M, Nivarthi H, Albu RI, Marty C, et al. Thrombopoietin receptor activation by myeloproliferative neoplasm associated calreticulin mutants. Blood. 2016;127(10):1325-35.

76. Araki M, Yang Y, Masubuchi N, Hironaka Y, Takei H, Morishita S, et al. Activation of the thrombopoietin receptor by mutant calreticulin in CALR-mutant myeloproliferative neoplasms. Blood. 2016;127(10):1307-16.
77. Balligand T, Achouri Y, Pecquet C, Chachoua I, Nivarthi H, Marty C, et al. Pathologic activation of thrombopoietin receptor and JAK2-STAT5 pathway by frameshift mutants of mouse calreticulin. Leukemia. 2016;30(8):1775-8.
78. Araki M, Yang Y, Imai M, Mizukami Y, Kihara Y, Sunami Y, et al. Homomultimerization of mutant calreticulin is a prerequisite for MPL binding and activation. Leukemia. 2019;33(1):122-31.
79. Pronier E, Cifani P, Merlinsky TR, Berman KB, Somasundara AVH, Rampal RK, et al. Targeting the CALR interactome in myeloproliferative neoplasms. JCI Insight. 2018;3(22).
80. Gardai SJ, McPhillips KA, Frasch SC, Janssen WJ, Starefeldt A, Murphy-Ullrich JE, et al. Cell-surface calreticulin initiates clearance of viable or apoptotic cells through trans-activation of LRP on the phagocyte. Cell. 2005;123(2):321-34.
81. Chao MP, Jaiswal S, Weissman-Tsukamoto R, Alizadeh AA, Gentles AJ, Volkmer J, et al. Calreticulin is the dominant pro-phagocytic signal on multiple human cancers and is counterbalanced by CD47. Science translational medicine. 2010;2(63):63ra94-63ra94.
82. Feng M, Chen JY, Weissman-Tsukamoto R, Volkmer JP, Ho PY, McKenna KM, et al. Macrophages eat cancer cells using their own calreticulin as a guide: roles of TLR and Btk. Proc Natl Acad Sci U S A. 2015;112(7):2145-50.
83. Feng M, Marjon KD, Zhu F, Weissman-Tsukamoto R, Levett A, Sullivan K, et al. Programmed cell removal by calreticulin in tissue homeostasis and cancer. Nature communications. 2018;9(1):3194.
84. Daitoku S, Takenaka K, Yamauchi T, Yurino A, Jinnouchi F, Nunomura T, et al. Calreticulin mutation does not contribute to disease progression in essential thrombocythemia by inhibiting phagocytosis. Exp Hematol. 2016;44(9):817-25.e3.
85. Liu P, Zhao L, Loos F, Marty C, Xie W, Martins I, et al. Immunosuppression by Mutated Calreticulin Released from Malignant Cells. Molecular cell. 2020;77(4):748-60.e9.
86. Garbati MR, Welgan CA, Landefeld SH, Newell LF, Agarwal A, Dunlap JB, et al. Mutant calreticulin-expressing cells induce monocyte hyperreactivity through a paracrine mechanism. American journal of hematology. 2016;91(2):211-9.
87. Han L, Schubert C, Köhler J, Schemionek M, Isfort S, Brümmendorf TH, et al. Calreticulin-mutant proteins induce megakaryocytic signaling to transform

hematopoietic cells and undergo accelerated degradation and Golgi-mediated secretion. Journal of hematology & oncology. 2016;9(1):45.
88. Balligand T, Achouri Y, Pecquet C, Gaudray G, Colau D, Hug E, et al. Knock-in of murine Calr del52 induces essential thrombocythemia with slow-rising dominance in mice and reveals key role of Calr exon 9 in cardiac development. Leukemia. 2020;34(2):510-21.
89. Pecquet C, Balligand T, Chachoua I, Roy A, Vertenoeil G, Colau D, et al. Secreted Mutant Calreticulins As Rogue Cytokines Trigger Thrombopoietin Receptor Activation Specifically in CALR Mutated Cells: Perspectives for MPN Therapy. Blood. 2018;132(Supplement 1):4-.
90. Di Buduo CA, Abbonante V, Marty C, Moccia F, Rumi E, Pietra D, et al. Defective interaction of mutant calreticulin and SOCE in megakaryocytes from patients with myeloproliferative neoplasms. Blood. 2020;135(2):133-44.
91. Rumi E, Pietra D, Ferretti V, Klampfl T, Harutyunyan AS, Milosevic JD, et al. JAK2 or CALR mutation status defines subtypes of essential thrombocythemia with substantially different clinical course and outcomes. Blood. 2014;123(10):1544-51.
92. Rotunno G, Mannarelli C, Guglielmelli P, Pacilli A, Pancrazzi A, Pieri L, et al. Impact of calreticulin mutations on clinical and hematological phenotype and outcome in essential thrombocythemia. Blood. 2014;123(10):1552-5.
93. Tefferi A, Guglielmelli P, Larson DR, Finke C, Wassie EA, Pieri L, et al. Long-term survival and blast transformation in molecularly annotated essential thrombocythemia, polycythemia vera, and myelofibrosis. Blood. 2014;124(16):2507-13.
94. Tefferi A, Lasho TL, Tischer A, Wassie EA, Finke CM, Belachew AA, et al. The prognostic advantage of calreticulin mutations in myelofibrosis might be confined to type 1 or type 1-like CALR variants. Blood. 2014;124(15):2465-6.
95. Pietra D, Rumi E, Ferretti VV, Di Buduo CA, Milanesi C, Cavalloni C, et al. Differential clinical effects of different mutation subtypes in CALR-mutant myeloproliferative neoplasms. Leukemia. 2016;30(2):431-8.
96. Cabagnols X, Defour JP, Ugo V, Ianotto JC, Mossuz P, Mondet J, et al. Differential association of calreticulin type 1 and type 2 mutations with myelofibrosis and essential thrombocytemia: relevance for disease evolution. Leukemia. 2015;29(1):249-52.
97. Verstovsek S, Mesa RA, Gotlib J, Gupta V, DiPersio JF, Catalano JV, et al. Long-term treatment with ruxolitinib for patients with myelofibrosis: 5-year update from the randomized, double-blind, placebo-controlled, phase 3 COMFORT-I trial. Journal of hematology & oncology. 2017;10(1):55.

98. Verstovsek S, Mesa RA, Gotlib J, Levy RS, Gupta V, DiPersio JF, et al. A Double-Blind, Placebo-Controlled Trial of Ruxolitinib for Myelofibrosis. New England Journal of Medicine. 2012;366(9):799-807.
99. Harrison CN, Schaap N, Vannucchi AM, Kiladjian JJ, Jourdan E, Silver RT, et al. Fedratinib in patients with myelofibrosis previously treated with ruxolitinib: An updated analysis of the JAKARTA2 study using stringent criteria for ruxolitinib failure. American journal of hematology. 2020;95(6):594-603.
100. Pardanani A, Tefferi A, Masszi T, Mishchenko E, Drummond M, Jourdan E, et al. Updated results of the placebo-controlled, phase III JAKARTA trial of fedratinib in patients with intermediate-2 or high-risk myelofibrosis. British journal of haematology. 2021;195(2):244-8.
101. Holmström MO, Martinenaite E, Ahmad SM, Met Ö, Friese C, Kjær L, et al. The calreticulin (CALR) exon 9 mutations are promising targets for cancer immune therapy. Leukemia. 2018;32(2):429-37.
102. Holmstrom MO, Ahmad SM, Klausen U, Bendtsen SK, Martinenaite E, Riley CH, et al. High frequencies of circulating memory T cells specific for calreticulin exon 9 mutations in healthy individuals. Blood cancer journal. 2019;9(2):8.
103. Tubb VM, Schrikkema DS, Croft NP, Purcell AW, Linnemann C, Freriks MR, et al. Isolation of T cell receptors targeting recurrent neoantigens in hematological malignancies. Journal for ImmunoTherapy of Cancer. 2018;6(1):70.
104. Gigoux M, Holmström MO, Zappasodi R, Park JJ, Pourpe S, Bozkus CC, et al. Calreticulin mutant myeloproliferative neoplasms induce MHC-I skewing, which can be overcome by an optimized peptide cancer vaccine. Sci Transl Med. 2022;14(649):eaba4380.
105. Arshad N, Cresswell P. Tumor-associated calreticulin variants functionally compromise the peptide loading complex and impair its recruitment of MHC-I. Journal of Biological Chemistry. 2018;293(25):9555-69.
106. Cimen Bozkus C, Roudko V, Finnigan JP, Mascarenhas J, Hoffman R, Iancu-Rubin C, et al. Immune Checkpoint Blockade Enhances Shared Neoantigen-Induced T-cell Immunity Directed against Mutated Calreticulin in Myeloproliferative Neoplasms. Cancer discovery. 2019;9(9):1192-207.
107. Kihara Y, Araki M, Imai M, Mori Y, Horino M, Ogata S, et al. Therapeutic Potential of an Antibody Targeting the Cleaved Form of Mutant Calreticulin in Myeloproliferative Neoplasms. Blood. 2020;136:9-10.

108. Tvorogov D, Thompson-Peach CAL, Foßelteder J, Dottore M, Stomski F, Onnesha SA, et al. Targeting human CALR-mutated MPN progenitors with a neoepitope-directed monoclonal antibody. EMBO reports. 2022;23(4):e52904.
109. Palacios R, Steinmetz M. IL3-dependent mouse clones that express B-220 surface antigen, contain ig genes in germ-line configuration, and generate B lymphocytes in vivo. Cell. 1985;41(3):727-34.
110. Kitamura T, Tange T, Terasawa T, Chiba S, Kuwaki T, Miyagawa K, et al. Establishment and characterization of a unique human cell line that proliferates dependently on GM-CSF, IL-3, or erythropoietin. Journal of Cellular Physiology. 1989;140(2):323-34.
111. Komatsu N, Kunitama M, Yamada M, Hagiwara T, Kato T, Miyazaki H, et al. Establishment and characterization of the thrombopoietin-dependent megakaryocytic cell line, UT-7/TPO. Blood. 1996;87(11):4552-60.
112. Komatsu N, Nakauchi H, Miwa A, Ishihara T, Eguchi M, Moroi M, et al. Establishment and characterization of a human leukemic cell line with megakaryocytic features: dependency on granulocyte-macrophage colony-stimulating factor, interleukin 3, or erythropoietin for growth and survival. Cancer research. 1991;51(1):341-8.
113. Masubuchi N, Araki M, Yang Y, Hayashi E, Imai M, Edahiro Y, et al. Mutant calreticulin interacts with MPL in the secretion pathway for activation on the cell surface. Leukemia. 2020;34(2):499-509.
114. Olschok K, Han L, de Toledo MAS, Böhnke J, Graßhoff M, Costa IG, et al. CALR frameshift mutations in MPN patient-derived iPSCs accelerate maturation of megakaryocytes. Stem cell reports. 2021.
115. Eglitis MA, Kantoff P, Gilboa E, Anderson WF. Gene Expression in Mice After High Efficiency Retroviral-Mediated Gene Transfer. Science. 1985;230(4732):1395-8.
116. Hatzoglou M, Lamers W, Bosch F, Wynshaw-Boris A, Clapp DW, Hanson RW. Hepatic gene transfer in animals using retroviruses containing the promoter from the gene for phosphoenolpyruvate carboxykinase. Journal of Biological Chemistry. 1990;265(28):17285-93.
117. Joyner A, Keller G, Phillips RA, Bernstein A. Retrovirus transfer of a bacterial gene into mouse haematopoietic progenitor cells. Nature. 1983;305(5934):556-8.
118. Dzierzak EA, Papayannopoulou T, Mulligan RC. Lineage-specific expression of a human β-globin gene in murine bone marrow transplant recipients reconstituted with retrovirus-transduced stem cells. Nature. 1988;331(6151):35-41.

119. Pear WS, Miller JP, Xu L, Pui JC, Soffer B, Quackenbush RC, et al. Efficient and Rapid Induction of a Chronic Myelogenous Leukemia-Like Myeloproliferative Disease in Mice Receiving P210 bcr/abl-Transduced Bone Marrow. Blood. 1998;92(10):3780-92.
120. Jaenisch R, Mintz B. Simian Virus 40 DNA Sequences in DNA of Healthy Adult Mice Derived from Preimplantation Blastocysts Injected with Viral DNA. Proceedings of the National Academy of Sciences. 1974;71(4):1250-4.
121. Gordon JW, Scangos GA, Plotkin DJ, Barbosa JA, Ruddle FH. Genetic transformation of mouse embryos by microinjection of purified DNA. Proceedings of the National Academy of Sciences. 1980;77(12):7380-4.
122. Evans MJ, Kaufman MH. Establishment in culture of pluripotential cells from mouse embryos. Nature. 1981;292(5819):154-6.
123. Martin GR. Isolation of a pluripotent cell line from early mouse embryos cultured in medium conditioned by teratocarcinoma stem cells. Proceedings of the National Academy of Sciences. 1981;78(12):7634-8.
124. Lewandoski M. Conditional control of gene expression in the mouse. Nature Reviews Genetics. 2001;2(10):743-55.
125. Kühn R, Schwenk F, Aguet M, Rajewsky K. Inducible Gene Targeting in Mice. Science. 1995;269(5229):1427-9.
126. Ogilvy S, Metcalf D, Gibson L, Bath ML, Harris AW, Adams JM. Promoter Elements of vav Drive Transgene Expression In Vivo Throughout the Hematopoietic Compartment. Blood. 1999;94(6):1855-63.
127. de Boer J, Williams A, Skavdis G, Harker N, Coles M, Tolaini M, et al. Transgenic mice with hematopoietic and lymphoid specific expression of Cre. European Journal of Immunology. 2003;33(2):314-25.
128. Göthert JR, Gustin SE, Hall MA, Green AR, Göttgens B, Izon DJ, et al. In vivo fate-tracing studies using the Scl stem cell enhancer: embryonic hematopoietic stem cells significantly contribute to adult hematopoiesis. Blood. 2005;105(7):2724-32.
129. Joseph C, Quach JM, Walkley CR, Lane SW, Lo Celso C, Purton LE. Deciphering hematopoietic stem cells in their niches: a critical appraisal of genetic models, lineage tracing, and imaging strategies. Cell Stem Cell. 2013;13(5):520-33.
130. Toppaldoddi KR, da Costa Cacemiro M, Bluteau O, Panneau-Schmaltz B, Pioch A, Muller D, et al. Rare type 1-like and type 2-like calreticulin mutants induce similar myeloproliferative neoplasms as prevalent type 1 and 2 mutants in mice. Oncogene. 2019;38(10):1651-60.

131. Shide K, Kameda T, Kamiunten A, Oji A, Ozono Y, Sekine M, et al. Mice with Calr mutations homologous to human CALR mutations only exhibit mild thrombocytosis. Blood cancer journal. 2019;9(4):42.
132. Benlabiod C, Cacemiro MdC, Nédélec A, Edmond V, Muller D, Rameau P, et al. Calreticulin del52 and ins5 knock-in mice recapitulate different myeloproliferative phenotypes observed in patients with MPN. Nature communications. 2020;11(1):4886.
133. Bosma GC, Custer RP, Bosma MJ. A severe combined immunodeficiency mutation in the mouse. Nature. 1983;301(5900):527-30.
134. Bosma MJ, Carroll AM. The SCID Mouse Mutant: Definition, Characterization, and Potential Uses. Annual Review of Immunology. 1991;9(1):323-50.
135. Shultz LD, Schweitzer PA, Christianson SW, Gott B, Schweitzer IB, Tennent B, et al. Multiple defects in innate and adaptive immunologic function in NOD/LtSz-scid mice. The Journal of Immunology. 1995;154(1):180.
136. Mazurier F, Doedens M, Gan OI, Dick JE. Rapid myeloerythroid repopulation after intrafemoral transplantation of NOD-SCID mice reveals a new class of human stem cells. Nature Medicine. 2003;9(7):959-63.
137. Christianson SW, Greiner DL, Schweitzer IB, Gott B, Beamer GL, Schweitzer PA, et al. Role of Natural Killer Cells on Engraftment of Human Lymphoid Cells and on Metastasis of Human T-Lymphoblastoid Leukemia Cells in C57BL/6J-scidMice and in C57BL/6J-scid bgMice. Cellular Immunology. 1996;171(2):186-99.
138. Ito M, Hiramatsu H, Kobayashi K, Suzue K, Kawahata M, Hioki K, et al. NOD/SCID/γcnull mouse: an excellent recipient mouse model for engraftment of human cells. Blood. 2002;100(9):3175-82.
139. Ishikawa F, Yasukawa M, Lyons B, Yoshida S, Miyamoto T, Yoshimoto G, et al. Development of functional human blood and immune systems in NOD/SCID/IL2 receptor {gamma} chain(null) mice. Blood. 2005;106(5):1565-73.
140. Shultz LD, Lyons BL, Burzenski LM, Gott B, Chen X, Chaleff S, et al. Human Lymphoid and Myeloid Cell Development in NOD/LtSz-scid IL2Rγ^{null} Mice Engrafted with Mobilized Human Hemopoietic Stem Cells. The Journal of Immunology. 2005;174(10):6477.
141. Rahmig S, Kronstein-Wiedemann R, Fohgrub J, Kronstein N, Nevmerzhitskaya A, Bornhäuser M, et al. Improved Human Erythropoiesis and Platelet Formation in Humanized NSGW41 Mice. Stem cell reports. 2016;7(4):591-601.

142. Cosgun Kadriye N, Rahmig S, Mende N, Reinke S, Hauber I, Schäfer C, et al. Kit Regulates HSC Engraftment across the Human-Mouse Species Barrier. Cell Stem Cell. 2014;15(2):227-38.
143. Wunderlich M, Chou FS, Link KA, Mizukawa B, Perry RL, Carroll M, et al. AML xenograft efficiency is significantly improved in NOD/SCID-IL2RG mice constitutively expressing human SCF, GM-CSF and IL-3. Leukemia. 2010;24(10):1785-8.
144. Wunderlich M, Chou F-S, Sexton C, Presicce P, Chougnet CA, Aliberti J, et al. Improved multilineage human hematopoietic reconstitution and function in NSGS mice. PloS one. 2018;13(12):e0209034.
145. Rongvaux A, Willinger T, Martinek J, Strowig T, Gearty SV, Teichmann LL, et al. Development and function of human innate immune cells in a humanized mouse model. Nature biotechnology. 2014;32(4):364-72.
146. Chao MP, Weissman IL, Majeti R. The CD47-SIRPα pathway in cancer immune evasion and potential therapeutic implications. Current opinion in immunology. 2012;24(2):225-32.
147. Willingham SB, Volkmer J-P, Gentles AJ, Sahoo D, Dalerba P, Mitra SS, et al. The CD47-signal regulatory protein alpha (SIRPa) interaction is a therapeutic target for human solid tumors. Proceedings of the National Academy of Sciences. 2012;109(17):6662-7.
148. Saito Y, Ellegast JM, Rafiei A, Song Y, Kull D, Heikenwalder M, et al. Peripheral blood CD34(+) cells efficiently engraft human cytokine knock-in mice. Blood. 2016;128(14):1829-33.
149. Song Y, Rongvaux A, Taylor A, Jiang T, Tebaldi T, Balasubramanian K, et al. A highly efficient and faithful MDS patient-derived xenotransplantation model for pre-clinical studies. Nature communications. 2019;10(1):366.
150. Wang X, Prakash S, Lu M, Tripodi J, Ye F, Najfeld V, et al. Spleens of myelofibrosis patients contain malignant hematopoietic stem cells. The Journal of Clinical Investigation. 2012;122(11):3888-99.
151. Ishii T, Zhao Y, Sozer S, Shi J, Zhang W, Hoffman R, et al. Behavior of CD34+ cells isolated from patients with polycythemia vera in NOD/SCID mice. Experimental Hematology. 2007;35(11):1633-40.
152. Reinisch A, Thomas D, Corces MR, Zhang X, Gratzinger D, Hong WJ, et al. A humanized bone marrow ossicle xenotransplantation model enables improved engraftment of healthy and leukemic human hematopoietic cells. Nat Med. 2016;22(7):812-21.

153. Lysenko V, Wildner-Verhey van Wijk N, Zimmermann K, Weller MC, Bühler M, Wildschut MHE, et al. Enhanced engraftment of human myelofibrosis stem and progenitor cells in MISTRG mice. Blood advances. 2020;4(11):2477-88.
154. Celik H, Krug E, Zhang CR, Han W, Issa N, Koh WK, et al. A Humanized Animal Model Predicts Clonal Evolution and Therapeutic Vulnerabilities in Myeloproliferative Neoplasms. Cancer discovery. 2021:candisc.1652.2020.
155. Watson JD, Crick FHC. Molecular Structure of Nucleic Acids: A Structure for Deoxyribose Nucleic Acid. Nature. 1953;171(4356):737-8.
156. Bessman MJ, Kornberg A, Lehman IR, Simms ES. Enzymic synthesis of deoxyribonucleic acid. Biochimica et biophysica acta. 1956;21(1):197-8.
157. Bessman MJ, Lehman IR, Simms ES, Kornberg A. Enzymatic synthesis of deoxyribonucleic acid. II. General properties of the reaction. The Journal of biological chemistry. 1958;233(1):171-7.
158. Lehman IR, Bessman MJ, Simms ES, Kornberg A. Enzymatic synthesis of deoxyribonucleic acid. I. Preparation of substrates and partial purification of an enzyme from Escherichia coli. The Journal of biological chemistry. 1958;233(1):163-70.
159. Olivera BM, Lehman IR. Linkage of polynucleotides through phosphodiester bonds by an enzyme from Escherichia coli. Proceedings of the National Academy of Sciences. 1967;57(5):1426-33.
160. Gefter ML, Becker A, Hurwitz J. The enzymatic repair of DNA. I. Formation of circular lambda-DNA. Proceedings of the National Academy of Sciences. 1967;58(1):240-7.
161. Zimmerman SB, Little JW, Oshinsky CK, Gellert M. Enzymatic joining of DNA strands: a novel reaction of diphosphopyridine nucleotide. Proceedings of the National Academy of Sciences. 1967;57(6):1841-8.
162. Meselson M, Yuan R. DNA restriction enzyme from E. coli. Nature. 1968;217(5134):1110-4.
163. Smith HO, Wilcox KW. A restriction enzyme from Hemophilus influenzae. I. Purification and general properties. J Mol Biol. 1970;51(2):379-91.
164. Cohen SN, Chang AC, Boyer HW, Helling RB. Construction of biologically functional bacterial plasmids in vitro. Proc Natl Acad Sci U S A. 1973;70(11):3240-4.
165. Crea R, Kraszewski A, Hirose T, Itakura K. Chemical synthesis of genes for human insulin. Proc Natl Acad Sci U S A. 1978;75(12):5765-9.
166. Mullis K, Faloona F, Scharf S, Saiki R, Horn G, Erlich H. Specific enzymatic amplification of DNA in vitro: the polymerase chain reaction. Cold Spring Harbor symposia on quantitative biology. 1986;51 Pt 1:263-73.

167. Kim YG, Cha J, Chandrasegaran S. Hybrid restriction enzymes: zinc finger fusions to Fok I cleavage domain. Proc Natl Acad Sci U S A. 1996;93(3):1156-60.
168. Bibikova M, Carroll D, Segal DJ, Trautman JK, Smith J, Kim YG, et al. Stimulation of homologous recombination through targeted cleavage by chimeric nucleases. Molecular and cellular biology. 2001;21(1):289-97.
169. Boch J, Scholze H, Schornack S, Landgraf A, Hahn S, Kay S, et al. Breaking the Code of DNA Binding Specificity of TAL-Type III Effectors. Science. 2009;326(5959):1509-12.
170. Christian M, Cermak T, Doyle EL, Schmidt C, Zhang F, Hummel A, et al. Targeting DNA Double-Strand Breaks with TAL Effector Nucleases. Genetics. 2010;186(2):757-61.
171. Miller JC, Tan S, Qiao G, Barlow KA, Wang J, Xia DF, et al. A TALE nuclease architecture for efficient genome editing. Nature biotechnology. 2011;29(2):143-8.
172. Zhang F, Cong L, Lodato S, Kosuri S, Church GM, Arlotta P. Efficient construction of sequence-specific TAL effectors for modulating mammalian transcription. Nature biotechnology. 2011;29(2):149-53.
173. Lander ES, Linton LM, Birren B, Nusbaum C, Zody MC, Baldwin J, et al. Initial sequencing and analysis of the human genome. Nature. 2001;409(6822):860-921.
174. International Human Genome Sequencing C. Finishing the euchromatic sequence of the human genome. Nature. 2004;431(7011):931-45.
175. Mojica FJ, Díez-Villaseñor C, García-Martínez J, Soria E. Intervening sequences of regularly spaced prokaryotic repeats derive from foreign genetic elements. Journal of molecular evolution. 2005;60(2):174-82.
176. Barrangou R, Fremaux C, Deveau H, Richards M, Boyaval P, Moineau S, et al. CRISPR provides acquired resistance against viruses in prokaryotes. Science. 2007;315(5819):1709-12.
177. Deltcheva E, Chylinski K, Sharma CM, Gonzales K, Chao Y, Pirzada ZA, et al. CRISPR RNA maturation by trans-encoded small RNA and host factor RNase III. Nature. 2011;471(7340):602-7.
178. Brouns SJ, Jore MM, Lundgren M, Westra ER, Slijkhuis RJ, Snijders AP, et al. Small CRISPR RNAs guide antiviral defense in prokaryotes. Science. 2008;321(5891):960-4.
179. Marraffini LA, Sontheimer EJ. CRISPR interference limits horizontal gene transfer in staphylococci by targeting DNA. Science. 2008;322(5909):1843-5.

180. Jinek M, Chylinski K, Fonfara I, Hauer M, Doudna JA, Charpentier E. A Programmable Dual-RNA–Guided DNA Endonuclease in Adaptive Bacterial Immunity. Science. 2012;337(6096):816-21.
181. Gasiunas G, Barrangou R, Horvath P, Siksnys V. Cas9-crRNA ribonucleoprotein complex mediates specific DNA cleavage for adaptive immunity in bacteria. Proc Natl Acad Sci U S A. 2012;109(39):E2579-86.
182. Bolotin A, Quinquis B, Sorokin A, Ehrlich SD. Clustered regularly interspaced short palindrome repeats (CRISPRs) have spacers of extrachromosomal origin. Microbiology (Reading, England). 2005;151(Pt 8):2551-61.
183. Garneau JE, Dupuis M-È, Villion M, Romero DA, Barrangou R, Boyaval P, et al. The CRISPR/Cas bacterial immune system cleaves bacteriophage and plasmid DNA. Nature. 2010;468(7320):67-71.
184. Cong L, Ran FA, Cox D, Lin S, Barretto R, Habib N, et al. Multiplex Genome Engineering Using CRISPR/Cas Systems. Science. 2013;339(6121):819.
185. Mali P, Yang L, Esvelt KM, Aach J, Guell M, DiCarlo JE, et al. RNA-guided human genome engineering via Cas9. Science. 2013;339(6121):823-6.
186. Lieber MR. The mechanism of double-strand DNA break repair by the nonhomologous DNA end-joining pathway. Annual review of biochemistry. 2010;79:181-211.
187. Liang F, Han M, Romanienko PJ, Jasin M. Homology-directed repair is a major double-strand break repair pathway in mammalian cells. Proceedings of the National Academy of Sciences. 1998;95(9):5172-7.
188. Mao Z, Bozzella M, Seluanov A, Gorbunova V. DNA repair by nonhomologous end joining and homologous recombination during cell cycle in human cells. Cell Cycle. 2008;7(18):2902-6.
189. Popp MW, Maquat LE. Leveraging Rules of Nonsense-Mediated mRNA Decay for Genome Engineering and Personalized Medicine. Cell. 2016;165(6):1319-22.
190. Hsu PD, Scott DA, Weinstein JA, Ran FA, Konermann S, Agarwala V, et al. DNA targeting specificity of RNA-guided Cas9 nucleases. Nature biotechnology. 2013;31(9):827-32.
191. Doench JG, Hartenian E, Graham DB, Tothova Z, Hegde M, Smith I, et al. Rational design of highly active sgRNAs for CRISPR-Cas9-mediated gene inactivation. Nature biotechnology. 2014;32(12):1262-7.
192. Doench JG, Fusi N, Sullender M, Hegde M, Vaimberg EW, Donovan KF, et al. Optimized sgRNA design to maximize activity and minimize off-target effects of CRISPR-Cas9. Nature biotechnology. 2016;34(2):184-91.

193. Slaymaker IM, Gao L, Zetsche B, Scott DA, Yan WX, Zhang F. Rationally engineered Cas9 nucleases with improved specificity. Science. 2016;351(6268):84-8.
194. Kleinstiver BP, Pattanayak V, Prew MS, Tsai SQ, Nguyen NT, Zheng Z, et al. High-fidelity CRISPR–Cas9 nucleases with no detectable genome-wide off-target effects. Nature. 2016;529(7587):490-5.
195. Chen JS, Dagdas YS, Kleinstiver BP, Welch MM, Sousa AA, Harrington LB, et al. Enhanced proofreading governs CRISPR-Cas9 targeting accuracy. Nature. 2017;550(7676):407-10.
196. Tsai SQ, Zheng Z, Nguyen NT, Liebers M, Topkar VV, Thapar V, et al. GUIDE-seq enables genome-wide profiling of off-target cleavage by CRISPR-Cas nucleases. Nature biotechnology. 2014;33:187.
197. Tsai SQ, Nguyen NT, Malagon-Lopez J, Topkar VV, Aryee MJ, Joung JK. CIRCLE-seq: a highly sensitive in vitro screen for genome-wide CRISPR-Cas9 nuclease off-targets. Nature methods. 2017;14(6):607-14.
198. Wienert B, Wyman SK, Richardson CD, Yeh CD, Akcakaya P, Porritt MJ, et al. Unbiased detection of CRISPR off-targets in vivo using DISCOVER-Seq. Science. 2019;364(6437):286.
199. Zhu X, Xu Y, Yu S, Lu L, Ding M, Cheng J, et al. An Efficient Genotyping Method for Genome-modified Animals and Human Cells Generated with CRISPR/Cas9 System. Scientific Reports. 2014;4(1):6420.
200. Kim S, Kim D, Cho SW, Kim J, Kim JS. Highly efficient RNA-guided genome editing in human cells via delivery of purified Cas9 ribonucleoproteins. Genome research. 2014;24(6):1012-9.
201. Shalem O, Sanjana NE, Hartenian E, Shi X, Scott DA, Mikkelsen TS, et al. Genome-Scale CRISPR-Cas9 Knockout Screening in Human Cells. Science. 2014;343(6166):84-7.
202. Xu CL, Ruan MZC, Mahajan VB, Tsang SH. Viral Delivery Systems for CRISPR. Viruses. 2019;11(1).
203. DeWitt MA, Corn JE, Carroll D. Genome editing via delivery of Cas9 ribonucleoprotein. Methods (San Diego, Calif). 2017;121-122:9-15.
204. Lin S, Staahl BT, Alla RK, Doudna JA. Enhanced homology-directed human genome engineering by controlled timing of CRISPR/Cas9 delivery. Elife. 2014;3:e04766.
205. Wang H, Yang H, Shivalila CS, Dawlaty MM, Cheng AW, Zhang F, et al. One-Step Generation of Mice Carrying Mutations in Multiple Genes by CRISPR/Cas-Mediated Genome Engineering. Cell. 2013;153(4):910-8.

206. DeWitt MA, Magis W, Bray NL, Wang T, Berman JR, Urbinati F, et al. Selection-free genome editing of the sickle mutation in human adult hematopoietic stem/progenitor cells. Science Translational Medicine. 2016;8(360):360ra134-360ra134.
207. Yin H, Song C-Q, Dorkin JR, Zhu LJ, Li Y, Wu Q, et al. Therapeutic genome editing by combined viral and non-viral delivery of CRISPR system components in vivo. Nature biotechnology. 2016;34(3):328-33.
208. Dever DP, Bak RO, Reinisch A, Camarena J, Washington G, Nicolas CE, et al. CRISPR/Cas9 beta-globin gene targeting in human haematopoietic stem cells. Nature. 2016;539(7629):384-9.
209. Kaulich M, Dowdy SF. Combining CRISPR/Cas9 and rAAV Templates for Efficient Gene Editing. Nucleic acid therapeutics. 2015;25(6):287-96.
210. Wang D, Tai PWL, Gao G. Adeno-associated virus vector as a platform for gene therapy delivery. Nature Reviews Drug Discovery. 2019;18(5):358-78.
211. Legut M, Dolton G, Mian AA, Ottmann OG, Sewell AK. CRISPR-mediated TCR replacement generates superior anticancer transgenic T cells. Blood. 2018;131(3):311-22.
212. Liu X, Zhang Y, Cheng C, Cheng AW, Zhang X, Li N, et al. CRISPR-Cas9-mediated multiplex gene editing in CAR-T cells. Cell Research. 2017;27(1):154-7.
213. Lapidot T, Sirard C, Vormoor J, Murdoch B, Hoang T, Caceres-Cortes J, et al. A cell initiating human acute myeloid leukaemia after transplantation into SCID mice. Nature. 1994;367(6464):645-8.
214. Passegué E, Wagner EF, Weissman IL. JunB Deficiency Leads to a Myeloproliferative Disorder Arising from Hematopoietic Stem Cells. Cell. 2004;119(3):431-43.
215. Castor A, Nilsson L, Åstrand-Grundström I, Buitenhuis M, Ramirez C, Anderson K, et al. Distinct patterns of hematopoietic stem cell involvement in acute lymphoblastic leukemia. Nature Medicine. 2005;11(6):630-7.
216. Mandal Pankaj K, Ferreira LMR, Collins R, Meissner Torsten B, Boutwell Christian L, Friesen M, et al. Efficient Ablation of Genes in Human Hematopoietic Stem and Effector Cells using CRISPR/Cas9. Cell Stem Cell. 2014;15(5):643-52.
217. Xu L, Yang H, Gao Y, Chen Z, Xie L, Liu Y, et al. CRISPR/Cas9-Mediated CCR5 Ablation in Human Hematopoietic Stem/Progenitor Cells Confers HIV-1 Resistance In Vivo. Molecular Therapy. 2017;25(8):1782-9.
218. Wu Y, Zeng J, Roscoe BP, Liu P, Yao Q, Lazzarotto CR, et al. Highly efficient therapeutic gene editing of human hematopoietic stem cells. Nature Medicine. 2019;25(5):776-83.

219. Wu Y, Zeng J, Roscoe BP, Liu P, Yao Q, Lazzarotto CR, et al. Highly efficient therapeutic gene editing of human hematopoietic stem cells. Nature Medicine. 2019.
220. Frangoul H, Altshuler D, Cappellini MD, Chen Y-S, Domm J, Eustace BK, et al. CRISPR-Cas9 Gene Editing for Sickle Cell Disease and β-Thalassemia. New England Journal of Medicine. 2020;384(3):252-60.
221. Heckl D, Kowalczyk MS, Yudovich D, Belizaire R, Puram RV, McConkey ME, et al. Generation of mouse models of myeloid malignancy with combinatorial genetic lesions using CRISPR-Cas9 genome editing. Nature biotechnology. 2014;32(9):941-6.
222. Tothova Z, Krill-Burger JM, Popova KD, Landers CC, Sievers QL, Yudovich D, et al. Multiplex CRISPR/Cas9-Based Genome Editing in Human Hematopoietic Stem Cells Models Clonal Hematopoiesis and Myeloid Neoplasia. Cell Stem Cell. 2017;21(4):547-55.e8.
223. Bak RO, Dever DP, Porteus MH. CRISPR/Cas9 genome editing in human hematopoietic stem cells. Nature Protocols. 2018;13(2):358-76.
224. Concordet J-P, Haeussler M. CRISPOR: intuitive guide selection for CRISPR/Cas9 genome editing experiments and screens. Nucleic Acids Research. 2018;46(W1):W242-W5.
225. Ran FA, Hsu PD, Wright J, Agarwala V, Scott DA, Zhang F. Genome engineering using the CRISPR-Cas9 system. Nature Protocols. 2013;8:2281.
226. Song L, Kauss MA, Kopin E, Chandra M, Ul-Hasan T, Miller E, et al. Optimizing the transduction efficiency of capsid-modified AAV6 serotype vectors in primary human hematopoietic stem cells in vitro and in a xenograft mouse model in vivo. Cytotherapy. 2013;15(8):986-98.
227. Prins D, González Arias C, Klampfl T, Grinfeld J, Green AR. Mutant Calreticulin in the Myeloproliferative Neoplasms. HemaSphere. 2020;4(1):0333.
228. Bradley TR, Metcalf D. The growth of mouse bone marrow cells in vitro. The Australian journal of experimental biology and medical science. 1966;44(3):287-99.
229. Sanada C, Xavier-Ferrucio J, Lu YC, Min E, Zhang PX, Zou S, et al. Adult human megakaryocyte-erythroid progenitors are in the CD34+CD38mid fraction. Blood. 2016;128(7):923-33.
230. McDermott SP, Eppert K, Lechman ER, Doedens M, Dick JE. Comparison of human cord blood engraftment between immunocompromised mouse strains. Blood. 2010;116(2):193-200.
231. Nam AS, Kim K-T, Chaligne R, Izzo F, Ang C, Taylor J, et al. Somatic mutations and cell identity linked by Genotyping of Transcriptomes. Nature. 2019;571(7765):355-60.

232. Cerezo M, Lehraiki A, Millet A, Rouaud F, Plaisant M, Jaune E, et al. Compounds Triggering ER Stress Exert Anti-Melanoma Effects and Overcome BRAF Inhibitor Resistance. Cancer Cell. 2016;29(6):805-19.
233. Richardson PG, Barlogie B, Berenson J, Singhal S, Jagannath S, Irwin D, et al. A Phase 2 Study of Bortezomib in Relapsed, Refractory Myeloma. New England Journal of Medicine. 2003;348(26):2609-17.
234. Salati S, Genovese E, Carretta C, Zini R, Bartalucci N, Prudente Z, et al. Calreticulin Ins5 and Del52 mutations impair unfolded protein and oxidative stress responses in K562 cells expressing CALR mutants. Sci Rep. 2019;9(1):10558.
235. Hendel A, Bak RO, Clark JT, Kennedy AB, Ryan DE, Roy S, et al. Chemically modified guide RNAs enhance CRISPR-Cas genome editing in human primary cells. Nature biotechnology. 2015;33(9):985-9.
236. Azhagiri MKK, Babu P, Venkatesan V, Thangavel S. Homology-directed gene-editing approaches for hematopoietic stem and progenitor cell gene therapy. Stem Cell Research & Therapy. 2021;12(1):500.
237. Dahlberg A, Delaney C, Bernstein ID. Ex vivo expansion of human hematopoietic stem and progenitor cells. Blood. 2011;117(23):6083-90.
238. Hubbard N, Hagin D, Sommer K, Song Y, Khan I, Clough C, et al. Targeted gene editing restores regulated CD40L function in X-linked hyper-IgM syndrome. Blood. 2016;127(21):2513-22.
239. Bibikova M, Golic M, Golic KG, Carroll D. Targeted chromosomal cleavage and mutagenesis in Drosophila using zinc-finger nucleases. Genetics. 2002;161(3):1169-75.
240. Shide K, Kameda T, Yamaji T, Sekine M, Inada N, Kamiunten A, et al. Calreticulin mutant mice develop essential thrombocythemia that is ameliorated by the JAK inhibitor ruxolitinib. Leukemia. 2017;31(5):1136-44.
241. Li J, Prins D, Park HJ, Grinfeld J, Gonzalez-Arias C, Loughran S, et al. Mutant calreticulin knockin mice develop thrombocytosis and myelofibrosis without a stem cell self-renewal advantage. Blood. 2018;131(6):649-61.
242. Notta F, Doulatov S, Laurenti E, Poeppl A, Jurisica I, Dick JE. Isolation of Single Human Hematopoietic Stem Cells Capable of Long-Term Multilineage Engraftment. Science. 2011;333(6039):218.
243. Schiroli G, Conti A, Ferrari S, Della Volpe L, Jacob A, Albano L, et al. Precise Gene Editing Preserves Hematopoietic Stem Cell Function following Transient p53-Mediated DNA Damage Response. Cell Stem Cell. 2019;24(4):551-65.e8.

244. Hu Z, Van Rooijen N, Yang Y-G. Macrophages prevent human red blood cell reconstitution in immunodeficient mice. Blood. 2011;118(22):5938-46.
245. Rahmig S, Kronstein-Wiedemann R, Fohgrub J, Kronstein N, Nevmerzhitskaya A, Bornhauser M, et al. Improved Human Erythropoiesis and Platelet Formation in Humanized NSGW41 Mice. Stem cell reports. 2016;7(4):591-601.
246. Wang J, Kimura T, Asada R, Harada S, Yokota S, Kawamoto Y, et al. SCID-repopulating cell activity of human cord blood–derived CD34− cells assured by intra–bone marrow injection. Blood. 2003;101(8):2924-31.
247. Hogan CJ, Shpall EJ, Keller G. Differential long-term and multilineage engraftment potential from subfractions of human CD34+ cord blood cells transplanted into NOD/SCID mice. Proceedings of the National Academy of Sciences. 2002;99(1):413-8.
248. Vannucchi AM, Rotunno G, Bartalucci N, Raugei G, Carrai V, Balliu M, et al. Calreticulin mutation-specific immunostaining in myeloproliferative neoplasms: pathogenetic insight and diagnostic value. Leukemia. 2014;28(9):1811-8.
249. Prins D, Park HJ, Watcham S, Li J, Vacca M, Bastos HP, et al. The stem/progenitor landscape is reshaped in a mouse model of essential thrombocythemia and causes excess megakaryocyte production. Science advances. 2020;6(48):eabd3139.
250. Jutzi JS, Marneth AE, Ciboddo M, Guerra-Moreno A, Jiménez-Santos MJ, Kosmidou A, et al. Whole-genome CRISPR screening identifies N-glycosylation as a genetic and therapeutic vulnerability in CALR-mutant MPN. Blood. 2022:blood.2022015629.
251. Ibarra J, Elbanna YA, Kurylowicz K, Ciboddo M, Greenbaum HS, Arellano NS, et al. Type I but Not Type II Calreticulin Mutations Activate the IRE1α/XBP1 Pathway of the Unfolded Protein Response to Drive Myeloproliferative Neoplasms. Blood Cancer Discovery. 2022:OF1-OF18.
252. Tefferi A, Wassie EA, Guglielmelli P, Gangat N, Belachew AA, Lasho TL, et al. Type 1 versus Type 2 calreticulin mutations in essential thrombocythemia: A collaborative study of 1027 patients. American journal of hematology. 2014;89(8):E121-E4.
253. Gething M-J. Role and regulation of the ER chaperone BiP. Seminars in Cell & Developmental Biology. 1999;10(5):465-72.
254. Wu J, Wu Y, Lian X. Targeted inhibition of GRP78 by HA15 promotes apoptosis of lung cancer cells accompanied by ER stress and autophagy. Biology open. 2020;9(11).

9. Appendix

Foßelteder J, Pabst G, Sconocchia T, Schlacher A, Auinger L, Kashofer K, Beham-Schmid C, Trajanoski S, Waskow C, Schöll W, Sill H, Zebisch A, Wölfler A, Thomas D, Reinisch A. **Human gene-engineered calreticulin mutant stem cells recapitulate MPN hallmarks and identify targetable vulnerabilities.** Leukemia 2023.